The Role of High-Salt Diet on Melanoma Growth

Doctoral thesis

to obtain a doctorate (PhD)

from the Faculty of Medicine

of the University of Bonn

Natascha Ellen Stumpf

from Lahnstein, Germany

2024

Written with authorization of
the Faculty of Medicine of the University of Bonn

First reviewer: Prof. Dr. med. Christian Kurts

Second reviewer: Prof. Dr. med. Jonathan Jantsch

Day of oral examination: 16.02.2024

From the Institute of Molecular Medicine and Experimental Immunology
Director: Prof. Dr. med. Christian Kurts

Table of content

List of Abbreviations

Abbreviation	Spelled
%	Percentage
°C	Degree Celsius
2-NBDG	2-Deoxy-2-[(7-nitro-2,1,3-benzoxadiazol-4-yl)amino]-D-glucose
ANOVA	Analysis of variance
ATP	Adenosine triphosphate
BCA	Bicinchoninic acid
BN-PAGE	Blue native polyacrylamide gel electrophoresis
BRAF	v-RAF murine sarcoma viral oncogene homolog B1
BSA	Bovine serum albumin
BODIPY™ FL C16	(*T*-4)-[1-[3-[5-[(3,5-Dimethyl-2*H*-pyrrol-2-ylidene-κ*N*)methyl]-1*H*-pyrrol-2-yl-κ*N*]-1-oxopropoxy]-2,5-pyrrolidinedionato]difluoroboron
Ca^{2+}	Calcium
cAMP	Cyclic adenosine monophosphate
CFU	Colony forming units
Cl^-	Chloride
d	day
ddH_2O	Double distilled water
DMSO	Dimethylsulfoxide
DNA	Deoxyribonucleic acid
dNTP	Nucleotide triphosphate
ECAR	Extracellular acidification rate
ECM	Extracellular matrix
EDTA	Ethylenediaminetetraacetic acid
EGF	Epidermal growth factor
ELISA	Enzyme-linked immunosorbent assay
EMT	Epithelial-to-mesenchymal-transition
FACS	Fluorescence-activated cell scanning
FCS	Fetal calf serum
FMO	Fluorescence minus one

g	g-force
G418	Geneticin G418 antibiotic
G-CSF	Granulocyte colony-stimulation factor
GR	Glucocorticoid receptor
HET	House of Experimental Therapy
Hif-1α	Hypoxia-inducible factor 1 alpha
HSD	High-salt diet
i.v.	intravenous
i.p.	intraperitoneal
IVIS	In Vivo Imaging System
K^+	Potassium
kDa	Kilodalton
LN	Lymph nodes
MDSC	Myeloid-derived suppressor cells
MFI	Mean fluorescence intensity
MFI-FM_0	Mean fluorescence intensity minus one
MHC	Major histocompatibility complex
M-MDSC	Monocytic myeloid-derived suppressor cells
mg	milligram
Mitf	Microphthalmia-associated transcription factor
ml	milliliter
mM	millimolar
mm^3	cubic millimeter (volume)
mTOR	Mammalian target of rapamycin
Na^+	Sodium
NaCl	Sodium chloride
Nfat5	Nuclear factor of activated T-cells 5
NaN_3	Sodium azide
ng	nanogram
nm	nanometer
NRAS	neuroblast RAS viral oncogene homolog
NSD	Normal-salt diet

OCR	Oxygen consumption rate
OVA	Ovalbumin
PBS	Phosphate buffer saline
PCR	Polymerase chain reaction
PMA	Phorbol 12-myristate 13-acetate
PMN-MDSC	Granulocytic myeloid-derived suppressor cells
POMC	Proopiomelanocortin
P/S	Penicillin and Streptavidin
RCB	Red cell removal buffer
RNA	Ribonucleic acid
ROS	Reactive oxygen species
rpm	Revolution per minute
RT	Room temperature
s.c.	subcutan
sec	seconds
SPF	Specific pathogen-free
Sgk1	Serum and glucocorticoid-regulated kinase 1
TCA	Tricarboxylic acid cycle
Th T cells	T helper cells
TLS	Tertiary lymphoid structures
TME	Tumor microenvironment
µ	micro
µg	microgram
µl	microliter
µm	micrometer
UMAP	Uniform Manifold Approximate and Projection
UV	Ultraviolet
VEGF	Vascular endothelial cell growth factor

1 Introduction

1.1. Skin structure and function

The skin is the mammal's biggest organ and functions as a natural barrier between the organism and the environment. The main role of the skin is to protect the body against the invasion of pathogens and fending off chemical and physical assaults, for instance, ultraviolet (UV) radiation (Proksch, Brandner, and Jensen 2008; Madison 2003). To ensure an effective barrier, the skin is built as a complex network, which can be divided into two major layers: the superficial nonvascular epidermis, which is composed of stratum corneum, stratum spinosum, and stratum basale, and the lower layer, the dermis (Figure 1). The outer layer of the epidermis, stratum corneum, is built by keratinocytes which migrate from the stratum basale through the epidermis towards the surface and anchor there in a lipid matrix composed of ceramides, cholesterol, and fatty acids (Prottey 1977; Sadowski et al. 2017). The lipid composition of stratum corneum plays an essential role in structuring and maintaining the water permeability barrier function in the skin and in preventing unregulated loss of water and solutes (Coderch et al. 2003). Beneath the stratum corneum is the stratified squamous epithelium, composed of proliferating basal and differentiated suprabasal keratinocytes as well as melanocytes (Breitkreutz, Mirancea, and Nischt 2009). Together with fibroblasts, keratinocytes constitute the majority of cellular components in the skin (Hoath and Leahy 2003). Keratinocytes are responsible for cell-cell junction formation in order to create a stable cytoskeleton (Bazzoni and Dejana 2002). They are in close contact with melanocytes. Melanocytes are pigmented cells, found in the skin, eye, mucosal epithelial, and meninges (Lo and Fisher 2014). A special feature of these cells is the production and storage of melanin, which protects the cells against UV radiation (Bonaventure, Domingues, and Larue 2013). The deepest layer of the epidermis, stratum basale, contains stem cells which are continually divided into different cell types to ensure the maintenance of skin homeostasis and repair (Blanpain and Fuchs 2006).

The dermis is localized beneath the epidermis and functions to anchor and nourish the vascular-free epidermis. The major structural components of the dermis are collagen, elastic fibers, and extrafibrillar matrix, which assure strength and elasticity of the skin (Dick 1947). The dermis further contains hair follicles, several glands, and thermoreceptors to regulate the heat and sense coolness, pain, tickling, and itching (Ewart 1842). Furthermore, blood vessels and lymphatic vessels are present in the dermis layer to ensure a provision and fast recruitment of innate and adaptive immune cells against harmful penetrations (Shirshin et al. 2017).

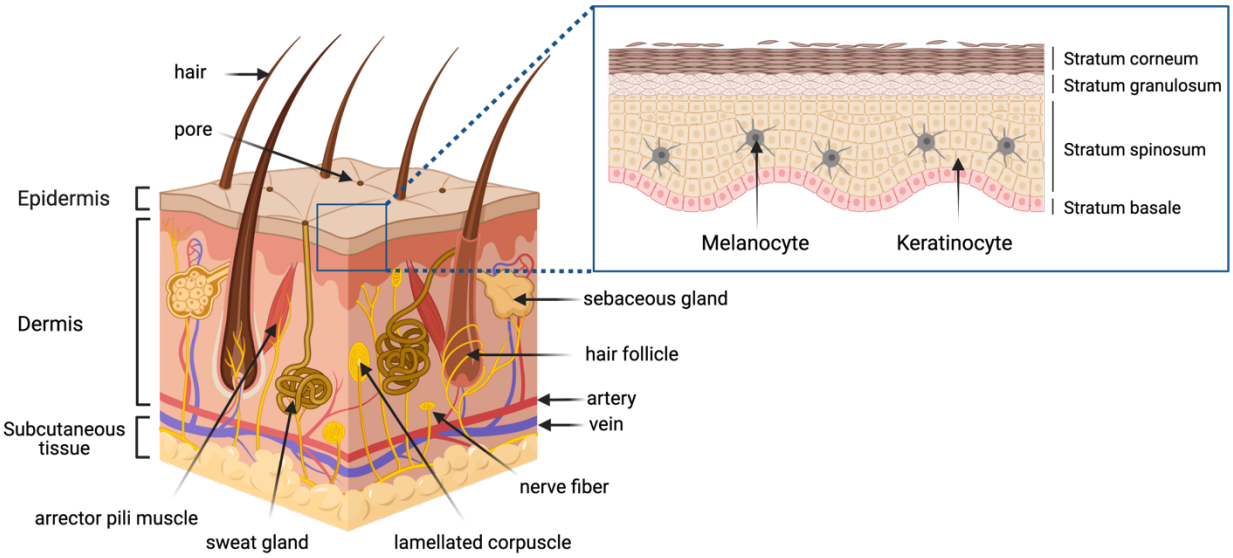

Figure 1: Structure of the skin. The skin can be divided into two major layers: the epidermis and the dermis. The epidermis provides a barrier function against the environment and regulates water balance. Within the epidermis, keratinocytes and melanocytes build a network with various functions, like the stability of the skin and the protection against UV light. The dermis is localized beneath the epidermis. Elastic fibers, extracellular matrix, and collagen assure the strength and elasticity of the skin. Hair follicles, sweat glands, and thermoreceptors play an essential role to regulate body homeostasis (modified from BioRender template and Laberge et al. 2020).

1.2. Skin immunity

To ensure a protective function of the skin, a branched network of skin-resident immune cells is crucial not only for the prevention of infection but also for tissue reconstruction. Dysregulation of the immune system leads to impaired wound healing and low tissue recovery function (Nguyen and Soulika 2019). Both myeloid and lymphoid cell populations are located in the skin. The most abundant skin-resident myeloid cells are Langerhans cells, macrophages, mast cells, and eosinophils.

Langerhans cells are specialized dendritic cells located in the epidermis. They form a network within the epidermis through interactions between epithelial cell adhesion molecules, such as E-cadherin, and keratinocytes (Choi et al. 2018). These cells contribute to skin homeostasis by secreting growth factors, such as granulocyte colony-stimulation factor (G-CSF), and epidermal growth factor (EGF), which are essential for the survival of keratinocytes, fibroblasts, and endothelial cells (Seggewiss and Einsele 2007; Schirmacher et al. 2001). Moreover, Langerhans cells are migratory cells and emigrate between the skin and their draining-lymph nodes to improve tolerance in homeostasis or initiate adaptive immune responses during infection (Romani et al. 1989; Ghigo et al. 2013).

Macrophages (Mø) are found in the dermal layer of the skin and can be categorized into M1/activated macrophages or M2/trophic macrophages, depending on their activation state (Malissen, Tamoutounour, and Henri 2014; Ginhoux and Jung 2014). The phagocytic characteristics of Mø allow the removal of debris and apoptotic cells in order to maintain skin health. During infection, M1 macrophages get activated and promote inflammatory responses, whereas M2 macrophages improve wound healing (Hassanshahi et al. 2022).

In addition to the innate immune system, the skin harbors different cell types of the lymphoid lineage. Conventional $\alpha\beta$ T cells are found in the epidermis and in the dermis layer where they function as resident memory T cells (Seidel et al. 2018). All known subpopulations of T cells, such as $CD8^+$ T cells, $CD4^+$ T cells, Th17 T cells, as well as regulatory T cells (Tregs) are represented in the skin for maintaining dermal homeostasis (Ariotti et al. 2014; Mackay et al. 2013; Ali and Rosenblum 2017). In addition to $\alpha\beta$ T cells, unconventional T cells, particularly $\gamma\delta$ T cells are located in the dermis within junctions

between keratinocytes (Elbe, Foster, and Stingl 1996). Unlike, $\alpha\beta$ T cells, $\gamma\delta$ T cells recognize free soluble antigens and non-peptide antigens with non-classical MHC-like molecules (Xiong and Raulet 2007). Once activated, $\gamma\delta$ T cells secrete a range of cytokines, e.g. interleukin (IL-)17, and growth factors to boost the antimicrobial defense in the skin and promotes wound healing (MacLeod et al. 2013; Jameson et al. 2004).
B lymphocytes are found in lower frequency in the skin during homeostasis (Egbuniwe et al. 2015). In addition to physical and microbiological barriers, the skin contains resident immune cells involved in tissue homeostasis and initiates various mechanisms of inflammatory responses to ensure optimal defense. Apart from that, tumor formation, in particular melanoma formation, also challenges skin immunity.

1.3. Malignant melanoma

Malignant melanoma is a neoplasm that originates in melanocytes and is the most lethal type of all skin cancer, contributing to 1.7 % of all cancers in the world population with rising incidence (Sung et al. 2021; Sandru et al. 2014). In 2022, recent data reported over 99000 new cases of melanoma patients in the United States which caused around 7700 disease-related deaths with overall a slight male predominance (Siegel et al. 2022). Melanoma is a multifaceted disease and bears a high mutational burden (Pagliuca, Di Leo, and De Zio 2022). Constant exposure of the skin to environmental stressors, including UV radiation and chemical compounds, results in genetic mutations and promotes tumor development (Moore 2002; Pandey et al. 2002). Early mutation in cancer development, particularly within the mitogen-activated protein kinase (MAPK) pathway, is a critical oncogenic event found in the majority of patients with malignant melanoma (Fecher, Amaravadi, and Flaherty 2008). Specifically, abnormalities in the v-RAF murine sarcoma viral oncogene homolog B1 (BRAF) and neuroblast RAS viral (v-RAS) oncogene homolog (NRAS) are found in around 40-50 % (for BRAF) and 15-20 % (for NRAS) of patients with melanoma (Omholt et al. 2003). Another risk factor represents the overexpression of c-KIT, a proto-oncogene encoding for the transmembrane receptor tyrosine kinase. Around 3 % of all patients with melanoma harbor the mutation which leads downstream of the activation of several signaling pathways, including MAPK/ERK and PI3K/Akt pathway, to induce cell proliferation, tumor growth, and metastasis (Pham,

Guhan, and Tsao 2020; Yuzawa et al. 2007; Sansal and Sellers 2004). However, unprotected sun exposure, especially in childhood, is the most environmental risk factor as it is responsible for the development of 60-70 % of all melanoma cases (Elwood and Jopson 1997; Arnold et al. 2018). Mechanistically, UV radiation induces DNA damage, frequently found in the cyclin-dependent kinase inhibitor 2a (*CDKN2A)* gene in cutaneous malignant melanoma. A mutation in this tumor suppressor protein can lead to permanent activation and further abnormal cell proliferation (Merlo et al. 1995).

The best survival rate for patients is the early diagnosis during tumor onset. However, if melanoma was diagnosed, the treatment possibilities depend mainly on the stage of cancer. The first treatment for melanoma is surgical removal or excision in the early stage of formation. Treatment with BRAF inhibitor (Vemurafenib®) was the first targeted agent in advanced melanoma. However, melanoma often showed a high rate of resistance in the first six months of treatment in 50 % of all patients (Chapman et al. 2011; McArthur et al. 2014). A combination of BRAF inhibitor and blocking the MEK pathway (Cobimetinib®) archives a higher clinical efficiency and longer overall survival rate in patients with melanoma (Mackiewicz and Mackiewicz 2018; Larkin et al. 2014). In recent years, successful treatments including immune checkpoint therapies such as PD-1 and CTLA-4 blockade significantly improve patient survival rate (Ribas 2012; Robert et al. 2014; Weber 2008). However, melanoma is a multifaceted disease with various unknown mechanisms that hamper novel therapeutic strategies.

1.4. Onset of melanoma formation

Cutaneous melanoma arises upon the malignant formation of melanocytes, the pigmented cells within the skin, which generally protects against UV radiation. Based on the Clark model, tumor progression can be well-defined and subdivided into several stages (Figure 2) (Clark 1991). Ultraviolet radiation, caused by sun exposure or artificial UV, provokes the formation of pyrimidine dimers between adjacent thymine and cytosine bases in the DNA. This results in a DNA excision repair system, where the dimer is cut out and replaced by the original sequence (Pfeifer and Besaratinia 2012). Besides external environmental factors, genetic pre-deposition is another key player in the development of melanoma. 25-50 % of people carry mutations increase their risk of the development of melanoma. For

example, a mutation in the tumor suppressor gene *CDKN2A* leads to uncontrolled melanocyte proliferation (Piepkorn 2000). Another mutation with high frequency found in melanoma progression was observed in BRAF. BRAF is a member of Raf kinases which are upstream elements of the MAPK pathway (Kong, Carlino, and Menzies 2016). The cytoplasmic protein kinase is regulated by its interaction with Ras and downstream activation of MAPK cascade, resulting in enriched signal transduction of cell proliferation (Peyssonnaux and Eychène 2001) (Figure 2, Step 1) (Ascierto et al. 2012). Abnormal growth of melanocytes in a pre-existing nevus, or newly generated cells, results in a pre-malignant lesion with random cytologic atypia (Figure 2, Step 2). Next, mutated melanocytes acquire the ability to proliferate in the horizontal layer of the epidermis (Figure 2, Step 3). During the epithelial-to-mesenchymal transition (EMT), the loss of E-cadherin and the expression of N-cadherin support the intraepidermal growth into the lower dermis and further allow the invasion of cancer cells. Malignant melanocytes invade the basement membrane where they proliferate vertically into the dermis, resulting in an expanded nodule growth (Figure 2, Step 4). In the end, melanoma cells reach the bloodstream and spread to other areas in the body, mainly lymph nodes, subcutaneous soft tissue, and further into the lung and the brain (Figure 2, Step 5) (Thompson and Shaw 2000).

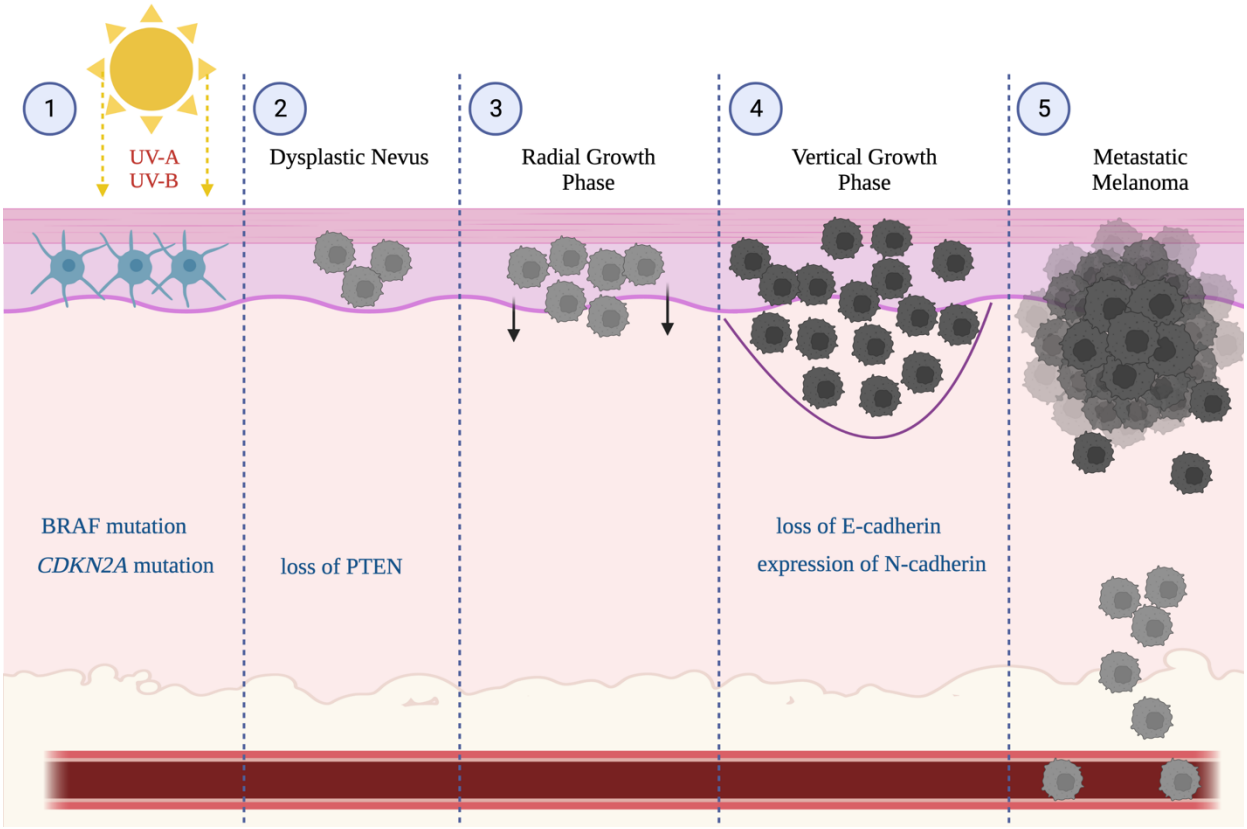

Figure 2: Melanoma formation in the skin. Dysplastic Nevus is the first step of uncontrolled proliferation of melanocytes in a pre-existing nevus or new location resulting in a pre-malignant lesion. Here, excessive UV exposure to melanocytes in the skin or genetic alterations leads to abnormal cell growth. In the radial growth phase, melanoma proliferates horizontally in the epidermis. Further, the loss of E-cadherin as well as the expression of N-cadherin allows malignant cells to invade lower layers of the skin and further expand with metastatic potential. Finally, malignant melanocytes reach the bloodstream and spread to other areas of the body, usually first the lymph nodes, lungs, and other subcutaneous soft tissues (modified from Abbasi et al. 2004).

1.5. Melanogenesis in melanocytes and melanoma

Melanocytes, as well as the malignant form, are melanin-producing cells that act to protect the skin from excessive exposure to UV. Melanin is crucial in the regulation of epidermal homeostasis and melanoma behavior (Slominski et al. 2004; Brożyna et al. 2013). Hereby, tyrosinase is the key enzyme in which L-tyrosine is converted into brown/black eumelanin and red pheomelanin. The entire process of melanin production is called melanogenesis and consists of the interaction between melanocytes and an associated pool of keratinocytes (Figure 3) (Hearing 1999). Here, UV exposure causes *TP53* transcription in keratinocytes and further leads to the translation of proopiomelanocortin (POMC) (Gilchrest et al. 1996). POMC is cleaved to multiple peptide hormones, including alpha-melanocytes stimulating hormone (α-MSH), which can bind to its receptor, melanocortin 1 receptor (Mc1r), on melanocytes as well as melanoma cells (Suzuki et al. 1996). Receptor binding activates cyclic adenosine monophosphate (cAMP) and further promotes the downstream PKA-CREB signaling pathway. CREB, in turn, activates the transcription of the microphthalmia-associated transcription factor (*MITF*), the master transcription factor of pigment genes. MITF further boosts the transcription of genes involved in melanogenesis, like tyrosinase (*TYR*), tyrosinase-related protein (*TYRP1*), dopachrome tautomerase (*DCT),* and premelanosome protein (*PMEL*) (Lei et al. 2002; Videira, Moura, and Magina 2013). *Via* enzymatic reactions, L-tyrosine is converted into either eumelanin or pheomelanin to form melanin-containing vesicles, called melanosomes. Matured melanosomes are transferred from melanocytes to keratinocytes and accumulate around the nucleus where they protect against UV light (Hida et al. 2020).

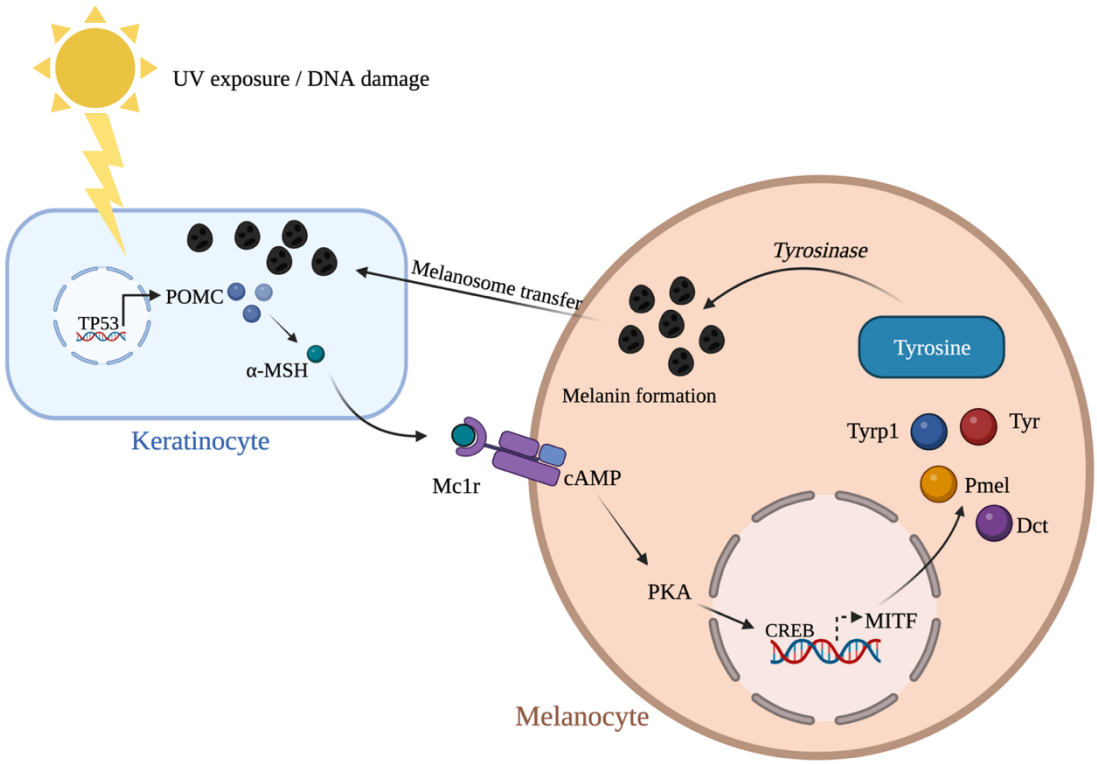

Figure 3: Melanogenesis signaling pathway. Upon UV exposure, epidermal keratinocytes activate TP53 transcription and downstream POMC. POMC is cleaved into α-MSH and secreted by keratinocytes, which in turn bind to its receptor, Mc1r, on melanocytes. The binding activates the cAMP-PKA-CREB signaling pathway and promotes the transcription of the master transcription factor MITF. MITF promotes the expression of pigment genes including *Dct, Pmel, Tyrp1*, and *Tyr*. Tyrosinase then catalyzes the conversion of L-Tyrosine into L-DOPA and further to eumelanin and pheomelanin. Matured melanosomes are transferred from melanocytes to keratinocytes and accumulate to prevent the cells from further UV damage (modified from Hida et al. 2020).

1.6. Hallmark of Cancer - Tumor metabolism

Cancer in general comprises a variety of heterogenic features that favor abnormal growth and thus complicate therapeutic strategies. The mutated cells show defects in regulatory circuits that manage normal cell proliferation and homeostasis. The conversion of normal cells into malignant cancer is a multistep process, which reflects genetic alterations that promote progressive transformation. These mutations produce oncogenes with a dominant gain of function, whereas tumor suppressor genes lose their function (Gutschner and Diederichs 2012). In 2000, Hanahan and Weinberg proposed six hallmarks of cancer that all together form the fundamental principle of malignant transformation. The six

essential alterations in cell physiology that prescript malignant growth have been determined as: sustaining proliferative signaling, evading growth suppressors, activating invasion and metastasis, enabling replicative immortality, inducing angiogenesis, and resisting cell death. Self-sufficiency in growth signals supports the tumor progression equally with the insensitivity to anti-growth signals. The fact of limitless replication potentially supports tissue invasion and metastasis. The induction of angiogenesis guarantees the access of the tumor to all nutrients and energy sources. Finally, the resistance to cell death represents the most unfavorable fact of tumor formation. All these factors lead to the development of a complex tumor microenvironment (Hanahan and Weinberg 2000).

In 2011, Hanahan and Weinberg extended four more specifications to their model of cancer characterization, including genome instability, avoiding immune destruction with simultaneous tumor-promoting inflammation, and deregulation of cellular energetics (Hanahan and Weinberg 2011). Investigation on tumor metabolism is one of the oldest fields in cancer research, which is based on the principle that metabolic activities are enhanced in cancer cells compared to normal cells supporting cell survival and proliferation (De Berardinis and Chandel 2016). For instance, activation of oncogenes and loss of tumor suppressors promotes metabolic reprogramming in cancer, resulting in enhanced nutrient uptake and energy production. The altered metabolic activity supports the anabolic growth of cancer cells during nutrient-replete conditions as well as catabolism to support cell survival during the limitation of supplements (Pavlova and Thompson 2016). Further, the reinforcement of the redox homeostasis system to counteract the metabolic effects on oncogene activation and other stress factors is crucial for cancer cell survival (Boroughs and DeBerardinis 2015). All of these factors support cell survival under stressful conditions and allow tumor growth and proliferation in a pathological way (Patra et al. 2013).

The two major processes involved in cellular energy generation are glycolysis and oxidative phosphorylation (OXPHOS). In normal cells, glycolysis can be performed during hypoxia and results in a high rate of pyruvate, which then is inserted into the tricarboxylic acid cycle (TCA) in the inner membrane of mitochondria. Here, a series of chemical reactions using carbohydrates are used to generate Acetyl-CoA which further promotes the production of fatty acids and amino acids. *Via* oxidative modifications, the cells

generate energy in the form of adenosine triphosphate (ATP) for nucleotide and lipid synthesis. However, rapidly proliferating cancer cells show enhanced glycolysis and OXPHOS activity, regardless of oxygen availability (Zheng 2012). The phenomenon was described first by Otto Warburg, who observed a constitutive uptake of glucose and the production of lactate regardless of oxygen availability (WARBURG 1956). Deregulation of cellular metabolism promotes harmful cell growth and the invasion of melanoma.

1.7. The role of the immune system in melanoma

Cutaneous cancer is an immunogenic tumor whose interaction with immune cells present in the microenvironment significantly influences cancer cell proliferation, progression, and metastasis. During melanoma formation, both immune and melanoma cells undergo immunoediting processes that include interconnected phases such as elimination, equilibrium, and escape or immune evasion (Dunn, Old, and Schreiber 2004; R. Kim, Emi, and Tanabe 2007). The balance between infiltrating immune cells and cancer cells decisively determines the patient's survival change.

1.7.1. Innate immune cell response

The tumor microenvironment (TME) is a highly heterogeneous tissue, including extracellular matrix (ECM), endothelial cells, fibroblast crisscrossed with blood vessels, and a variety of immune cells (Villanueva and Herlyn 2008). The effector cells on the innate immune system that directly target cancer cells are natural killer cells (NK) and macrophages (Mø). Furthermore, dendritic cells (DC), myeloid-derived suppressor cells (MDSCs), as well as polymorphonuclear leukocytes (PMN) with the subpopulation of neutrophils, eosinophils, and basophils are detected in the TME of melanoma (Y. Liu and Zeng 2012).

NK cells are the primary innate immune cell type responsible for killing non-MHC-related cancer cells. By releasing small cytotoxic proteins such as perforin and granzyme, NK cells initiate apoptosis in the affected cell (Yokoyama and Plougastel 2003). New therapeutic approaches targeting melanoma suggest enhanced NK cell responses, by blocking Tim-3 on their surface to improve cytotoxic ability (da Silva et al. 2014).

Furthermore, adoptive NK cell therapy could be a promising treatment strategy for metastatic melanoma in the future (van Vliet et al. 2021).

Tumor-associated macrophages (TAMs) are present in a high number in the microenvironment of melanoma. Based on their polarization, TAMs are either involved in cancer-related inflammation or tumor progression (Hussein 2006). Apoptotic tumor cells can efficiently be eliminated by Mø. By recognizing characteristic structures on tumor cells, such as lipid phosphatidylserine (PS), oxidized PS, or the multifunctional protein calreticulin (CRT), these cells become visible for Mø and subsequently get phagocytosed (Jeannin, Jaillon, and Delneste 2008). M1/activated Mø have cytotoxic, antitumor effects on cancer cells. *Via* secretion of a variety of proinflammatory cytokines, such as TNF-α, IL1-β, and IL-6, Mø promote inflammation in the tumor environment and favor tumor regression. On the other hand, M2/trophic Mø beneficially promote cancer progression, tumor proliferation, invasion, and migration (C.-Y. Liu et al. 2013). By secretion of anti-inflammatory cytokines, such as IL-4, IL-10, and TGF-β, Mø inhibit the differentiation of bone marrow cells into functional immune cells, and by this their anti-tumor activity (Baek et al. 2020). Furthermore, M2 Mø induce the activity of myeloid-derived suppressor cells that additionally inhibit the response of the immune system (Mao et al. 2013).

Myeloid-derived suppressor cells (MDSCs) are a heterogeneous population that belongs to the myeloid cell lineage. Two major subsets of MDSCs have been described: polymorphonuclear MDSCs (PMN-MDSCs) resemble phenotypically granulocytic cells, whereas M-MDSCs were defined based on their surface marker identifying them as monocytes. Both cell types were found in increased numbers and activation state in tumor tissue, resulting in a strong impairment of anti-tumor immune response (Gabrilovich 2017). They can effectively suppress NK cells as well as T cells by upregulation of immunosuppressive factors, such as arginase and nitric oxides synthase (NOS2) which further promote the release of anti-inflammatory cytokines, like TGF-β and IL-10 and thus harmfully promote tumor growth (Ostrand-Rosenberg et al. 2012; Kumar et al. 2016).

Dendritic cells are professional Antigen-Presenting Cells (APCs) which are active players that directly counteract the proliferation of melanoma cells. After recognition of tumor cells, DCs can interact *via* cognate TCR-peptide MHC complexes with $CD4^+$ and $CD8^+$ T cells to elicit cellular immunity (Manicassamy and Pulendran 2011). Similar to Mø, dendritic cells can also detect apoptotic cancer cells *via* specific translocated molecules. This

benefit is used in immunotherapies, where cancer patients have been immunized with their own DCs loaded *ex vivo* with tumor antigens (Gilboa 2007). In line with this, DC vaccination leads to an increase in tumor-infiltrating T cells, which in turn has positive effects on melanoma reduction (Bulgarelli et al. 2019).

Tumor-associated PMN, especially neutrophils, can have a great impact on tumorigenesis and metastasis formation. Many cell types within the tumor microenvironment are capable of secreting neutrophil-chemotactic substances. On the one hand, neutrophils show a significant role in the TME by their production of cytokines and chemokines, which induce inflammatory cell recruitment and activation (Granot and Jablonska 2015). However, the secretion of reactive oxygen species (ROS) and proteinases by neutrophils, was associated with a positive effect on tumor progression, angiogenesis, and metastasis formation (Gregory and Houghton 2011). In some instances, the tumor cells themselves mediate neutrophil recruitment by secreting IL-8, strongly suggesting that tumor-associated neutrophils (TANs) are not helpful in host defense and rather promote tumor angiogenesis (Tazzyman, Lewis, and Murdoch 2009).

In summary, the innate immune response can either fight or support tumor development. Thus, many attempts are currently being made to skew the innate immunity towards one with anti-tumor properties.

1.7.2. Adaptive immune response

Besides innate immune cells, the TME also contains adaptive immune cells such as B cells and T cells, including T helper 1 (Th1), T helper 2 (Th2), regulatory T cells (Treg), and cytotoxic T cells. These cells are located in the center of tumors, in the invasive margin, or in the adjacent tertiary lymphoid structures (TLS) (Galon, Fridman, and Pagès 2007). Different types of infiltrating immune cells have different effects on tumor progression, which can vary according to cancer type (Fridman et al. 2012). The tumor-associated antigens (TAAs) are the major players in the recruitment of immune cells into the TME. By presenting of TAAs on MHC II molecules, $CD4^+$ T helper cells secrete cytokines and chemokines that regulate different aspects of the immune response. $CD8^+$ T cells themselves are directly cytotoxic and can be activated both by direct presentation of antigen *via* MHC I, or $CD4^+$ T cell-mediated activation (Spurrell and Lockley 2014). On

the other hand, Th2 $CD4^+$ T cell activation acts on B cells and results in humoral immunity (Batista and Harwood 2009).

The persistence of tumors despite host immunity implies that tumor cells develop immune avoidance. Some malignant tissues can lose the expression of MHC molecules making them unable to present TAAs, thus evading T cell recognition. Other tumors create their own immune-privileged site, therefore generating a physical barrier by enhanced collagen and fibrin production (Lu, Weaver, and Werb 2012; Miskolczi et al. 2018). Another evasion strategy generated by tumors is the secretion of anti-inflammatory cytokines, such as IL-10, resulting in the expansion of $FoxP3^+$ regulatory T cells (Tregs) in the TME (Zou and Chen 2008; Salmi et al. 2021).

Providentially, research has made enormous progress in tumor control in the last decade, where tumor antigens can be targeted by monoclonal antibodies for specific recognition and elimination of tumor cells. These investigations proved to be so essential in the field of immunotherapy that the Nobel Prize 2018 in Physiology and Medicine was awarded to James P. Allison and Tasuku Honjo for their work on cancer therapy by inhibition of negative immune regulations (nobleprize.org). Successful treatments include immune checkpoint therapies such as PD-1 and CTLA-4 blockade and the inhibition of oncogenic MAPK (mitogen-activated protein kinase) signaling to increase patient survival rate. Blocking of CTLA-4 with a monoclonal antibody (Ipilimumab©) promotes anti-tumor immunity (Hodi et al. 2010). The second mechanism in anti-tumor treatment is the blockage of Programmed-Death 1 (PD-1) on T cells. Thus, blocking PD-1 *via* anti-PD-1 antibodies can be an efficient cancer therapy (Nivolumab©, Pembrolizumab©) (Davar et al. 2021; Sari and Saip 2018). However, lower efficiency and some side effects diminish the success rate. Therefore, there is an ongoing interest in targeting PD-1 in different ways, for example, targeting one of the ligands with an anti-PD-L1 antibody on tumor cells, as well as combining blockade of PD-1 and CTLA-4 on immune cells to strengthen their activity (Wolchok et al. 2013).

A completely new approach in the tumor research field is the different diet forms in our modern society. The influence of individual components, such as high-fat, high-glucose as well as high-salt is being investigated in melanoma studies.

1.8. High-salt diet as part of the Western diet

Over the last decades, the Western diet has become more and more in the focus of biological studies. Researchers showed that many immune parameters are determined by non-heritable factors such as diet. This modern dietary pattern is generally characterized by high intakes of red and processed meat, fried foods, and high-fat dairy dishes. Therefore, characteristic components of the Western diet are high fat, high glucose, and increased protein levels, but low in fiber and vitamins (Cordain et al. 2005). Additionally, westernized food products also contain a high level of sodium chloride (NaCl). According to the World Health Organization, a daily consumption of 5-6 grams of NaCl is recommended for an adult person (Holbrook et al. 1984). However, a Western diet nutrition contains between 9 and 12 grams of NaCl per day, which is twice the amount of recommended value and can have substantial effects on homeostasis and diseases (Manzel et al. 2014). Therefore, researchers started to focus on the influence of high-salt diet (HSD) on disease outcomes and the impact on the immune system.

1.9. Effects of high-salt diet on homeostasis and disease

Excessive salt consumption is associated with several changes in body homeostasis. Sodium binds water and therefore increases the volume of fluid in the body. The increase of fluid promotes higher blood pressure and further enhances the risk of hypertension and cardiovascular complications (Mente et al. 2014; Weinberger 1996). HSD has been linked to autoimmune diseases such as multiple sclerosis and inflammatory bowel disease (Kleinewietfeld et al. 2013; Kuang et al. 2023) Furthermore, an increased risk of developing rheumatoid arthritis has been found in association with excessive salt intake (Bae et al. 2021).

The kidneys are the central organ affected by HSD. High sodium levels have to excrete through the urine, but a certain amount of water still needs to be conserved in order to avoid dehydration. Consequently, the renin-angiotensin-aldosterone-system (RAAS), located in the kidneys and adrenal glands, is modulated by HSD. Angiotensin II and aldosterone, which stimulate sodium reabsorption are downregulated in individuals on HSD (Drenjančević-Perić et al. 2011; Rakova et al. 2017). Furthermore, excessive salt

consumption is associated with hormonal changes, especially stress-related responses. Plasma analysis revealed a significant increase in noradrenaline and cortisol during high-salt intake (de la Sierra et al. 1996; A. X. Chen et al. 2020). Consistent with that, urinary sodium concentration as well as cortisol and its metabolites were increased in patients on HSD. Moreover, the researchers showed a correlation between high sodium intake and insulin resistance, suggesting an additive mechanism in obesity-related metabolic disorders (Baudrand et al. 2014). Besides stress hormones, it has been recently demonstrated that HSD leads to plasma glucocorticoid increase in humans and mice (Kitada et al. 2017; Rakova et al. 2017). Glucocorticoids belong to the class of corticosteroids produced by the adrenal glands and regulate physiological processes, mainly anti-inflammatory responses (Sapolsky, Romero, and Munck 2000). They stimulate the maturation of the Na^+/K^+ pump and support the development of the neonate's renal system by increasing glomerular filtration. On the other hand, glucocorticoids carry anti-inflammatory functions for instance reducing the number of thymocytes and peripheral T cell under homeostatic conditions, and preventing autoimmunity (Pazirandeh et al. 2002).

In contrast, it was shown that excessive salt leads to sodium accumulation in the skin which is believed to have pro-inflammatory effects (Jantsch et al. 2015). Further investigations showed that an hypertonic environment stimulates the p38/MAPK pathway, leading to increased gene expression of the Nuclear factor of activated T-cells (Nfat5), also known as Tonicity-Responsive Enhancer Binding Protein (TonEBP) (Kino et al. 2009). Nfat5 can also increase the transcription of proinflammatory modulators, like TNF-α, IL1-β, IL-6, and the serum-glucocorticoid kinase 1 (Sgk1) (Cheung and Ko 2013; Neuhofer 2010). Sgk1 is regulated by extracellular tonicity and plays an important role in cellular osmotic stress response (S. Chen et al. 2009). Due to the activation by glucocorticoids, Sgk1 enhances several ion channels, like the Na^+ channel on epithelial cells (ENaC), K^+ channels in the renal outer medulla (ROMK1), or Ca^{2+} channels in renal epithelial cells, to rebalance cell´s osmolarity (Loffing et al. 2001; Welling and Ho 2009; Xu et al. 2005). Furthermore, the infiltration of sodium depolarizes the cells and allows cellular uptake of Cl^- by simultaneous removal of Ca^{2+} (MacGregor, Cappuccio, and Markandu 1987; Kirchner 1992).

In summary, excessive salt intake negatively affects physiological processes in the body. In addition, immunological changes due to high-salt diet have been observed.

1.10. Impact of excessive sodium on the immune system

Diet has long been postulated as a potential environmental risk factor for developed countries. A common dietary factor, which is associated with the Western diet and increased consumption of “fast food” is salt (Appel 2008). The excess intake of sodium chloride modulates the innate and adaptive immune system. Hypertonicity results in an increase of Th1 and Th17 cell polarization and proliferation, as well as a significant rise of IL-2 production (Kleinewietfeld et al. 2013). Th17 differentiation is closely related to the development of multiple sclerosis. *In vivo* studies could show that administration of HSD induces Th17 proliferation and worsens experimental autoimmune encephalomyelitis outcome (EAE = animal model of multiple sclerosis). Recent publications reveal that HSD increases local sodium accumulation in POMC neurons, located in the hypothalamus, and represents key regulators of metabolic homeostasis. The excessive salt leads to channel activation, specifically the transient receptor potential vanilloid 1 (TRPV1), and further enhances the production of adrenocorticotropic hormone (ACTH) (Zhang et al. 2022). Furthermore, negative impacts of HSD were found in the gastrointestinal tract of mice, where sodium exacerbates colitis by decreasing *Lactobacillus* (Aguiar et al. 2018). In addition, an increasing number of *Bifidobacterium* causes gut leakage and affects the development and function of NK cells (Miranda et al. 2018; Zeng et al. 2020). Consequences of excessive salt intake could also be observed in the kidneys. HSD worsens pyelonephritis outcome by impairing neutrophil functionality (Jobin et al. 2020).
Negative effects of HSD were also described in the skin. Here, high salt intake lowers ECM remodeling and therefore impairs dermal tissue remodeling in mice (Pajtók et al. 2021). In line with this, wound healing of the skin was delayed under HSD, which was associated with decreased M2 macrophages activation at the wound site (Binger et al. 2015). On the other hand, sodium accumulation in the skin favors a pro-inflammatory environment and strengthens the antimicrobial barrier function to protect the body against *Leishmania* infections (Jantsch et al. 2015).

In summary, high-salt diet on long-term aggravation can have both, beneficial and deleterious effects on body homeostasis and the immune system (Figure 4).

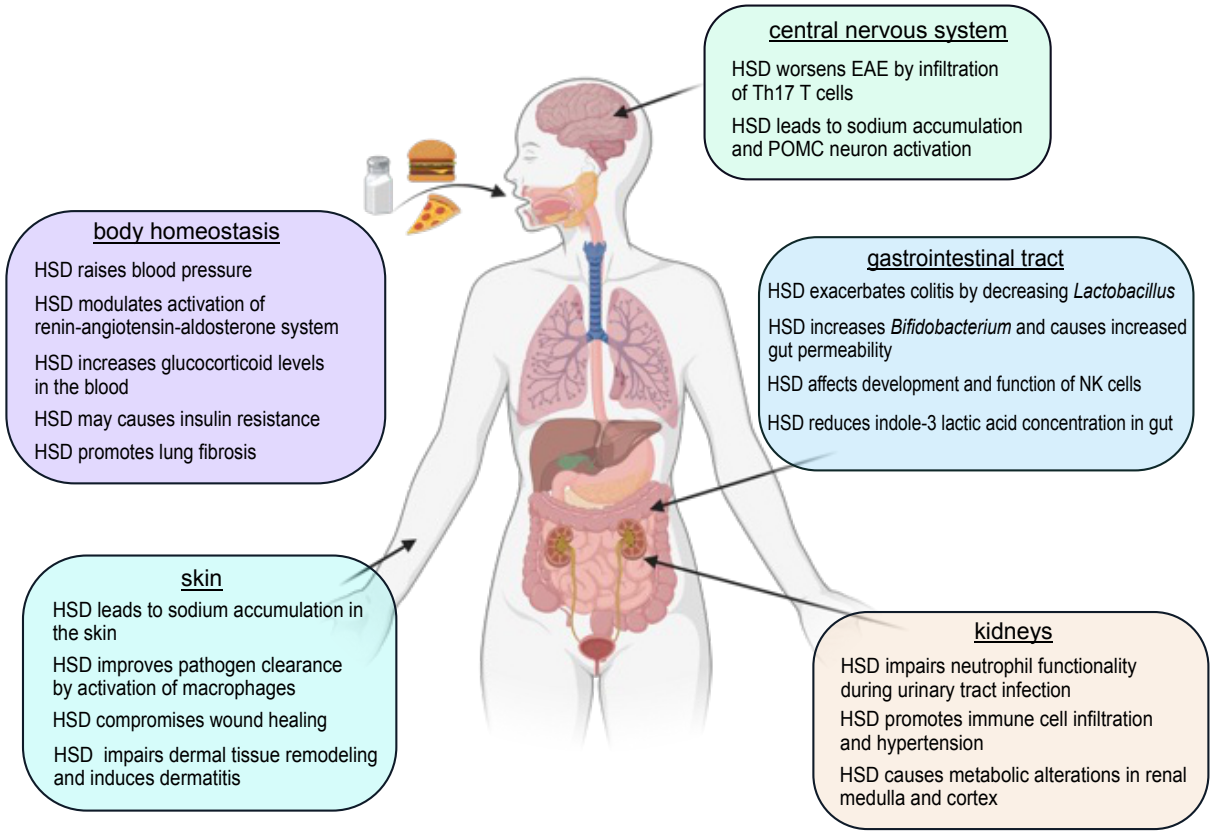

Figure 4: HSD-related changes in body homeostasis and diseases. Various organs are modified caused by high-salt diet. The central nervous system showed increased immune cell infiltration leading to EAE progression. The gastrointestinal tract undergoes physiological and immunological differences. In addition to that, HSD negatively affects kidney homeostasis and worsens bacterial infections by impairing the immune system. Sodium accumulation in the skin promotes macrophage activation and improves anti-microbial activity (modified from Wilck et al. 2019).

1.11. Aim of the project

The main goal of this thesis was to investigate the influence of high-salt diet on cutaneous cancer growth, in order to identify cellular and molecular mechanisms for new potential therapeutic strategies.

First, the role of the immune system during melanoma growth under high-salt diet was examined. Therefore, the characterization of immune cells in the tumor microenvironment and the draining lymph nodes was performed for a better understanding of how an enriched sodium environment may change the immune cell compartment. Furthermore, blood kinetics should provide information on how high-salt diet changes the circulating lymphocytes.

Secondly, the effect of high-salt diet on tumor cells was examined in detail. Here, possible effects of osmo-protective mediators, which can be upregulated by HSD in melanoma were investigated. Further cell-intrinsic changes in tumor cells were explored to better understand how high-salt diet can affect melanoma growth and whether they could be useful for possible therapeutic approaches.

2 Material and Methods

2.1. Material

2.1.1 Technical equipment

Table 1: Technical Equipment

Equipment	Manufacturer
Autoclave	Belimed, Cologne, Germany
	Bergisch Gladbach, Germany
Bright field scanner	Leica Biosystems, Nussloch, Germany
Caliber	Fine Science Tools,
	Heidelberg, Germany
Centrifuge (5430R)	Eppendorf AG, Hamburg, Germany
Centrifuge (5810R)	Eppendorf AG, Hamburg, Germany
Centrifuge (Biofuge pico)	Heraeus, Hanau, Germany
Clean Bench HeraSafe	Heraeus, Hanau, Germany
Dissecting set	FST Dumont Biology,
	Dumont, Switzerland
Electronic balance	Sartorius Lab Instruments,
	Goettingen, Germany
Electronic precision balance	Sartorius Lab Instruments,
	Goettingen, Germany
Flow Cytometers Canto II, LSRFortessa	Becton, Dickinson and Co.,
	Franklin Lakes, NJ, USA
Freezer (-20°C)	Liebherr, Biberach a.d. Riß, Germany
Freezer (-80°C)	Heraeus, Hanau, Germany
Fume Hood	Wesemann, Syke, Germany
Heating block ThermoMixer	Eppendorf AG, Hamburg, Germany
	Hohenpleißbenberg, Germany
Homogenizer Fast Prep 24	MP Biomedicals Germany
Ice machine	Frimont Bettlonic, Pogliano, Italy
Incubator HeraCell 240	Heraeus, Hanau, Germany

IVIS Lumina LT Series III	Caliper Life Science, Massachusetts, USA
Light Cycler 480 machine	Roche, Frankfurt a.M., Germany
MACS® cell separator	Miltenyi Biotec, Bergisch Gladbach, Germany
Mice cages	Techniplast, Hohenpeißenberg, Germany
Micro centrifuge	Biozym, Hessisch Oldendorf, Germany
Micropipettes	Eppendorf AG, Hamburg, Germany
Microplates absorbance reader	Tecan group, Männedrof, Switzerland
Microscope (IX71)	Olympus, Hamburg, Germany
Microscope Leica DMIL	Leica Mircosystems, Wetzlar, Germany
Multichannel pipette	Eppendorf AG, Hamburg, Germany
NanoDrop Spectrophotometer	Thermo Fisher Scientific, Waltham, USA
Neubauer chamber	Labomedic, Bonn, Germany
PCR Mastercycler	Eppendorf AG, Hamburg, Germany
Photometer	Thermo Fisher Scientific, Waltham, USA
Pipetboy acu 2	Integra Bioscience, Biebertal, Germany
Refrigerators (+4°C)	Liebherr, Bieberach a.d. Riß, Germany
Scalpel	Fine Science Tools, Heidelberg, Germany
Scissors	Fine Science Tools, Heidelberg, Germany
Sterile workbench	Scanlaf Mars, Wertheim, Germany
Thermomixer MaxQ	Thermo Fisher Scientific, Waltham, US
Vaccum pump	Vacuubrand, Wertheim, Germany
Vortex	VWR, Pennsylvania, USA
Water bath	Memmert, Schwabach, Germany
WES™ Western blot machine	Protein simple Biotechne, California, USA

2.1.2. KITs

Table 2: KITS

KITs	Manufacturer
α-MSH ELISA	Abbexa Ltd, Cambridge, UK
BCA KIT for protein detection	Thermo Fisher Scientific, Waltham, USA
cDNA reverse transcriptase	Thermo Fisher Scientific, Waltham, USA
FoxP3 Fixation/Permeabilization KIT	Thermo Fisher Scientific, Waltham, USA
GoTaq qPCR Master Mix	Promega, Mannheim, Germany
Permeabilization KIT	BD, New Jersey, USA
RNA NucleoSpin isolation KIT	Macherey Nagel, Düren, Germany
SYBR Green PCR MasterMix	Thermo Fisher Scientific, Waltham, USA
WES™ α-rabbit detection KIT	Protein simple Biotechne, California, USA
WES™ E2 Standard pack 12-230 kDa	Protein simple Biotechne, California, USA
WES™ Standard pack 60-300 kDa	Protein simple Biotechne, California, USA

2.1.3. Cell lines

Table 3: Cell lines

Cell lines	Manufacturer
B16-OVA $Gr^{-/-}$ melanoma cell line	AG Kurts / AG Hölzel
B16-OVA luciferase melanoma cell line	AG Kurts / AG Hölzel
B16-OVA melanoma cell line	AG Kurts / AG Hölzel
B16-OVA $Nfat5^{-/-}$ melanoma cell line	AG Kurts / AG Hölzel
B16-OVA Nfat5 mNeon melanoma cell line	AG Kurts / AG Hölzel
B16-OVA $Sgk1^{-/-}$ melanoma cell line	AG Kurts / AG Hölzel
B16-OVA Sgk1 mNeon melanoma cell line	AG Kurts / AG Hölzel
B16 TyrKO melanoma cell line	AG Kurts / AG Hölzel
CCL79 adrenal gland cancer cell line	AG Kurts / J. Yin

2.1.4. Consumables

Table 4: Consumables

Consumables	Manufacturer
12-well plate	VWR, Pennsylvania, USA
150 cm^2 cell culture flask	Biozym Scientific, Oldendorf, Germany
384-well PCR plate	Roche, Frankfurt a.M., Germany
96-well plate, flat bottom	VWR, Pennsylvania, USA
96-well plate, round bottom	VWR, Pennsylvania, USA
Compensation beads	Thermo Fisher Scientific, Waltham, USA
Counting beads	BD Biosciences, Heidelberg, Germany
Cryo conservation tubes (2 ml)	Thermo Fisher Scientific, Waltham, USA
FACS tubes	Sarstedt AG + Co., Nümbrecht, Germany
Falcon tubes (5 ml, 15 ml, 50 ml)	Greiner, Kremsmünster, Austria
Filter (30 µm, 100 µm)	Labomedic, Bonn, Germany
Filter tips (10 µl, 200 µl, 1000 µl)	Nerbe-plus, Winsen, Germany
Injection needles (0.45x12 mm)	Labomedic, Bonn, Germany
MACS® LS-columns for cell isolation	Miltenyi Biotec, Bergisch Gladbach, Germany
MACS® Tumor-isolation beads	Miltenyi Biotec, Bergisch Gladbach, Germany
Micro tubes (0.5 ml 1.5 ml, 2 ml)	Sarstedt AG + Co., Nümbrecht, Germany
Micro-Hematocrit-Capillary	Brand, Berlin, Germany
Microscope cover glasses	Paul Marienfeld GmbH & Co. KG, Königshofen, Germany
Microscope slides	Paul Marienfeld GmbH & Co. KG, Königshofen, Germany
Multichannel pipette (10 µl, 300 µl)	Eppendorf AG, Hamburg, Germany
Neubauer chamber	Labomedic, Bonn, Germany
Parafilm M	Sigma Aldrich, Missouri, USA
PCR micro seal stripe	Biozym Scientific, Oldendorf, Germany
PCR rubes, 8-stripes	Biozym Scientific, Oldendorf, Germany
Pipetboy acu 2	Integra Bioscience, Biebertal, Germany

Seahorse® 96-well plate	Agilent Technologies, Santa Clara, USA
Serological pipet (5 ml, 10 ml, 25 ml)	Sarstedt AG + Co., Nümbrecht, Germany
Syringe (1 ml, 2 ml)	Labomedic, Bonn, Germany
	Waldbronn, Germany
Weighing pans	Brand GmbH & Co. KG,
	Wertheim, Germany
Wes™ capillary 25	Protein simple Biotechne,
	California, USA

2.1.5. Media and buffers

Table 5: Media and buffers

Media and Buffers	Manufacturer
Aqua Bidest	Kurts lab material
Digestion media	100 mg/ml DNAse I + 10 mg/ml
	Collagenase IV in media
FACS buffer	0.1 % BSA + 0.1 % NaN_3 in PBS
RIPA lysis buffer	Thermo Fisher Scientific, Waltham, USA
RPMI 1640 + GlutaMax™ media	Thermo Fisher Scientific, Waltham, USA
Sterile Phosphate buffered saline (PBS)	Life Technologies, California, USA
Solution A for mitochondria isolation	20 mM HEPES/KOH (pH 7.6) + 220 mM
	D-Mannitol + 70mM sucrose + 1 mM
	EDTA + 0.5 mM PMSF in PBS
Solution B for mitochondria isolation	Solution A + 2 mg/ml BSA

2.1.6. Chemicals and reagents

Table 6: Chemicals and reagents

Chemicals and Reagents	Manufacturer
2-NBDG	AAT Bioquest, California, USA
BODIPY™ FL C16	Thermo Fisher Scientific, Waltham, USA
Bovine serum albumin (BSA)	PAN-Biotech, Aidenbach, Germany
Collagenase IV (100 mg/ml)	Sigma Aldrich, Missouri, USA
Crystal-Violet	Thermo Fisher, Waltham, USA
D-Mannitol	Sigma Aldrich, Missouri, USA
Deoxyribonuclease I (10 mg/ml)	Sigma Aldrich, Missouri, USA
Dimethylsulfoxid (DMSO)	Carl Roth, Karlsruhe, Germany
Fetal calf serum (FCS)	Kurts lab material
G418 Geneticin antibiotics	Thermo Fisher, Waltham, USA
Glucose	AppliChem, Darmstadt, Germany
HEPES/KOH	Sigma Aldrich, Missouri, USA
High-salt diet food (4 % NaCl)	ssnift Spezialdiät GmbH, Soest, Germany
Indole-3-lactic-acid	Sigma Aldrich, Missouri, USA
Luciferin	Thermo Fisher, Waltham, USA
Natrium acid (NaN_3)	Sigma Aldrich, Missouri, USA
Natrium chloride (NaCl)	AppliChem GmbH, Darmstadt, Germany
Natriumdodecylsulfat (SDS)	Sigma Aldrich, Missouri, USA
Penicillin/Streptavidin antibiotic mix	Sigma Aldrich, Missouri, USA
Phenylmethansulfonylfluorid (PMSF)	Sigma Aldrich, Missouri, USA
Phorbol 12-myristate 13-acetate (PMA)	Sigma Aldrich, Missouri, USA
Protease inhibitor tablets	Thermo Fisher, Waltham, USA
RCB Lysis Buffer	Lonza, Walersville MD, USA
Sodium acid (NaN_3)	Thermo Fisher, Waltham, USA
Sucrose	Sigma Aldrich, Missouri, USA
Trypan blue solution	Sigma Aldrich, Missouri, USA
Trypsin EDTA	Thermo Fisher, Waltham, USA

2.1.7. Software

Table 7: Software

Software	Manufacturer
Affinity Designer	Serif, Nottingham, United Kingdom
BioRender	BioRender, Toronto, ON, Canada
Compass for Simple Western™	Protein simple Biotechne, California, USA
FACS Diva V8.0.1	BD Biosciences, Heidelberg, Germany
Fiji ImageJ	National Institute of Health, Bethesda, USA
FlowJo V10	Tree star Inc, USA
GraphPad Prism9	GraphPad Software, La Jolla, USA
MagellanTM6	Tecan Trading AG, Männedorf, Switzerland
Microsoft Excel 2019	Microsoft, Redmond, USA
Microsoft Word 2019	Microsoft, Redmond, USA
Nanodrop 2000/2000c	Thermo Fisher Scientific, Waltham, USA
Wheel Manager	Caliper Life Science, Massachusetts, USA

2.1.8. Websites

Table 8: Websites

Subject	Website
Gorilla Gene Ontology	https://cbl-gorilla.cs.technion.ac.il
NCBI Nucleotides	https://www.ncbi.nlm.nih.gov/nucleotide/
Primer3Plus	https://www.bioinformatics.nl/cgi-bin/primer3plus/primer3plus.cgi
Primer Blast	www.ncbi.nlm.nih.gov/tools/primer-blast/
Proteome Discoverer	https://thermofisher.commass-spectrometry/
SequenceHT node	https://www.ibm.com/docs/en/integration-bus

2.1.9. Antibodies for flow cytometry analysis

Table 9: Antibodies for flow cytometry analysis

Antibody	Clone	Conjugate	Isotype	Company
CD45	30-F11	BV421	mIgG2a	BioLegend, San Diego, USA
CD4	GK1.5	BV421	rIgG2b	BioLegend, San Diego, USA
CD8α	53-6.7	BV510	rIgG2b	BioLegend, San Diego, USA
CD3e	17A2	PECy7	rIgG2b	Thermo Fisher Scientific, USA
TCRβ	H57-597	APC/BV421	hmIgG	BioLegend, San Diego, USA
CD11c	HL3	APC/BV421	rIgG2b	BioLegend, San Diego, USA
CD11b	M1/70	APC	rIgG2b	BioLegend, San Diego, USA
F4/80	BM8	PE	rIgG2a	BioLegend, San Diego, USA
MHCII	M5/114	FITC	rIgG2b	BioLegend, San Diego, USA
Ly6G	1A8	APC/FITC	rIgG2a	BioLegend, San Diego, USA
Ly6C	HK1.4	PerCP-Cy5.5	rIgG2c	BioLegend, San Diego, USA
GR1	RB6-8C	PE-Cy7	rIgG2b	BioLegend, San Diego, USA
NK1.1	PK136	APC	mIgG2a	BioLegend, San Diego, USA
CD25	PC61.5	APC/PE	rIgG1	BioLegend, San Diego, USA
FoxP3	F-JK-116s	FITC	rIgG2a	Thermo Fisher Scientific, USA
mTOR	MRRBY	PE/BV421	rIgG	Thermo Fisher Scientific, USA
pmTOR	MRBBY	PECy7	rIgGκ	Thermo Fisher Scientific, USA
Fixable Viability Dye		eF780		Thermo Fisher Scientific, USA
AnnexinV		FITC		Miltenyi Biotec, Germany
$\gamma\delta$TCR	GL-3	FITC/BV510	mIgG1	BioLegend, San Diego, USA
IL-17A	TC11-18H	APC	rIgG1	Creative Biolabs, Shirley, USA
IFNγ	XMG1.2	PE	rIgG1	BioLegend, San Diego, USA
RORγT	Q31-378	PE/APC	mIgG2a	Thermo Fisher Scientific, USA
Tim-3	RMT3-23	APC	rIgG2a	Thermo Fisher Scientific, USA
CD44	IM7	FITC	rIgG2b	BioLegend, San Diego, USA
PD-1	29F.1A12	BV421	rIgG2aκ	BioLegend, San Diego, USA

2.1.10. Antibodies for Western blot analysis

Table 10: Antibodies for Western blot analysis

Antibody	Class	Host	Isotype/	Company
β-Actin	polyclonal	rabbit	IgG	Cell Signaling Technology, NL
Mc1r	polyclonal	rabbit	IgG	Thermo Fisher Scientific, USA
mTOR	polyclonal	rabbit	IgG	Thermo Fisher Scientific, USA
p-mTOR$^{Ser-288}$	polyclonal	rabbit	IgG	Thermo Fisher Scientific, USA
Hif-1α	polyclonal	mouse	IgG1	Novus Biologicals, USA
Mitf	polyclonal	rabbit	IgG	Cell Signaling Technology, NL

2.1.11. Primer sequences for gene expression analysis

Table 11: Primer sequences

Name	Forward 5´-3´	Reverse 5´-3´
Actb	CTAAGGCCAACCGTGAAAAG	ACCAGAGGCATACAGGGACA
Acta	CTCTCTTCCAGCCATCTTTCAT	TATAGGTGGTTTCGTGGATGC
Aldoa	GGAGGAGTACATCAAGCGC	TGGGAAAGAGCCTGAAGACC
Eno1	CCCCTGGCCAAATAAAGCAT	GCTGGGATGACATCAGGGAT
Hif1α	CATGATGGCTCCCTTTTTCA	GTCACCTGGTTGCTGCAATAA
Hk1	CTTCGACAAAGTGGTGGACG	TTACGGACGATCTCACCCAG
Hk2	CCCTGTGAAGATGTTGCCCAC	TGCCCATGTACTCAAGGAAGT
Ldha	ATGAAGGACTTGGCGGATGA	CGCCCTTGAGTTTGTCTTCC
Ldhb	GCGTTGGACAAGTGGGTATG	CACCAGGGCAAGTTCATCAG
Mc1r	TCATCGTCCTCTGCCCTCAG	GCAGCACCTCCCTTGAGTGTC
Mmp2	CTGGTGCTCCACCACATACA	GGCCATGGGTTGGATCTT
Mmp3	TGCAGCTCTACTTTGTTCTTTGA	AGAGATTTGCGCCAAAAAGTG
mt-Atp6	AAATATTAGCCCACCAACAG	CTAGGAGGGTGAATACGTAG
mt-Atp8	AGTCTCATCACAAACATTCCC	GTTAGTGATTTTGGTGAAGGTG
mt-Co1	CCTTTGCTTCAAAACGAGAA	ATAGGTTGGTTCCTCGAATG
mt-Co2	CAAGCAACAGTAACATCAAACC	GTGGAACCATTTCTAGGACAA
mt-Co3	TGTTTGCCTACTACGACAAC	GGAAAAGTCAGACTACGTCTAC
mt-Cytb	GTACTGAATCCTAGTAGCCAA	AGTATGAGATGGAGGCTAGT

mt-Nd1	CGCCCTAACAACTATTATCTTCC	GAAGCGTGGATAAGATGCTC
mt-Nd2	GGCCTTCCACCACTAACAGG	AGGGTGGAAAATATTAGGTTGGGT
mt-Nd3	ACAAGCTCTGCACGTCTACC	GCTCATGGTAGTGGAAGTAGAAGAG
mt-Nd4	TTAACCTCCAACCCTCACAC	AGGCCTGTAATTAGTTTTGGAC
mt-Nd4L	CCATACCAATCCCCATCACC	CGTAATCTGTTCCGTACGTGTT
mt-Nd5	ACCCATAAAATCTCTCAACC	GTGGTTATGTTTGTGTGAAG
mt-Nd6	AAAACGATCCACCAAACCCT	GGTTAGCATTAAAGCCTTCACC
Mtor	TTGAGGTTGCTATGACCAGAGAGA	TTACCAGAAAGGACACCAGCCAATG
Nfat5	GTGTTTAGCTCTTCAGCCAATCT	CTGCATGGACAGCTTGAGATA
Nr3c1	GGTGGGTTTTGTTTTGTAATTTTTT	AATTTCTTTAATTTCTCTTCTCCCTAA
Pdha	TACGGACCACCTCATCACTG	CAACCTCCTCTTCGTCCTGT
Pdhb	CAGCTAGTAGAGGACACGGG	TGAAAACGCCTCTTCAGCAG
Pfkl	GGGTCATGTACAGCGAGGA	GGGTCATGTACAGCGAGGA
Pfkp	CAAGAGAGATCTCCTGTTTCAACC	CTTGGGGATCCTGTGCTC
Pgk1	AAGACTGGCCAAGCTACTGT	AATCTGCTTAGCTCGACCCA
Pgm2	GTCCTAGCCAATGACCCAGA	CACTCTCCACTCACCACTGT
Slc2a1	GCTGTGCTTATGGGCTTCTC	CACATACATGGGCACAAAGC
Slc2a3	TAAACCAGCTGGGCATCGTTGTTG	AATGATGGTTAAGCCAAGGAGCCC
Slc3a2	TGATGAATGCACCCTTGTACTTG	TCCCCAGTGAAAGTGGA
Slc7a5	TCCCCAGTGAAAGTGGA	CTTGTCCCATGTCCTTCCCC
Slc27a1	GACAAGCTGGATCAGGCAAG	GAGGCCACAGAGGCTGTTC
Slc27a2	GCGTGCCTCAACTACAACATT	CCTCCTCCACAGCTTCTTGT
Slc27a3	GAGAACTTGCCACCGTATGC	GGTCTCACGTAGTGGCCAAAGA
Slc27a4	CTATGACTGCCTCCCCCCTCT	CATGCCGTGGAGTAAGCAC
Slc27a5	GCCTTCGAGCTACGATTAAGTG	GATAAGATGGCTGGCTTTGG
Slc27a6	CAACACCTGTGAACCCACTG	TCTTCTATGCTTCCAAGCAAATCT
Sdha	CAGTTCCACCCCACAGGTA	TCTCCACGACACCCTTCTG
Sdhb	ACTGGTGGAACGGAGACAAG	CCTCTGAAGTCGTCTCTGG
Sdhc	TGCGCTCTTGCTGAGACAT	GTGGTTCCCAAAGGAGCAG
Sdhd	CCTGCTCTGTGGTGGACTACT	CCCATGAACGTAGTCGGTAAC
Tyr	AAGAATGCTGCCCACCATGG	CACGGTCATCCACCCCTTTG
Tyrp1	CAGTGCAGCGTCTTCCTGAG	TTCCCGTGGGAGCACTGTAA

2.1.12. Mouse strains

All mice were bred and maintained on a C57BL/6J background under specific pathogen-free (SPF) conditions and in accordance with institutional animal guidelines at the animal facility of the University Hospital Bonn (House of Experimental Therapy, HET). For the experimental setup, female mice between 7-10 weeks were used and housed in individually ventilated cages. Mice were not randomized in cages, but each cage was randomly assigned to a specific treatment group. All animal studies were approved by the governmental committees (Landesamt für Natur, Umwelt und Verbraucherschutz, NRW) with the license: 84-02. 04. 2015. A530.

2.1.13. Illustrations

Introduction figures and schematic drawings of experimental setups were created with BioRender.com. The result figures were compiled with Affinity Designer.

2.2. Methods

2.2.1. Melanoma culturing and harvesting for *in vivo* experiments

Melanoma cells can be isolated directly from patient-derived samples or, in this case, using modified B16 mouse melanoma cell lines. Here, Ovalbumin-expressing melanoma cells (B16-OVA) were used in order to facilitate strong immune responses to tumor antigens. The cells were kindly provided by the group of Prof. Dr. Hölzel, University Clinics Bonn. Melanoma cells were cultured in complete media (RPMI 1640 GlutaMAX^{TM}, pH 7.6) + 10 % fetal calf serum (FCS) and 1 % Penicillin and Streptavidin (P/S) antibiotic mix. Geneticin antibiotic (G418 0.4 mg/ml) as a selection marker was added to the cells, so that only the OVA-expressing cells can grow (Wagman et al. 1974). Melanoma cells were grown adherent under controlled humid conditions (37°C and 5 % CO_2) and the culturing of the cells started one week prior to *in vivo* application. During that time, cells were collected and split (1:5) every second day and fresh media was added. On experimental day, media was aspirated and cells were washed with 10 ml PBS. After aspiration, 5 ml

of trypsin EDTA was added and incubated under controlled humidity conditions for 5 to 10 minutes until the cells detached. The cell suspension was transferred into a 50 ml tube and washed with 30 ml PBS. After centrifugation for 5 min at 1200 rpm and 4°C, the pellet was resuspended in 1 ml PBS. Living cells were counted using trypan blue staining and a Neubauer chamber. Subsequently, cell concentration was adjusted with PBS to the final concentration of 0.5 x 10^6 cells/100 µl and kept on ice until injection.

2.2.2. *In vivo* mouse model for skin melanoma growth

Female C57BL/6J wild-type mice between 7 and 10 weeks of age were used. Seven days before tumor injection (d-7) mice were grouped into different diet conditions: mice on normal-salt diet (NSD) were fed with normal mice chow, containing 0.3 % NaCl and received autoclaved tap water (control group). Mice under high-salt diet (HSD) were fed with 4 % NaCl-rich chow and additionally were given 0.9 % NaCl water *ad libitum*. On day 0 of experiment initiation, mice were shaved using an electric shaver and 0.5 x 10^6 B16-OVA melanoma cells in 100 µl PBS were injected *subcutaneously* into each mouse. On day 14 after tumor implantation, mice were euthanized with CO_2 to harvest tumor tissue, and the whole tumor mass was weighed. For the analysis of gene expression levels, tumor tissue was immediately frozen in liquid nitrogen. The rest was stored in digestion media for further processing.

2.2.3. Monitoring of tumor growth

In order to determine how HSD affects tumor growth *in vivo*, all mice were examined daily for their general health status. Here, weight changes were recorded over the entire period of the experiment, starting from day -7 onwards. Five days after tumor implantation, the first tumors could be seen by eye. The growth was documented daily over the entire observation time. Tumor volume was determined by caliber and calculated using the formula:

$$\text{Tumor volume } (mm^3) = \text{length (mm)} \times \text{width } (mm)^2$$

2.2.4. Mouse model of lung metastasis

A similar experimental setup was used to investigate the tumor growth in the lung. To visualize the tumor growth in living mice over time, the luciferin-luciferase reaction assay was used. For this purpose, genetically-modified melanoma cells expressing the luciferase gene were provided by the group of Prof. Dr. Hölzel. After one week of different diet conditions (NSD vs. HSD), 0.5 x 10^6 B16-OVA luciferase-expressing melanoma cells in 100 µl PBS were injected *intravenously* into the tail vein of each mouse. To quantify metastasis formation, mice were anesthetized with a mixture of 3 % isoflurane/O_2 (v/v) and received 250 µl of luciferin (50 mM) *intraperitoneally*. *Via* enzymatic reaction, the tumor cells emitted a visual light signal, which could be detected by the In Vivo Imaging System (IVIS) Lumina III machine. This measurement was repeated five times during the experiment. 14 days after tumor injection, mice were anesthetized with isoflurane and sacrificed *via* cervical dislocation and the lungs were removed. The nodules of metastatic formation in the lung were counted manually. Lung tissue was collected and digested in RPMI media + 10 mg/ml DNase I + 100 mg/ml Collagenase IV for further analysis. For gene expression analysis, lung tissue was immediately frozen in liquid nitrogen.

2.2.5. Blood collection during the experimental time

To investigate the influence of HSD on possible differences in the immune cell compartment, blood samples were collected from mice under NSD vs. HSD at different time points during the experiment (d-7, d0, d7 and d14). Therefore, mice were kept under infrared light to dilate the blood vessel and put into a retainer. The tail was disinfected with 70 % ethanol and a small incision was made using a blade. 30 µl of blood was collected with heparinized capillaries and transferred into a FACS tube containing 100 µl EDTA (50 mM). After washing with 1 ml FACS buffer and centrifugation at 1200 rpm for 5 min at 4°C, red blood cells were removed by adding 1 ml of RCB lysis buffer and incubated for 10 min at RT. The reaction was stopped by adding 1 ml FACS buffer. After another centrifugation step (1200 rpm for 5 min at 4°C), cells were stained for FACS analysis.

2.2.6. Mouse model for skin melanoma growth with immune cell depletion

Myeloid-derived suppressor cells (MDSCs) were depleted by using Gemcitabine 60 mg/kg *i.p.* injection every third day starting from day -7 on. Weekly blood analysis *via* FACS confirmed sufficient depletion of MDSCs.

2.2.7. Collection of tumor tissue, blood, and tumor-draining lymph nodes

On day 14 after tumor implantation, animals were deeply anesthetized with CO_2. Once the animal stopped breathing, blood was collected from the heart and transferred into a 1.5 ml tube. 100 µl of blood was used for FACS analysis, the rest was mixed with EDTA for further experiments. The skin was cut without opening the intraperitoneal region. The tumor was separated and the connective tissue was removed. After dissection, the total tumor tissue was weighed and the tumor was divided for further analysis. Some material was frozen in liquid nitrogen for further analysis. The rest was transferred into 2 ml digestion media (RPMI media + 10 mg/ml DNase I + 100 mg/ml Collagenase IV) to isolate the melanoma cells. Furthermore, the tumor-draining lymph nodes (LNs) were collected and stored in digestion media to obtain a cell suspension.

2.2.8. *Ex vivo* tumor cell processing

After transferring the tumor tissue and lymph nodes into digestion media, the solid bulk was homogenized using a plumber of a 2 ml syringe and incubated for 20 minutes at 37°C. Afterward, cell homogenate was resuspended by pipetting the suspension “up and down” and further incubated for another 20 minutes at 37°C. Single-cell suspension was filtered with a 100 µm nylon filter into a 15 ml falcon tube. The filter was washed three times with 2 ml PBS and the tubes were centrifuged for 5 minutes at 1200 rpm at 4°C. The supernatant was aspirated and the pellet was resuspended in 1 ml media. Red cell lysis was performed as written in section 2.2.5. and the homogenate was washed and centrifugated again. Living cells were counted using trypan blue and cell concentration was calculated by using the following equation:

$$\text{Total live cell number} = \frac{\text{counted cells}}{4} \text{ x } 10^4 \text{ x dilution factor x volume (suspension)}$$

2.2.9. Tumor cell isolation *via* MACS® magnetic beads isolation

Mice were humanely sacrificed as described in section 2.2.7. and skin tumor cells were removed and digested as mentioned in section 2.2.8. To obtain isolated tumor cells from the tumor microenvironment, single-cell suspension was incubated with magnet-labeled beads from Miltenyi Biotec according to the manufacturer´s description. Here, magnet-labeled beads bound on immune cells and discarded. The unlabeled tumor cells (negative isolation) were collected and used for further experiments.

2.2.10. Mitochondria isolation from melanoma cells

For further studies on mitochondrial function, mitochondria were isolated from tumor cells as described by Priesnitz et al. (Priesnitz, Pfanner, and Becker 2020). Shortly, tumor tissue was collected from mice on HSD and NSD and mixed with solution A (20 mM HEPES/KOH (pH 7.6) + 220 mM D-Mannitol + 70mM sucrose + 1 mM EDTA + 0.5 mM PMSF in PBS) and homogenized. After centrifugation at 800 g for 5 min at 4°C, the supernatant was transferred into a new tube and again centrifugated at 10000 g for 20 min at 4°C. The supernatant was aspirated and the formed pellet was resuspended with solution B and again centrifugated for 20 min at 10000 g and 4°C. The purified mitochondria were resuspended in solution B (solution A + 2 mg/ml BSA) and the total concentration was measured via Bicinchoninic Acid KIT (BCA).

2.2.11. Measurement of mitochondrial complex activity

Isolated mitochondria were further analyzed on their complex activity by our collaborators Prof. Dr. Thomas Becker and Dr. Matthias Eckhardt, Institute of Biochemistry and Molecular Biology, University of Bonn. Here, mitochondrial complex activity was measured by using blue native polyacrylamide gel electrophoresis (BN-PAGE). *Via* using antibodies, complex II (anti-SDHA) as well as complex III (Rieske) activity could be measured.

2.2.12. Flow cytometry of *ex vivo* samples

Single-cell suspension from the tumor microenvironment and LNs was prepared for flow cytometric analysis immediately after collection as described in section 2.2.8. Samples were centrifuged at 1200 rpm for 5 minutes at 4°C and the supernatant was discarded. Tumor samples were resuspended in 1 ml FACS buffer and 100 µl transferred into a 96-well F-bottom microplate. Lymph nodes were mixed with 200 µl FACS buffer and distributed on a 96-well F-bottom microplate. Cells were centrifuged again at 1200 rpm for 5 minutes at 4°C and the supernatant was discarded. Blood samples (100 µl) were transferred into FACS tubes and lysis of erythrocytes was performed by adding 1 ml of RCB buffer to the cell suspension. Samples were incubated for 10 minutes at room temperature and the reaction stopped by adding 2 ml FACS buffer. Cells were centrifuged at 1200 rpm for 5 minutes at 4°C and the supernatant was discarded. If necessary, red cell lysis was repeated as described. Before further processing, 1 x 10^4 counting beads (APC labeled) were added to each sample. Afterwards, samples were stained for 10 minutes at 4°C in 50 µl FACS buffer supplemented with live/dead discrimination dye. The reaction was stopped by adding 100 µl FACS buffer and the cells were centrifuged at 1200 rpm for 5 minutes at 4°C. 50 µl of antibody mix for surface markers was added to the cells and incubated for 20 minutes at room temperature in the dark. After resuspending in 100 µl FACS buffer the cells were centrifuged at 1200 rpm for 5 minutes at 4°C. Different cell populations were identified with flow cytometric analysis *via* expression of surface markers shown in Figure 5. Samples were analyzed according to cell number and clusters by flow cytometry using BD FACS Canto II or BD LSR Fortessa and quantified with FlowJo 10 software.

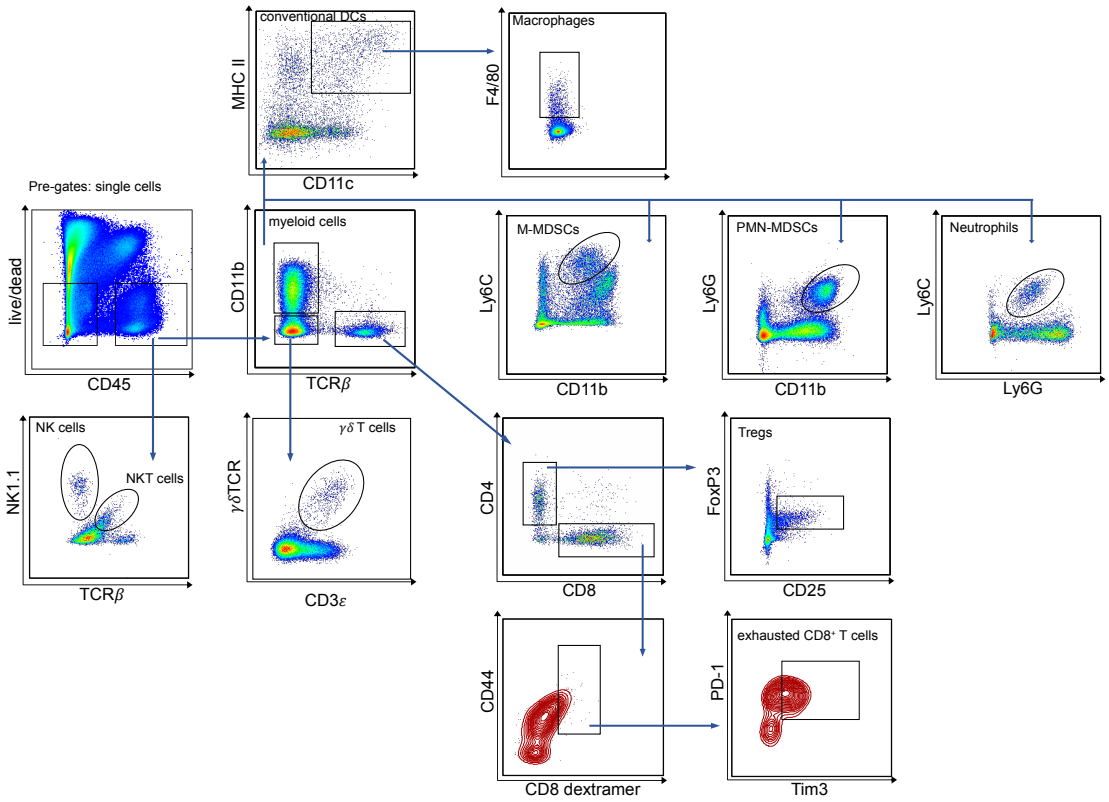

Figure 5: Gating strategy to identify immune cell population in the tumor microenvironment and draining lymph nodes. Data show flow cytometric dot plots and counterplots of tumor tissue of single cell suspension. Different immune cells were identified as:

Leukocytes	single Fixable Viability Dye$^-$ CD45$^+$ events
Myeloid cells	CD11b$^+$ TCRβ^- leukocytes
Conventional DC	CD11b$^+$ MHC II$^+$ CD11c$^+$ leukocytes
Macrophages	CD11b$^+$ MHC II$^+$ CD11c$^+$ F4/80$^+$ leukocytes
M-MDSCs	CD11b$^+$ Ly6C$^+$ leukocytes
PMN-MDSCs	CD11b$^+$ Ly6G$^+$ leukocytes
Neutrophils	CD11b$^+$ Ly6G$^+$ Ly6C$^+$ leukocytes
CD4 $\alpha\beta$ T cells	CD11b$^-$ CD11c$^-$ TCRβ^+ NK1.1$^-$ CD8$^-$ CD4$^+$ leukocytes
CD8 $\alpha\beta$ T cells	CD11b$^-$ CD11c$^-$ TCRβ^+ NK1.1$^-$ CD4$^-$ CD8$^+$ leukocytes
Exhausted CD8$^+$ T cells	CD8$^+$ T cells CD44$^+$ CD8 SIINFEKL-loaded MHCI dextramer$^+$ PD-1$^+$ Tim3$^+$
Regulatory T cells	CD4$^+$ T cells FoxP3$^+$ CD25$^+$ leukocytes
$\gamma\delta$ T cells	CD11b$^-$ CD11c$^-$ CD3ε^+ CD4$^-$ CD8$^-$ $\gamma\delta$TCR$^+$
NK cells	CD11b$^-$ CD11c$^-$ TCRβ^- NK1.1$^+$
NKT cells	CD11b$^-$ CD11c$^-$ TCRβ^+ NK1.1$^+$

2.2.13. Staining of intracellular molecules

To stain for intracellular molecules, samples had to be further processed using FoxP3 Fixation/Permeabilization KIT© from Thermo Fisher according to the manufacturer´s protocol. Fixation solution was prediluted 1:3 in the appropriate buffer and cells were resuspended in 200 µl fixation buffer. After 1 hour of permeabilization/fixation at room temperature in the dark, the reaction was stopped by the manufacturer´s washing buffer (1:10 pre-diluted in PBS). After centrifugation at 1200 rpm for 5 minutes at 4°C, the supernatant was discarded and 50 µl of antibody mix (in wash buffer) was added to the cells. The samples were stained for 30-45 minutes at 4°C. The reaction was stopped by adding 100 µl of wash buffer and the samples were centrifuged at 1200 rpm for 5 minutes at 4°C. After removing the supernatant, cell pellet was washed and stored in FACS buffer until measurement. Different cell populations were identified with flow cytometric analysis *via* surface marker expression and further on their intracellular signal by measuring the mean fluorescence intensity minus one (MFI-MFI_0).

2.2.14. UMAP analysis

Dimensionality reduction of flow cytometric data was performed using the Uniform Manifold Approximation and Projection for Dimension Reduction (UMAP) plug-in in FlowJo v. 10.6. Prior to UMAP, doublets and dead cells were excluded and specific cell populations were identified by standard gating as described in Figure 5.

2.2.15. ROS staining

To quantify reactive oxygen species (ROS), single-cell suspensions of tumor cells were stained with dihydrorhodamine 123 (DHR123) for 30 min at 37°C and measured *via* FACS. The positive control was treated with 1 µg/ml Phorbol 12-myristate 13-acetate (PMA) for 30 min at 37°C.

2.2.16. Glucose uptake assay

Tumor cells were collected after 14 days from HSD- and NSD-fed mice as described in section 2.2.7. and isolated as written in section 2.2.8. After the generation of a single-cell suspension, live tumor cells were determined *via* trypan blue staining and counted in a Neubauer chamber. Then 0.5 x 10^6 of B16-OVA cells in 100 µl were seeded into a 96-well plate, washed and starved for one hour in starvation buffer (PBS + 10 % FCS) at 37°C and 5 % CO_2. 100 mM of fluorescently-labeled 2-deoxy-glucose (2-NBDG) was added to each well and incubated for 1 hour under humidity conditions (37°C and 5 % CO_2). Afterward, cells were washed again in starvation buffer and stained with a fixable viability dye for 10 minutes at 4°C. Cells were washed and centrifuged again and the mean fluorescence intensity minus one (MFI-MFI_0) was measured using BD FACS Canto II.

2.2.17. Fatty acid uptake

Ex vivo collected tumor cells from both diet groups were processed into a single-cell suspension and live cells were determined *via* trypan blue staining. 0.5 x 10^6 of B16-OVA cells in 100 µl were seeded into a 96-well plate, washed and rested for 1 hour in starvation buffer (PBS + 20 µM BSA) under humidity conditions. 5 µM of fluorescent BODIPY™ FL C16 was added to the cells and incubated for 30 minutes at 37°C and 5 % CO_2. Afterward, cells were washed and stained with fixable viability dye for 10 minutes at 4°C and the mean fluorescence intensity minus one (MFI-MFI_0) was measured using BD FACS Canto II.

2.2.18. Puromycin assay

Tumor cells were collected after 14 days from HSD- and NSD-fed mice as described in section 2.2.8. After the generation of a single-cell suspension, live tumor cells were determined *via* trypan blue staining and 0.5 x 10^6 cells were seeded into a 96-well plate. 10 µg/ml Puromycin was added to the cells and incubated for 30 minutes at 37°C and 5 % CO_2. After washing and centrifugation, fixable viability staining was performed for 10 minutes at RT.

FoxP3 Fixation/Permeabilization KIT was used as described in section 2.2.13. Afterward, cells were stained with anti-puromycin antibody for 1 hour at 4°C. Mean fluorescence intensity minus one (MFI-MFI_0) was measured using BD FACS Canto II.

2.2.19. Seahorse® real-time metabolic cell analysis

Ex vivo collected tumor cells from both investigated groups were processed to get single-cell suspension as described in section 2.2.8. and 0.2 x 10^5 cells were seeded into a Seahorse® XF96 Cell Culture microplate. After the attachment of the cells, a bicarbonate-free media was added and the oxygen consumption rate (OCR) and extracellular acidification rate (ECAR) were measured using the Seahorse® XFe Analyzer by following the manufacturer´s instructions in cooperation with Prof. Dr. Christoph Wilhelm, Institute of Clinical Chemistry and Clinical Pharmacology, University Clinics Bonn.

2.2.20. Metabolome analysis

Skin tumors from mice fed with either HSD or NSD were harvested after 14 days and immediately stored in liquid nitrogen. Analysis of metabolites within the tumor samples was carried out by METABOLON® INC (Morrisville, NC).

2.2.21. Proteome analysis of isolated skin tumor cells

Skin tumors of mice fed with HSD or NSD were harvested after 14 days and single-cell suspensions were generated as described in section 2.2.7. Tumor cells were further isolated with MACS® isolation KIT as written in section 2.2.9. and 0.2 x10^6 cells were resuspended in 50 µl RIPA buffer + 10 % SDS and stored ad -80°C. Samples were processed and analyzed by Prof. Dr. Christian Münch and Süleyman Bozkurt, Mass Spectrometry Facility, Institute of Biochemistry II, University Hospital Frankfurt. Briefly, pure proteins were obtained with methanol/chloroform precipitation and digested with trypsin (1:1000) and LysC (1:50) at 37°C overnight. Digested peptides were further purified using Seq-Pak tC18 cartridges and peptide concentrations were determined *via* BCA assay. Samples were labeled with 2.5 µg TMT, adjusted to an equal amount and pooled.

For mass spectrometry (LC-MS^3) analysis, the fractions were resuspended in 2 % acetonitrile and 0.1 % formic acid and separated on fused-silica column. 1 µg of peptides were eluted by a non-linear gradient over 150 minutes and directly sprayed into a Orbitrap Fusion Lumos mass spectrometer equipped with a nanoFlex ion source. Sprayed peptides were analyzed with Multi-Notch MS3-based TMT method in order to minimize ratio compression and ion interferences. Raw data were analyzed with Proteome Discoverer 2.4 and SequenceHT node was selected for database searches of MS2-spectra. Ranked enriched gene ontology terms were identified using GOrilla website.

2.2.22. RNA isolation and gene expression analysis

Frozen tumor and lung samples were used for RNA isolation with the RNA NucleoSpin isolation KIT© from Macherey Nagel according to the manufacturer's protocol. Total RNA was extracted from homogenized samples by the selective binding properties of a silica-based membrane using RNeasy Mini Kit including DNase I treatment according to the manufacturer´s protocols. Total RNA concentration was determined *via* NanoDrop Spectrophotometer (ratio absorbance 260/280 nm and 260/230 nm). 1 µg RNA was reverse transcribed with Moloney murine leukemia virus reverse transcriptase, RNAsin and dNTPs master mix (Promega, 2020). Quantitative Real-Time PCR was performed by using Quantstudio 5 and GoTaq® qPCR Master Mix with SYBR green. PCR primer sequences were designed using the online-based databases: NCBI Nucleotides, Primer3, and Primer Blast shown in Table 8.
Gene expression was normalized to the housekeeping gene (β-Actin) and ΔΔCT method was used for comparing relative expression to the control group.

2.2.23. Protein isolation for Western blot

Melanoma tissues were harvested from mice under HSD and NSD as described in section 2.2.8. and tumor cells were isolated as written in section 2.2.10 and stored at -80°C. Frozen tumor cells were homogenized in RIPA buffer + 10 % Protease inhibitor. After cooling down on ice for 10 min, the solution was centrifuged at high speed for 15 min and

4°C. The supernatant was taken and protein concentration was determined using BCA protocol.

2.2.24. Western blot analysis using Simple Western™

Protein content was measured by using Simple Western™ technologies, combining size-based capillary electrophoresis with immunodetection *via* primary antibodies. Therefore 0.25 µg/µl of total protein was used and primary antibodies were added according to the manufacturer's protocol. Data were analyzed with the Software Compass for Simple Western™.

2.2.25. Hormone level quantification in serum

α-MSH levels were quantified in the serum of mice under HSD and NSD by ELISA according to the manufacturer´s description.

2.2.26. RNA Sequencing data processing

Skin tumors were collected from mice either on HSD or NSD and immediately stored in liquid nitrogen. Afterwards, total RNA was isolated as described in section 2.2.22. and sequenced with Standard 3' mRNA-Seq Library Kit for Illumina Protocol by the Next Generation Sequencing (NGS) Core Facility from the University Clinics Bonn. Briefly, size distribution and yield of the 3'mRNA-seq library after the PCR step were determined by the D1000 high-sensitivity tape station prior to pooling of the barcoded libraries. The pooled 3'mRNA-Seq libraries were loaded on the Illumina HiSeq2500 platform and analyzed by a 50-cycle high-output run. FASTQ files were aligned to the mm10 mouse reference genome using the StarAligner. Further computational 3'mRNA-seq analysis was done with the Bioconductor/R computing environment. The voom method of the limma package was used for normalization and linear modeling with quantile normalization. To obtain mRNA expression values, the read counts per million (cpm) were transformed to log2 values according to the voom algorithm. Differentially expressed genes were determined by an empirical Bayes moderated t-test statistic using the limma package. For gene set enrichment analysis, the gene ontology gene set collection GO-

biological processes provided by the Molecular Signature Database (MSigDb) from the Broad Institute was used (https://software.broadinstitute.org/gsea/msigdb/). The t-test statistic values as input ranking parametric for GSEA pre-ranked gene list mode and default settings. For GSEA analysis, javaGSEA stand-alone version was used. Bioinformatical analysis was done with the help of Prof. Dr. Michael Hölzel, University Clinics Bonn.

2.2.27. Histology

The fibrotic state of tumor tissue was assessed by Sirius Red staining on paraffin-embedded tissue sections. Therefore, the entire tumor as well as the surrounding skin was collected from mice on NSD or HSD and incubated in 4 % methanol-fee PFA in PBS at 4°C overnight. On the next day, the samples were transferred into a histology cassette and soaked under running tap water for 4 h before transferring to a tissue drainage automat. Here, samples were automatically dehydrated over a total period of 17 h. Subsequently, organs were placed in a histokinette, embedded in liquid paraffin and dried. Afterwards, the samples were sectioned in 2 µm thick slices using a rotary microtome and were dried overnight at 60°C before the staining was performed. After de-waxing and hydration of the samples, the slides were washed five times with BiDest and transferred into a glass cassette with Pico Sirius Red solution (in saturated picric acid) for one hour protected from light. The slides were washed twice with acidified water and dried afterwards. Tissues were dehydrated three times with 100 % ethanol and fixed with xylene and further with ROTI® Histokitt. The scanning was performed at 20x and 40x magnification using a bright field scanner. The fibrotic array was visualized and determined using Fiji ImageJ tool.

2.2.28. Cell confluence measurement of melanoma cells *in vitro*

Besides the investigation of melanoma growth *in vivo*, B16-OVA and B16 Tyrosinase$^{-/-}$ cells were also kept *in vitro* for further experiments. Cells were cultured under the same conditions as described in section 2.2.1. To mimic *in vivo* conditions, melanoma cells were treated with high sodium media (+ 40 mM NaCl) or D-Mannitol (+ 80 mM) to discriminate between salt-specific alterations or osmotic stress responses. To investigate growth

changes, 0.1 x 10^4 live cells were seeded into a 12-well plate and incubated at 37°C and 5 % CO_2 until they get attached. The adjusted media was added to the different groups; control cells received normal media. Cells were kept at 37°C and 5 % CO_2. Media was changed every second day and cell confluence was measured daily *via* Tecan Spark until the wells reached 100 % confluence.

2.2.29. Statistically analysis

The results were graphically represented as the average of the measured values together with their standard deviation (SD) or standard error of the mean (SEM). Significances were calculated either with an unpaired two-tailed t-test (when comparing two groups) or with a 2-way ANOVA analysis with Tukey´s multiple comparison test and defined as follows: *$p<0.05$, **$p<0.01$, ***$p<0.001$.
Outliers were identified and removed by using the ROUT method (Robust regression and Outlier removal) with Q = 1%.

3 Results

3.1 High-salt diet slows down B16 tumor growth in the skin and lungs of mice without major involvement of the immune system

In this thesis, the influence of high-salt diet on cutaneous melanoma growth was investigated. In particular, changes in the immune cell compartment due to excessive salt intake were in the focus. Furthermore, the question was raised whether metastatic melanoma, formed in the lungs, was similarly altered by HSD than solid tumors.

3.1.1. HSD significantly reduces B16 tumor growth in the skin

To assess the influence of high-salt diet on melanoma pathogenesis, a murine melanoma model using a B16 melanoma cell line expressing ovalbumin (B16-OVA) was chosen. *Subcutaneously* injected B16-OVA cells formed a palpable tumor between 5 to 10 days after injection, and without intervention, a tumor volume of approximately 1 cm^3 was reached by day 14. In this experimental setup, female C57BL/6J wild-type (WT) mice were used to investigate tumor growth under two different dietary conditions. Mice on normal-salt diet (NSD) received a regular chow and were allowed free access to autoclaved tap water. Mice under high-salt diet (HSD) were fed with 4 % NaCl-rich chow and additionally received 0.9 % sodium chloride autoclaved water *ad libitum* over the entire experimental time. After 7 days on the respective diet, 0.5 x 10^6 B16-OVA melanoma cells were injected *s.c.* into the mice and tumor growth was measured daily as soon as a tumor was palpable (Figure 6, A). Similar body weights between both groups were observed, indicating that HSD nor the implantation of melanoma cells had an effect on mice well-being (Figure 6, B). Mice under HSD showed reduced tumor volume compared to the NSD group after 14 days (Figure 6, C). Investigation on melanoma formation over time showed similar tumor growth in both groups in the beginning. While the NSD group displayed sustained B16-OVA tumor growth over the experimental time, mice under HSD started to slow down melanoma growth, starting from day 9 onwards, which became statistically significant from day 11 until the end of experiment (Figure 6, D).

In conclusion, high-salt diet significantly delayed B16-OVA tumor growth.

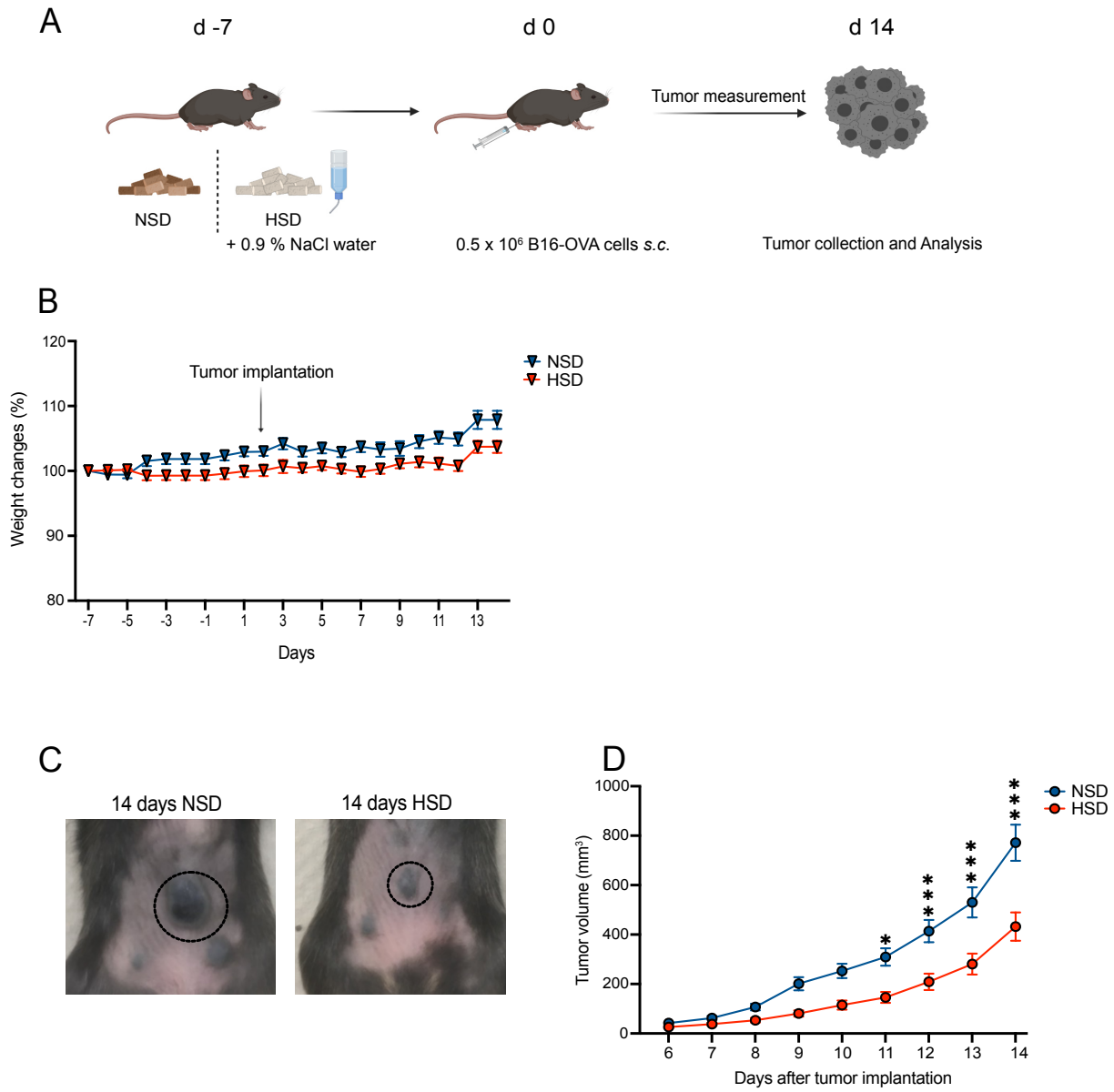

Figure 6: HSD significantly reduces B16-OVA tumor growth in the skin. Mice were fed with high-salt diet (HSD) and given 0.9 % NaCl water one week before tumor injection. The control group received normal chow. On day 0, 0.5 x 10^6 B16-OVA melanoma cells were injected *subcutaneously* into all mice. Tumor volume and weight changes were measured daily. After 14 days, tumor tissue was collected and further analyzed. (A) Experimental setup. (B) Percentage of weight changes in mice under HSD (red, n=17) compared to NSD (blue, n=17). (C) Representative picture of tumor size after 14 days of tumor growth under either diet. (D) Measurement of tumor volume (mm^3) over time of mice under NSD (blue, n=33) and HSD (red, n=33). (D) Data shown as mean ± SEM of 6 independent experiments (C) and 3 independent experiments (D) and analyzed with 2-way ANOVA. * - p<0.05; **- p<0.01; ***- p<0. 001.

3.1.2. *Ex vivo* tumor cells after HSD are significantly lower in cell number, without altering cell proliferation or apoptosis

To further investigate the reduced melanoma growth under HSD observed in mice, the tumors were harvested and analyzed in depth. Consistent with the reduced tumor volume, melanoma isolated from HSD-fed mice weighed significantly less than tumors isolated from NSD-fed mice (Figure 7, A) and contained significantly lower numbers of live tumor cells (Figure 7, B). Potential reasons for the differences in tumor growth could be explained by differences in tumor cell survival or proliferation caused by HSD. Therefore, the next question was whether the excessive salt content leads to alterations in apoptosis as well as the proliferation capacity of tumor cells. Staining with Annexin V revealed no differences in apoptosis between tumor cells isolated from HSD and NSD, indicating that HSD did not influence the apoptosis of tumor cells (Figure 7, C). Furthermore, the analysis of Ki-67, a proliferation marker, indicated comparable proliferation rates in both groups (Figure 7, D).

In conclusion, HSD diminished melanoma cells but had no effect on tumor cell proliferation or apoptosis.

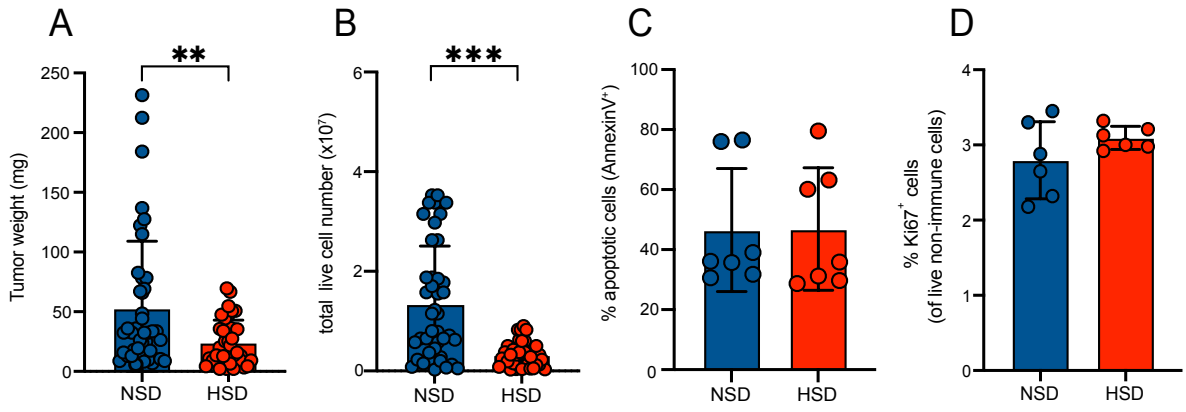

Figure 7: HSD reduces tumor weight and lowers the number of live tumor cells *ex vivo*. (A) Weight of tumors isolated from HSD (red, n=30) and NSD mice (blue, n=30) on day 14 after tumor implantation. (B) Number of live tumor cells under HSD (red, n=38) and NSD (blue, n=38) on day 14 after tumor implantation. (C) Percentage of apoptotic cells identified by staining with Annexin V among all tumor cells (n=7/group). (D) Percentage of Ki-67$^+$ cells among all live tumor cells (n=6/group). Data shown as mean ± SD of 8 independent experiments (A+B) and 2 independent experiments (C+D) and statistically analyzed by unpaired t-Test. * - p<0.05; **- p<0.01; ***- p<0. 001.

3.1.3. Excessive salt intake also causes tumor regression in the lung

Since melanoma shows a high potential to metastasize in other organs, the question was, whether the effect of reduced tumor growth under HSD can be also observed in other organs. Besides lymph nodes, the lung is one of the first organs affected by metastatic melanoma and recent publications negate a sodium storage capacity like in the skin (He et al. 2020). To answer this question, mice were fed with NSD or HSD, and tumor formation in the lung was investigated. Here, luciferase-expressing melanoma cells were used to measure melanoma formation *in vivo* over time. After 7 days on the diet, 0.5 x 10^6 B16- OVA luciferase-expressing cells were injected *i.v.* into the mice and metastatic melanoma formation was quantified with In Vivo Imaging System (IVIS) (Figure 8, A). 14 days after tumor implantation, the lungs were collected and visible tumor nodules were counted. Mice on HSD displayed only a minor number of visible melanoma nodules compared to the control group (Figure 8, B). Quantification of these nodules confirmed significantly fewer counted melanoma spots in HSD-fed mice compared to NSD (Figure 8, C) Consistent with this observation, during the course of the experiment, HSD-fed mice showed lower luminescence signal at the end of experiment than the NSD group, indicating a reduced melanoma growth in the lungs under HSD (Figure 8, D). Until day 10 after tumor application, HSD- and NSD-fed mice displayed a similar luminescence signal. Afterwards, luminescence signal under HSD was slightly decreased as compared to the control, indicating less tumor formation. No differences were detected in the weight change of both investigated groups (Figure 8, E). Gene expression analysis of Ovalbumin (*Oval*) mRNA in the lungs confirmed that excessive salt intake additionally diminished tumor growth in the lung (Figure 8, F).

Taken together, these data showed that HSD-mediated tumor suppression is not limited to solid tumors in the skin, but also delayed metastasis growth in the lung.

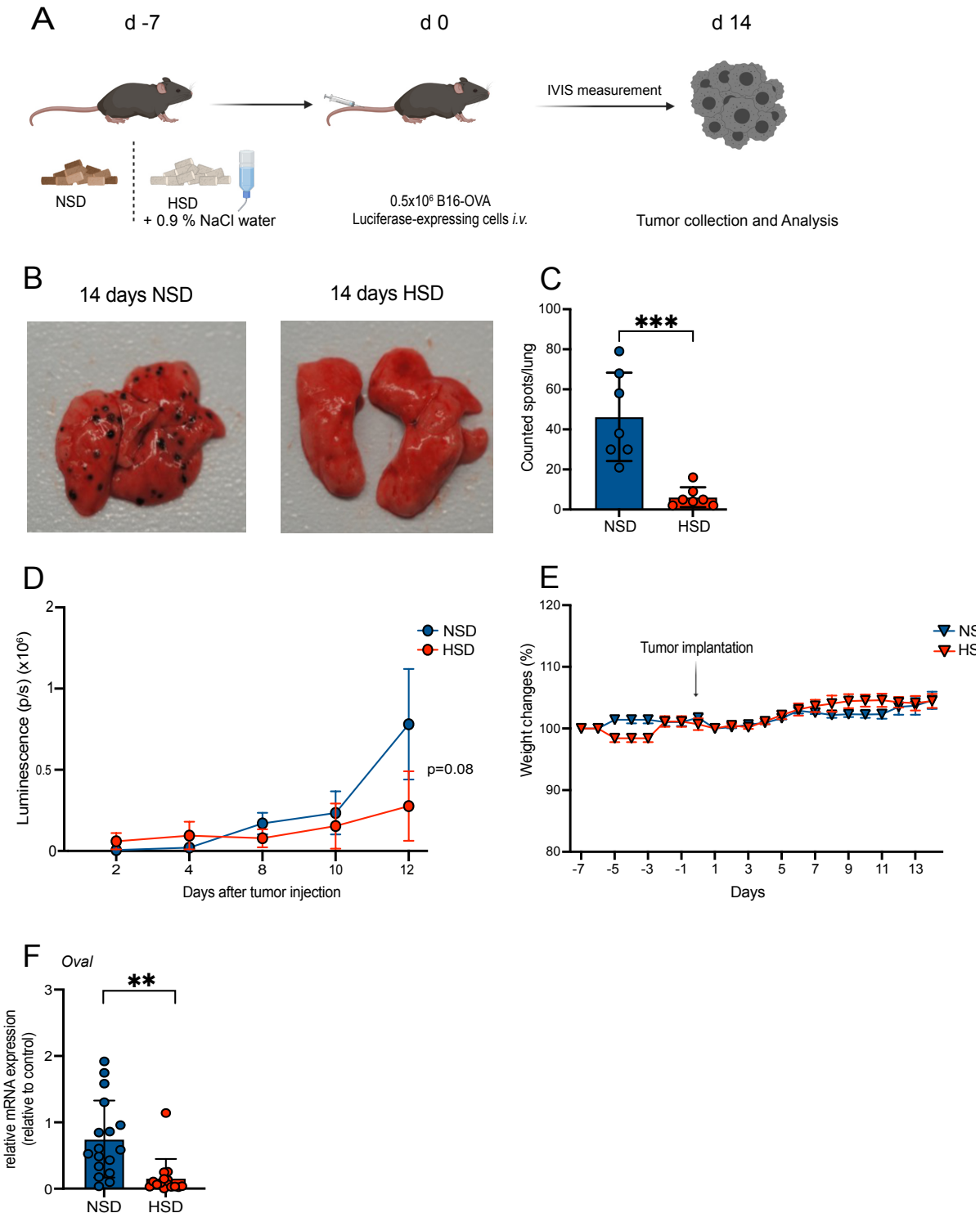

Figure 8: HSD delays B16-OVA melanoma growth in the lung. After 7 days on either HSD or NSD, mice received 0.5 x 10^6 B16-OVA luciferase-expressing cells *i.v.* and lung tumor formation was measured *via* IVIS. (A) Experimental setup. (B) Representative picture of lung tumor formation. (C) Quantification of lung tumor nodules out of mice fed with NSD or HSD (n=7 mice/group). (D) Luminescence measurement over the experimental time in mice fed with NSD or HSD (n=7

mice/group). (E) Weight changes of mice on HSD and NSD (n=7 mice/group). (F) Gene expression analysis of Ovalbumin (*Oval*) in the lung out of mice fed with HSD or NSD (n=7 mice/group). Data show mean ± SD of 2 independent experiments, analyzed with unpaired t-Test (C+F) or with 2-way ANOVA (D+E). * - $p<0.05$; **- $p<0.01$; ***- $p<0.001$. Experiments were done with the help of K. Jobin and M. Meißner.

3.1.4. HSD does not change the immune cell compartment in the blood

As it has already been shown that HSD polarizes the immune systems towards an inflammatory state (Ip and Medzhitov 2015; Jantsch et al. 2015) the next question was how the immune system changes during melanoma growth and whether HSD has additional effects on it. Therefore, blood was collected from the tail veil before diet change (day -7) and after 7 days on either HSD or NSD to assess the diet effect on the immune cell composition *via* FACS (Figure 9, A). HSD did not change the total live $CD45^+$ cells/ml blood (Figure 9, B) nor the number of $CD4^+$ or $CD8^+$ T cells per ml blood in comparison to NSD (Figure 9, C + D). Also, the number of neutrophils (Figure 9, E) and monocytes (Figure 9, F) did not change upon HSD. Overall, 7 days on HSD did not affect the composition of immune cells in the blood.

When assessing the abundance of immune cells after tumor implantation, melanoma transplantation in the skin induced the expansion of total live $CD45^+$ cells, total $CD4^+$ T cells, neutrophils, and monocytes in both investigated groups but without significant changes between the diet forms (Figure 9, B+C+E+F). Interestingly, $CD8^+$ T cells were increased on day 7 after tumor application but dropped back to normal cell count by day 14 (Figure 9, D).

In summary, HSD alone did not affect the immune cell composition in the blood. The transplantation of melanoma cells increased the total cell count in both groups, indicating a reaction of the immune system to the tumor. However, no salt-specific modulations were observed.

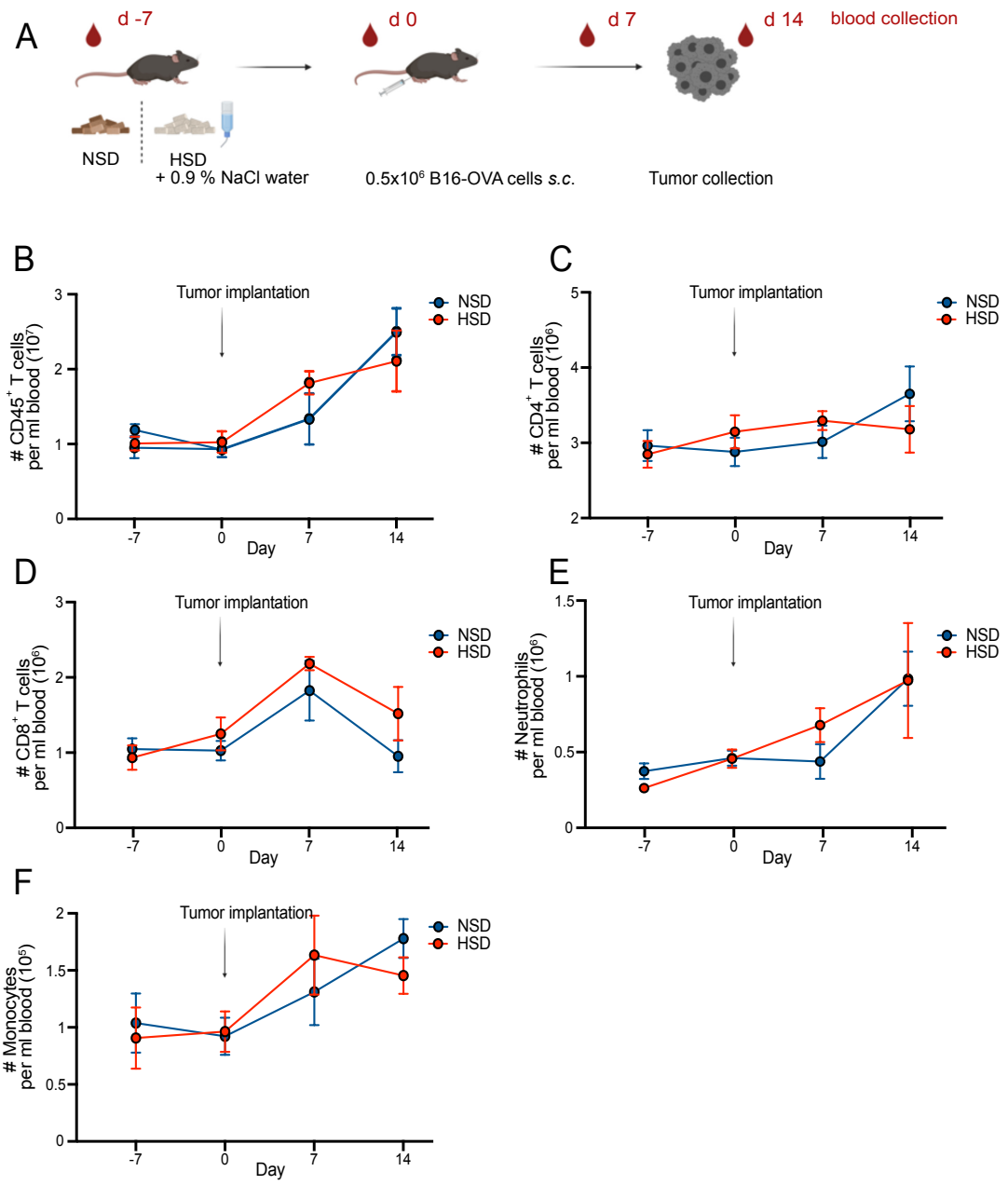

Figure 9: HSD does not change total cell numbers of blood immune cells. Blood samples were collected on day -7 (before changing the diet), day 0 (7 days on a different diet and before tumor implantation), day 7 (after tumor implantation) and day 14 (end of experiment). (A) Experimental setup. (B) Blood kinetic analysis of live $CD45^+$ cells from mice on NSD and HSD. (C) Total $CD4^+$ T cells (D) $CD8^+$ T cells (E) neutrophils and (F) monocytes per ml blood were investigated. Data shown as mean ± SEM of 2 independent experiments with 10 mice per group and analyzed with 2-way ANOVA. * - $p<0.05$; **- $p<0.01$; ***- $p<0.001$.

3.1.5. HSD does not change the intratumoral composition of immune cells

Excessive salt intake was shown to increase local sodium concentration in the skin and exert proinflammatory effects. This has been shown to boost classically-activated macrophages to promote bacterial clearance (Jantsch et al. 2015). To analyze whether HSD also affects the infiltration of immune cells into B16-OVA tumors, melanoma tissue was collected after 14 days of tumor growth in mice under HSD or NSD. Using Uniform Manifold Approximate and Projection (UMAP) analysis, the intratumoral immune cell distribution was visualized. HSD did not provoke immune cell infiltration divergent from the control group. Similar patterns of immune cells were detected in the tumor microenvironment (TME) under NSD compared to HSD (Figure 10, A). Detailed analysis confirmed similar numbers of live $CD45^+$ cells per mm^3 tumor between HSD and NSD (Figure 10, B). Analysis of the innate immune cell compartment in TME did not reveal any influences attributed to HSD. Similar numbers of macrophages, dendritic cells, neutrophils, and NK cells were found in the TME isolated from HSD-fed mice in comparison to NSD (Figure 10, C-F). Further investigations of the adaptive immune system showed comparable results between HSD and NSD. Similar numbers of $CD4^+$ T cells, Th17 T cells, regulatory T cells, $\gamma\delta$ T cells, and NKT cells were found in the TME of both investigated groups (Figure 10, G-K). Moreover, comparable numbers of $CD8^+$ T cells as well as PD-1^+ $CD8^+$ T cells were found in the TME of both investigated groups (Figure 10, L+M).

In summary, HSD had no great impact on the intratumoral immune cell compartment. Similar numbers of immune cells in the tumor tissue were detected which could not explain the HSD-mediated tumor reduction

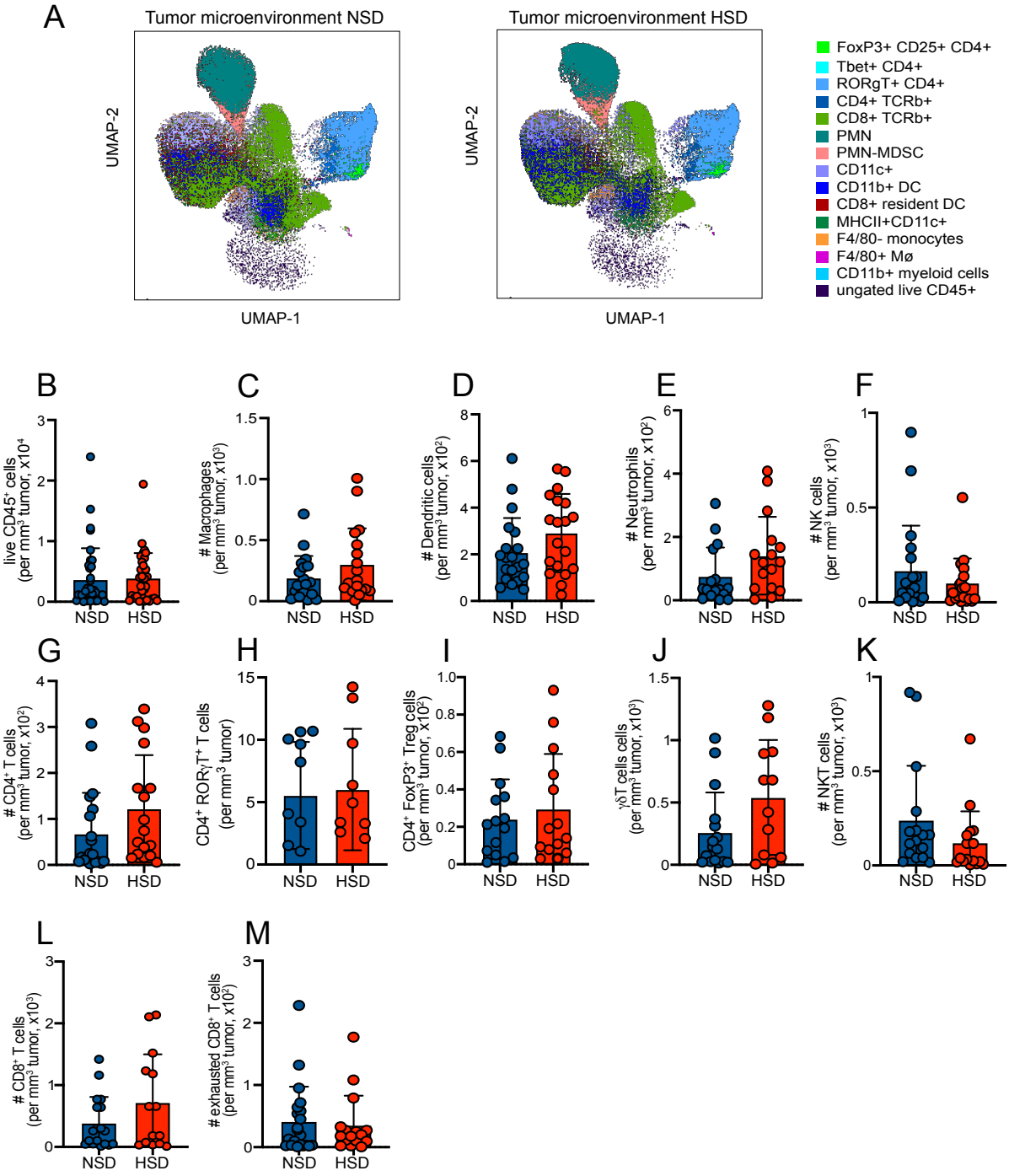

Figure 10: HSD does not change the intratumoral immune cell compartment. Quantitative UMAP dimensionally reduction displays by FACS data revealed similar distribution of immune cells in the TME from HSD and NSD-fed mice. (A) Representative example of UMAP analysis of tumor composition under NSD (n=5) and HSD (n=7). (B) Total number of live CD45$^+$ cells per mm^3 tumor of mice fed with HSD or NSD (n=28 mice/group). (C) Number of macrophages (n=14 mice/group), dendritic cells (D, n=14 mice/group), neutrophils (E, n=15 mice/group) and NK cells (F, 12 mice/group) per mm^3 tumor in mice fed with HSD or NSD. (G) Number of CD4$^+$ T cells (n=25 mice/group),

Th17 T cells (H, n=9 mice/group), regulatory T cells (I, n=20 mice/group), $\gamma\delta$ T cells (J, n=15 mice/group) and NK T cells (K, n=12 mice/group) per mm^3 tumor in mice fed with HSD or NSD. (L) Total number of $CD8^+$ T cells (n=19 mice/group) and $PD1^+$ $CD8^+$ T cells per mm^3 tumor both investigated groups (M, n=20 mice/group). UMAP shows 1 experiment. FACS data shows 3-5 independent experiments and analyzed with unpaired t-Test. * - $p<0.05$; **- $p<0.01$; ***- $p<0.001$. FACS analysis was done with the assistance of K. Jobin.

3.1.6. HSD does not influence immune cell numbers in tumor-draining lymph nodes

As a consequence of melanoma formation, the tumor-draining lymph nodes (LN) increase in size from day 2 after tumor application and boost the accumulation of immune cells (Commerford et al. 2018). Additionally, to assess the immune cell compartment in the blood and the tumors themselves, the tumor-draining LN and their changes during melanoma formation and HSD were analyzed. UMAP analysis visualized a similar distribution of immune cell populations in tumor-draining LN after 14 days of tumor growth under NSD and HSD (Figure 11, A). Detailed analysis revealed no differences in the number of live $CD45^+$ cells in the LN of both investigated groups (Figure 11, B). Comparable numbers of macrophages, dendritic cells, and NK cells were detected in LN on either diet (Figure 11, C-E). In contrast, the number of neutrophils significantly decreased in LN under HSD (Figure 11, F). Analysis of the adaptive immune system revealed no changes in the total number of $CD4^+$ T cells, Th17 T cells, regulatory T cells, or NKT cells (Figure 11, G-J). Comparable numbers of $CD8^+$ T cells and $PD1^+$ $CD8^+$ T cells were detected in LN in mice under HSD and NSD (Figure 11, K+L).

Taken together, the overall immune cell composition in tumor-draining LN was not affected by the excessive salt intake, but a decrease in neutrophils was observed.

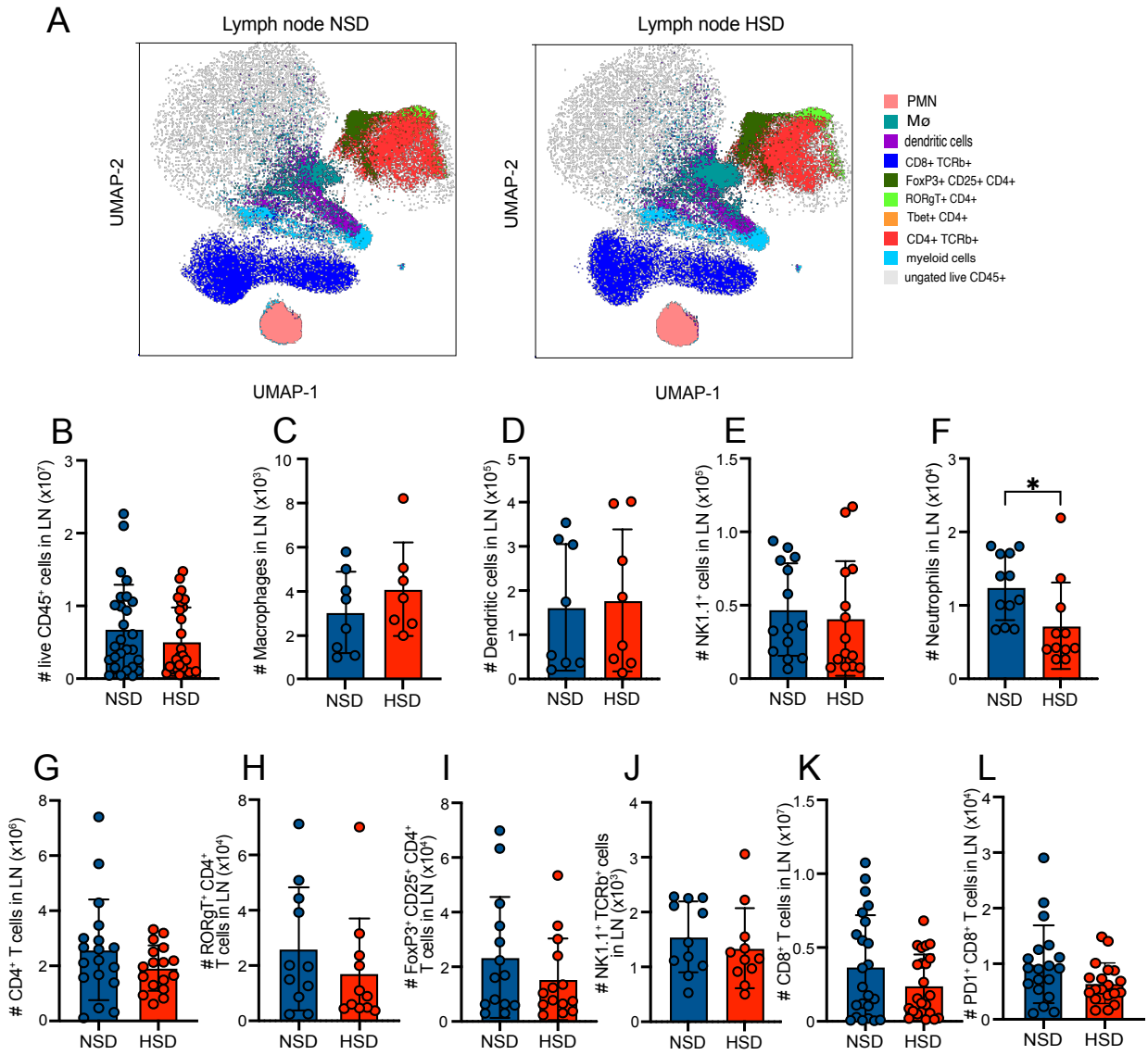

Figure 11: HSD does not change immune cell numbers in tumor-draining lymph nodes. After 14 days of tumor growth in mice on HSD or NSD, the tumor-draining LNs were analyzed by FACS. (A) Representative UMAP analysis of LN out of NSD-fed mice (n=5) and HSD-fed mice (n=7). (B) Number of total live CD45$^+$ cells (n=27 mice/group), macrophages (C, n=11 mice/group), dendritic cells (D, n=8 mice/group), NK cells (E, n=14 mice/group), and neutrophils (F, n=12 mice/group) in LN of both investigated groups. (G) Total number of CD4$^+$ T cells (n=18 mice/group), Th17 T cells subtype (H, n=11 mice/group), regulatory T cells (I, n=14 mice/group) and NKT cells (J, n=11 mice/group) in LN under HSD and NSD. (K) Total number of CD8$^+$ T cells (n=23 mice/group) and PD-1$^+$CD8$^+$ T cells (L, n=19 mice/group) in LN of both investigated groups. UMAP shows 1 experiment. FACS data shows 2-5 independent experiments and analyzed with unpaired t-Test. * - p<0.05; **- p<0.01; ***- p<0. 001. FACS analysis was done with the assistance of K. Jobin.

3.1.7. Myeloid-derived suppressor cells are no key players in HSD-mediated tumor reduction

The effect of dietary changes on tumor progression and their therapeutic potential is a highly researched topic. In the course of this thesis, HSD has been shown by Willebrand et al. to inhibit melanoma growth by suppressing myeloid-derived suppressor cells (MDSC) and in turn shifts lymphocytes toward a pro-inflammatory state (Willebrand et al. 2019). As this publication stands in contrast to the observation of this thesis, that the immune cell composition remains unchanged by HSD, MDSCs were investigated in greater detail in both blood and the tumor under HSD. Therefore, blood was collected at different time points, as described in section 3.1.4. and myeloid MDSCs (M-MDSCs) as well as granulocytic MDSCs (PMN-MDCs) were quantified. HSD did not change the frequency of M-MDSCs or PMN-MDSCs per ml blood compared to NSD before and after tumor implantation (Figure 12, A+B). Furthermore, the excessive salt intake did not change the frequency of M-MDSCs or PMN-MDSCs in the tumor compared to the control group (Figure 12, C+D). To evaluate the potential role of MDSCs in the reduced tumor growth under HSD, MDSCs were depleted and tumor growth was assessed. For this, mice were treated every three days with *i.p.* injection of Gemcitabine (60 mg/kg) (Le et al. 2009) and tumor formation was measured as described before (Figure 12, E). Analysis of the TME revealed significantly lower frequencies of MDSCs and PMN-MDSCs after Gemcitabine treatment in comparison to the untreated groups, indicating a sufficient depletion of myeloid-derived suppressor cells (Figure 12, F+G). The loss of MDSCs significantly decreased tumor volume in mice on NSD and HSD in combination with Gemcitabine treatment compared to the untreated control group after 14 days (Figure 12, H). No dietary-dependent differences were detected in melanoma growth between both Gemcitabine-treated groups.

Taken together, HSD did not change the population of myeloid-derived suppressor cells in the blood and tumor microenvironment. The loss of MDSCs did not further inhibit tumor growth in HSD-fed mice.

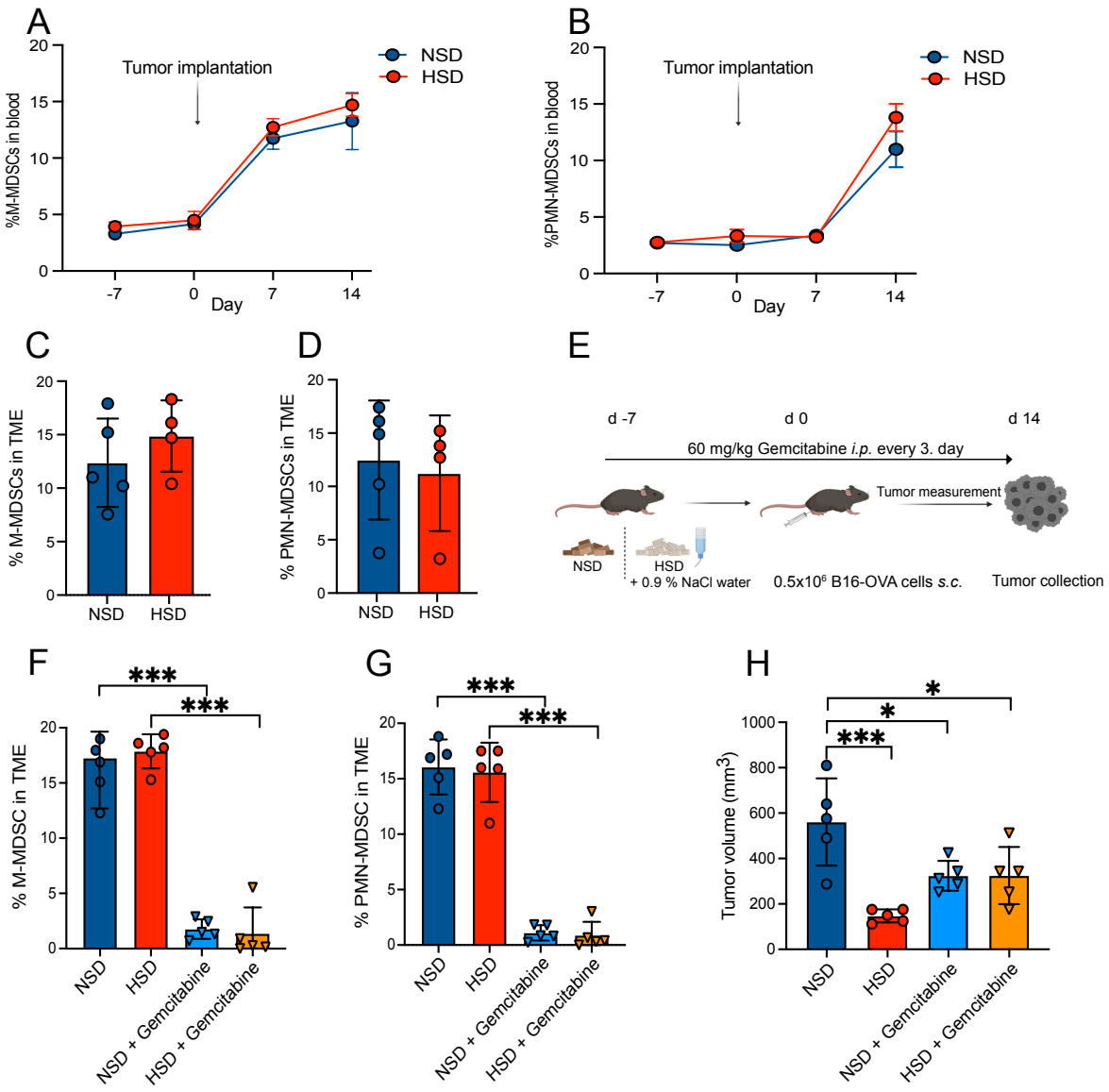

Figure 12: HSD has no impact on myeloid-derived suppressor cells. The percentage of M-MDSCs, as well as PMN-MDSCs, were similar in the blood and the tumor between HSD vs. NSD-fed mice. Nonetheless, tumor implantation led to an increase of both investigated cell populations in mice fed with HSD and NSD. Treatment with Gemcitabine does not further decrease HSD-mediated tumor reduction. (A) % M-MDSCs in the blood of mice under NSD (blue, n=7) and HSD (red, n=7). (B) % PMN-MDSCs in the blood of mice fed with NSD (n=7) or HSD (n=7). (C) % M-MDSCs as well as (D) PMN-MDSCs analyzed in the TME of both investigated groups. (E) Experimental setup of MDSC depletion. (F) % M-MDSCs and (G) PMN-MDSCs in the TME with Gemcitabine treatment. (H) tumor volume at day 14 of all investigated groups. (G) Data show mean ± SEM for kinetics and analyzed with 2-way ANOVA. Box blots were calculated with mean ± SD and analyzed with unpaired t-Test. Experiment was done once with 5 mice per group. * - p<0.05; **- p<0.01; ***- p<0. 001.

3.1.8. *In vitro* treated B16 cells under high salt conditions indicate a similar growth deficit as melanoma formation *in vivo*

After having observed *in vivo* that HSD strongly impairs the growth of B16 melanoma, and that this effect appeared to be independent of the immune system, the direct effect of salt in the growth of B16 cells was analyzed in greater depth *in vitro. In vitro* experiments allow the study of direct effects of high sodium conditions on the tumor cells without the influence of salt-induced factors such as hormones or the immune system. Based on the publication by Machnik et al. has shown that HSD can increase sodium levels in the skin of mice by up to 40 mM (Machnik et al. 2009). Therefore, media + 40 mM NaCl was used to mimic these conditions *in vitro*. As an increase in sodium concentration also induces osmotic stress, a suitable control to allow the discrimination of effects actually caused by high sodium or by osmotic pressure in general was required. For this control, D- Mannitol which has been shown to cause hyperosmotic stress was chosen (Yancey 2005) and melanoma cells were treated with 80 mM D-Mannitol. 0.1 x 10^5 B16-OVA melanoma cells were seeded into each well of a 12-well plate and cultured either in regular medium, under high sodium (HS) or under high Mannitol (Man) as described in section 2.2.28. The confluence of these cells was measured daily and the media was refreshed every other day to ensure optimal nutrient conditions (Figure 13, A). Representative pictures of the cell confluence measurement between day 4 and day 10 could be visualized for all investigated groups (Figure 13, B). Until day 5, a similar increase in cell confluence could be observed in all three groups. While the cells of the control group reached a cell confluence of 100 % by day 9 of the experiment, the cells cultured under HS and Man showed a significantly delayed increase in confluence (Figure 12, B+C), indicating a slower or reduced proliferating of B16-OVA cells under these conditions. However, no differences were detected between cells treated with high sodium in comparison to cells under hyperosmotic stress (Figure 13, B+C).

In summary, melanoma cells treated *in vitro* with high sodium conditions displayed a lower proliferation capacity than control cells. However, this effect was rather caused by osmotic stress than by salt-specific effects, as Mannitol-treated cells also showed a proliferating deficit.

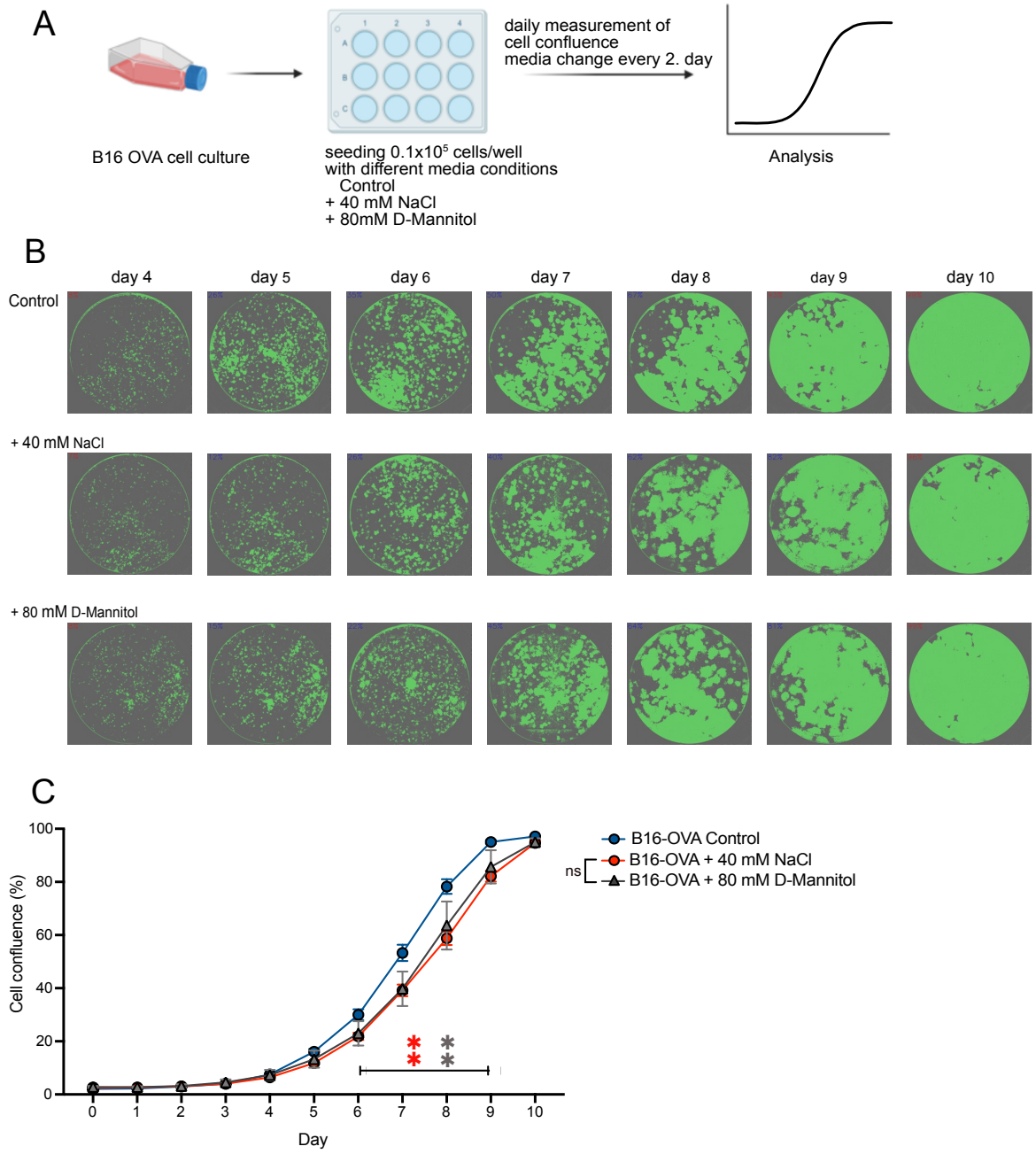

Figure 13: *In vitro* cultured melanoma cells show delayed cell growth under high sodium conditions as well as hyperosmotic stress. 0.1 x 10^5 B16-OVA cells were seeded into a 12-well plate under different media conditions: control media, high sodium (+ 40 mM NaCl) or D-Mannitol (+ 80 mM). Cell confluence was daily measured *via* Tecan and media was changed every second day. (A) Experimental setup. (B) Representative images of cell confluence over the experimental time of all three treatment groups. (C) Quantification of cell confluence (%). Data show mean ± SD of 6 independent experiments and analyzed with 2-way ANOVA. * - p<0.05; **- p<0.01; ***- p<0. 001.

3.2. Salt-induced tumor reduction is independent of osmo-protective mediators

The initial data of the thesis showed that HSD significantly diminished melanoma growth in the skin and could additionally reduce metastasis formation in the lung. Moreover, no great changes in the immune cell composition could be observed, in particular, an influence of MDSCs on HSD-mediated tumor reduction was excluded. Furthermore, *in vitro* studies showed that melanoma growth was also diminished under high sodium conditions. Therefore, mediators known to be activated by HSD were investigated.

3.2.1. Suppressed tumor growth under HSD is Nfat5 independent

Next, the question was whether HSD induces salt-sensitive mediators in the tumor microenvironment and that might be involved in the reduced tumor growth. In response to osmotic stress, the nuclear factor of activated T cell (Nfat5) gets activated and signals to protect cells from hypertonic stress (Miyakawa et al. 1999). To assess whether Nfat5 is also induced in the tumor during HSD, melanoma cells tagged with fluorescence on Nfat5 gene (mNeon) were generated and injected into mice on NSD or HSD. After 14 days of tumor growth, intracellular Nfat5 expression was measured (Figure 14, A). Gene expression analysis showed no differences in *Nfat5* mRNA expression in tumor cells under HSD compared to NSD (Figure 14, B). The data were confirmed by FACS, showing similar Nfat5 signal in tumor cells of both investigated groups (Figure 14, C). To verify that Naft5 does not play a role in HSD-mediated melanoma reduction, B16-OVA melanoma cells lacking Nfat5 were generated. Mice were fed with NSD or HSD and 0.5 x 10^6 B16-OVA Nfat5$^{-/-}$ melanoma cells were injected *s.c.* and tumor growth was documented over time (Figure 14, D). Similar to previous findings, mice under HSD displayed less tumor volume compared to the control group with a significant difference measurable at the end of the experiment (Figure 14, E).

In summary, melanoma cells did not upregulate Nfat5 in response to HSD and the tumor cell-specific loss of this transcription factor did not reverse the tumor-suppressive effect of HSD.

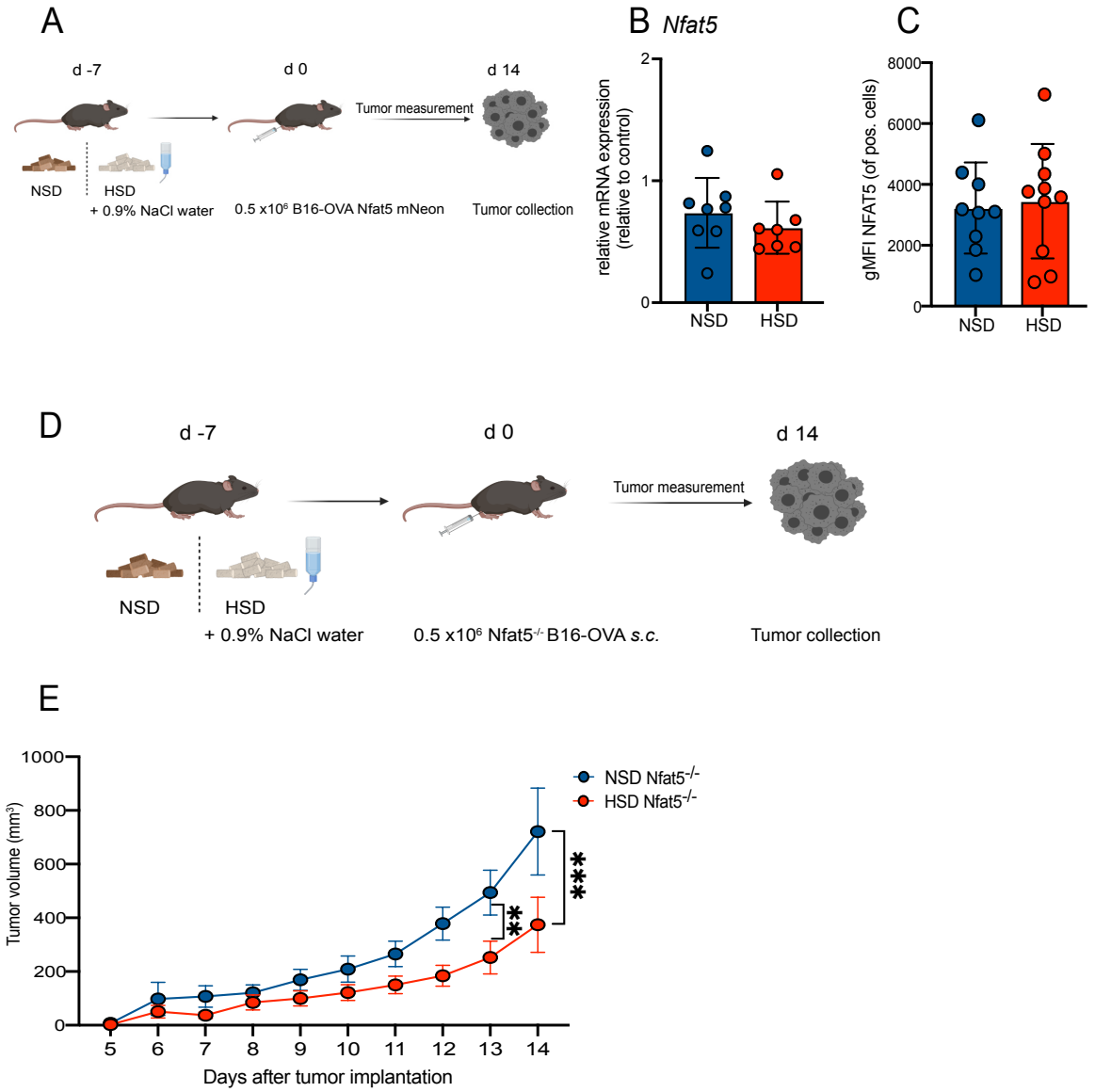

Figure 14: Reduced tumor growth under HSD is independent of the osmoprotective factor Nfat5. Gene expression analysis as well as FACS data indicate similar Nfat5 levels in melanoma cells under HSD in comparison to melanoma cells from the control group. Additionally, the loss of Nfat5 in melanoma cells could not recover the salt-induced tumor reduction. (A) Experimental setup. (B) relative mRNA expression of *Nfat5* (n=7 mice/group). (C) Geometric mean of fluorescence (gMFI) of intracellular Nfat5 (n=9 mice/group). (D) Experimental setup of mice under HSD vs. NSD, treated with Nfat5$^{-/-}$ melanoma cells. (E) Statistical analysis of Nfat5$^{-/-}$ tumor growth (n=12 mice/group). Data show mean ± SD of 2 independent experiments and analyzed with unpaired t-Test (Figure B+C) or 2-way ANOVA (Figure E). * - p<0.05; **- p<0.01; ***- p<0. 001.

3.2.2. HSD does not change Sgk1 levels in melanoma cells

Besides Nfat5, other osmoregulatory mechanisms get activated during high-salt diet. Hyperosmolarity has been shown to cause an increase of serum- and glucocorticoid-induced kinase 1 (Sgk1) which is able to regulate the epithelial sodium transport and constitutes a cellular response to stress (Farjah et al. 2003; Muller et al. 2003). To investigate the levels of Sgk1, melanoma cells tagged with fluorescence on Sgk1 gene (mNeon) were generated and injected into mice on either HSD or NSD. Tumor samples were collected after 14 days and intracellular Sgk1 levels were determined (Figure 15, A). Gene expression analysis showed no differences in *Sgk1* mRNA expression in tumor cells under HSD compared to NSD (Figure 15, B). The data were confirmed by FACS, showing similar Sgk1 signal in tumor cells of both investigated groups (Figure 15, C). To exclude the role of Sgk1 in HSD-mediated tumor suppression, melanoma cells lacking Sgk1 were generated and used in the current mouse model. Mice were injected *s.c.* with 0.5 x 10^6 B16-OVA Sgk1$^{-/-}$ melanoma after one week on either HSD or control diet and the tumor growth was measured over the next 14 days (Figure 15, D). Mice on HSD showed less tumor volume compared to the control group which became significant after 13 days (Figure 15, E).

In conclusion, HSD did not increase the expression of Sgk1 in melanoma cells. The effect of reduced tumor growth is still detectable even in the absence of Sgk1.

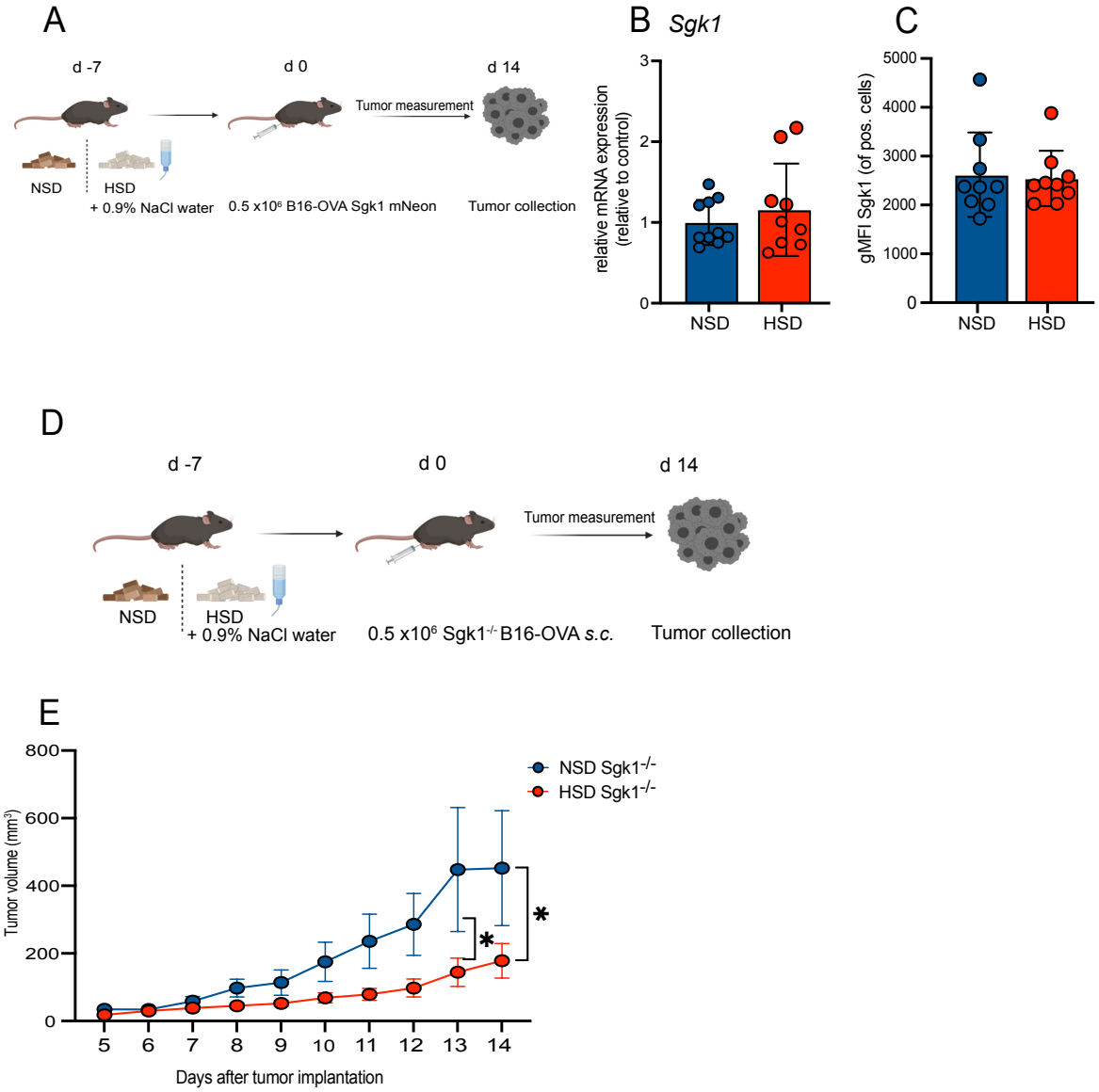

Figure 15: HSD-mediated tumor reduction is independent of Sgk1. Melanoma cells under HSD showed similar Sgk1 expression on genomic levels and protein levels. Injection of Sgk1 deficient melanoma cells in mice under HSD still showed reduced tumor growth compared to control diet. (A) Experimental setup. (B) Relative mRNA expression of *Sgk1* (n=9 mice/group). (C) Geometric mean of fluorescence (gMFI) of intracellular Sgk1 expression (n=9 mice/group). (D) Experimental setup. (E) Melanoma growth of Sgk1 deficient melanoma cells (n=9 mice/group). Data show mean ± SD of 2 independent experiments and analyzed unpaired t-Test (Figure B+C) or 2-way ANOVA (Figure E). * - p<0.05; **- p<0.01; ***- p<0. 001.

3.2.3. HSD directly suppresses melanoma formation independent of glucocorticoid receptor signaling

Besides osmo-protective mediators, tumor reduction under HSD might be mediated by the production of glucocorticoid receptor on melanoma cells. High sodium intake is associated with increased glucocorticoid (GC) production, such as corticosterone, which binds to its receptor (GR) (Baudrand et al. 2014). Downstream signaling activates transcription factors of mainly anti-inflammatory modulates in response to salt stress (Hayashi et al. 2004). Therefore, the question came up whether melanoma exposed to HSD express higher GR levels. After 14 days of tumor formation in mice fed with either HSD or NSD, melanoma tissue was collected and glucocorticoid receptor levels were measured in both groups (Figure 16, A). Interestingly, RT-PCR data revealed significantly less GR mRNA expression (*Nr3c1*) in melanoma cells under HSD compared to control group (Figure 16, B). FACS analysis confirmed less intracellular GR levels in tumor cells from HSD-fed mice compared to the control group (Figure 16, C). Furthermore, melanoma cells lacking the glucocorticoid receptor were injected into mice on NSD and HSD and tumor growth was measured over time (Figure 16, D). Mice under high-salt diet developed lower tumor volume compared to the control group, which was significantly less from day 12 on (Figure 16, E).

In summary, HSD diminished glucocorticoid receptor expression in tumor cells compared to the control. However, melanoma lacking GR still showed reduced tumor growth under HSD indicating a GR-independent regulation of tumor growth under HSD.

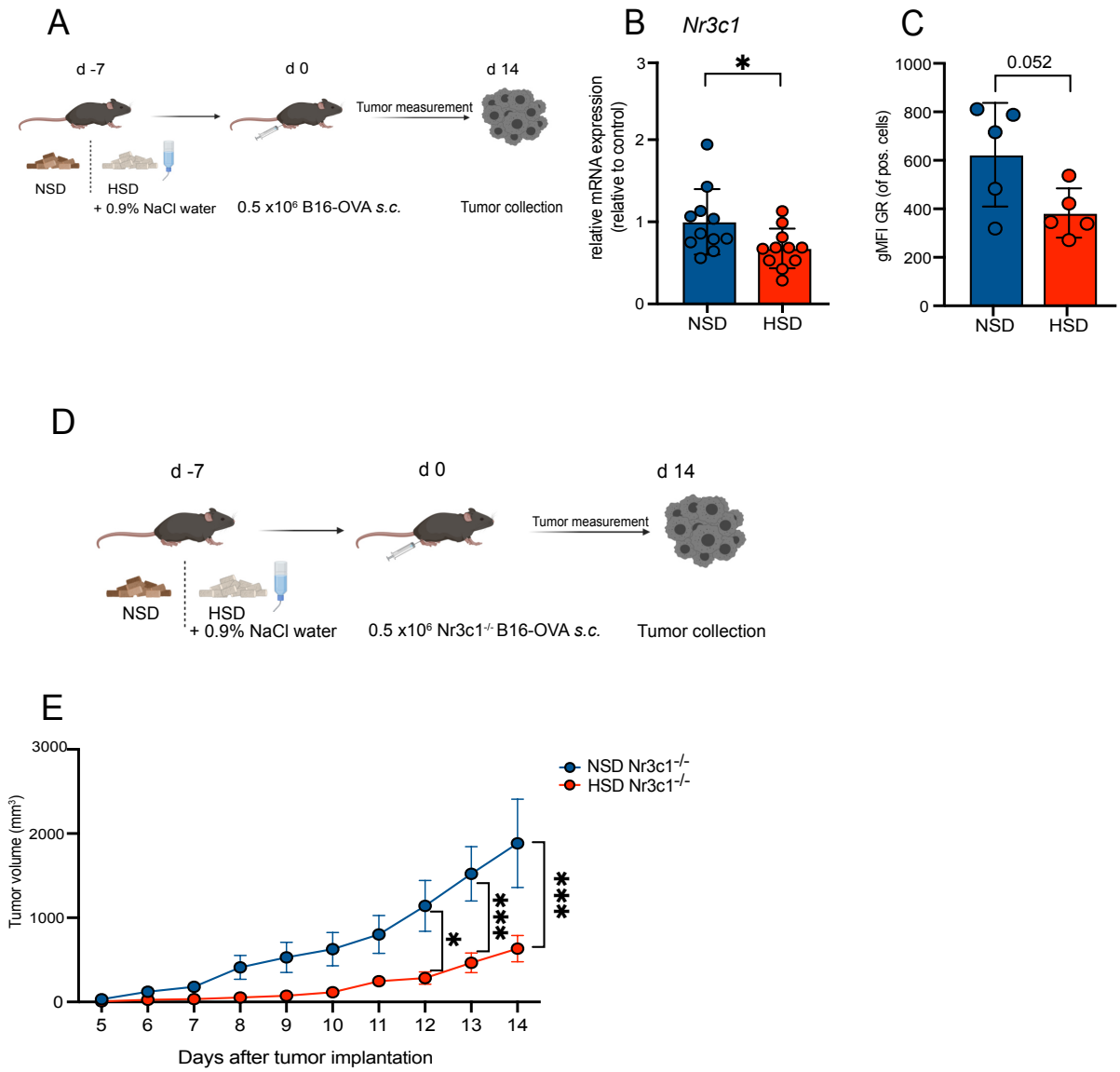

Figure 16: Melanoma cells under HSD trend toward lower glucocorticoid receptor expression. GR expression was measured in melanoma cells under HSD compared to control group. RT-PCR data as well as FACS analysis indicated lower expression of GR in melanoma cells after HSD. Further, melanoma lacking GR was injected into mice on either HSD or NSD and tumor formation was measured. (A) Experimental setup. (B) Relative mRNA expression of *Nr3c1* in tumor cells (n=11 mice/group). (C) FACS analysis of intracellular GR expression (n=5 mice/group). (D) Experimental setup. (E) Tumor formation of $Nr3c1^{-/-}$ melanoma in mice fed with either HSD or NSD (n=10 mice/group). Data show mean ± SD of 2 experiments (B) and 1 independent experiment (B) and analyzed with unpaired t-Test. in Figure E shows data from 2 independent experiments ± SD and analyzed with 2-way ANOVA. * - p<0.05; **- p<0.01; ***- p<0. 001.

3.2.4. Melanoma cells under HSD tend towards more fibrosis in the surrounding skin, while fibrosis-inducing mediators remain unaffected

Since cancer cells, and thus melanoma, cause chronic inflammation, the probability of fibrotic tissue formation is very high. Fibrosis is a pathological feature of chronic inflammation and enhances cancer initiation and progression (Coussens and Werb 2002). In recent years, several studies demonstrated a connection between increased salt consumption and fibrosis in various organs. Therefore, the role of fibrosis in melanoma growth under HSD was investigated. Sirius Red staining of the respective tumor tissue and the surrounding skin revealed a significant increase in fibrotic area at the border of tumor tissue to skin tissue under HSD (Figure 17, A+B). Also, inside the tumors themselves a trend towards more fibrosis under HSD was observed in comparison to NSD (Figure 17, C+D). Next, to the analysis *via* histology, the expression of genes involved in fibrosis was assessed on mRNA levels. Fitting to the histology results, elevated mRNA levels of matrix metallopeptidase 2 (*Mmp2*), matrix metallopeptidase 3 (*Mmp3*), and metallopeptidase inhibitor 3 (*Tim-3*) were detected in HSD tumors (Figure 17 F-H). Similar gene expression of actin alpha 2 smooth muscle (*Acta2*) was found in both investigated groups (Figure 17, E). Moreover, excessive salt consumption was found to increase the expression of transforming growth factor-beta (TGF-β) in renal fibrosis (Yu et al. 1998). No differences in the mRNA and protein expression of TGFβ were detected between melanoma cells from either diet (Figure 17, I+J). Based on the literature, it was shown that HSD induced liver fibrosis, which could be explained by excessive ROS production (G. Wang et al. 2016). Contrary to the literature, similar levels of ROS were measured when melanoma cells were grown under salty conditions compared to control group (Figure 17, K).

In conclusion, HSD slightly increased fibrosis at the border of tumor tissue and healthy skin tissue, but not inside the tumors. However, the increase in fibrosis did not appear to be caused by the known fibrosis modulators, such as TGF-β and ROS production, as their production remained unaffected by HSD.

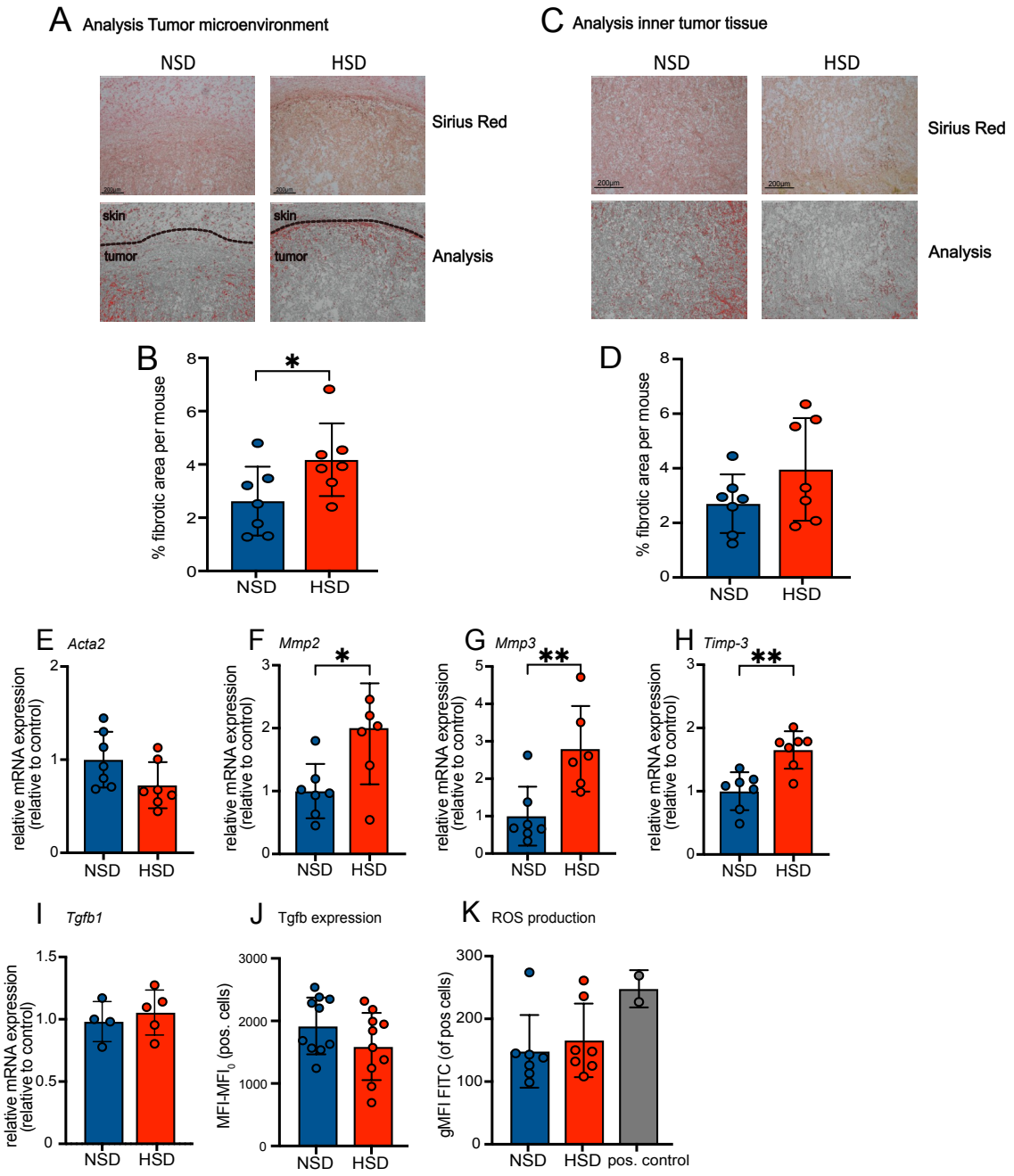

Figure 17: Melanoma cells under HSD trend towards more fibrosis. Fibrotic area was analyzed *via* Sirius Red staining of the inner tumor and the surrounding skin. Furthermore, fibrotic-related genes were investigated, as well as *Tgfb1* expression and ROS production. (A) Representative picture of Sirius Red staining of melanoma tissue and surrounding skin. (B) Quantification and statistical analysis of fibrotic area (n=7 mice/group). (C) Representative picture of Sirius Red staining of inner tumor environment. (D) Quantification and statistical analysis of fibrotic area in inner tumor without surrounding skin out of mice fed with either NSD or HSD (n=7 mice/group). (E) Gene expression analysis of smooth muscle actin alpha 2 (*Acta2,* n=7 mice/group). (F+G) Gene expression analysis of matrix metallopeptidase 2+3 (*Mmp2* + *Mmp3*, n=7 mice/group) as well as metallopeptidase inhibitor 3 (H, *Timp-3*, n=7 mice/group). (I)

Gene expression (n=5 mice/group) and (J) FACS analysis of transforming growth factor-beta 1 (TGF-β, n=10 mice/group)). (K) Intracellular ROS production (n=7 mice/group). Data shows mean ± SD of 3 independent experiments for Sirius Red analysis (A-D) which were analyzed with unpaired t-Test. Gene expression analysis as well as FACS analysis show 1-2 independent experiments which were analyzed with unpaired t-Test. * - $p<0.05$; **- $p<0.01$; ***- $p<0.001$.

3.3. HSD significantly diminishes tumor metabolism, particularly by reducing glycolysis

3.3.1. RNA sequencing data reveal downregulation of tumor metabolism and reduced cell cycle progression in melanoma cells after HSD

After having excluded several salt-specific modulators, the melanoma cells themselves were deeper analyzed. RNA sequencing data were generated to provide an overview of the changes in melanoma cells under HSD. RNA was isolated from tumor tissue after 14 days on either HSD or NSD and the sequencing was performed at the Next Generation Sequencing Core Facility (Figure 18, A). The RNA sequencing data revealed 9666 differentially expressed genes between HSD and NSD tumor cells (Figure 18, B). Gene Set Enrichment Analysis (GSEA) identified pathways that were significantly downregulated (Figure 18, C) or upregulated in melanoma cells after HSD (Figure 18, D). HSD was found to reduce the expression of genes involved in cell cycle progression (E2F targets, G2M checkpoints and less DNA repair), proliferation (Myc targets) and metabolic activity (oxidative phosphorylation, fatty acid metabolism and glycolysis) (Figure 18, C). On the other hand, HSD increased the expression of genes involved in the inflammatory responses (complement system, TNF-α response and protein secretion) as well as epithelial-to-mesenchymal transformation (EMT), coagulation and apoptosis in these melanoma cells (Figure 18, D).

In conclusion, the results of the RNA sequencing data indicated cell-intrinsic changes after HSD. In particular, excessive salt intake significantly downregulated genes that are mainly involved in metabolic activity and cell proliferation.

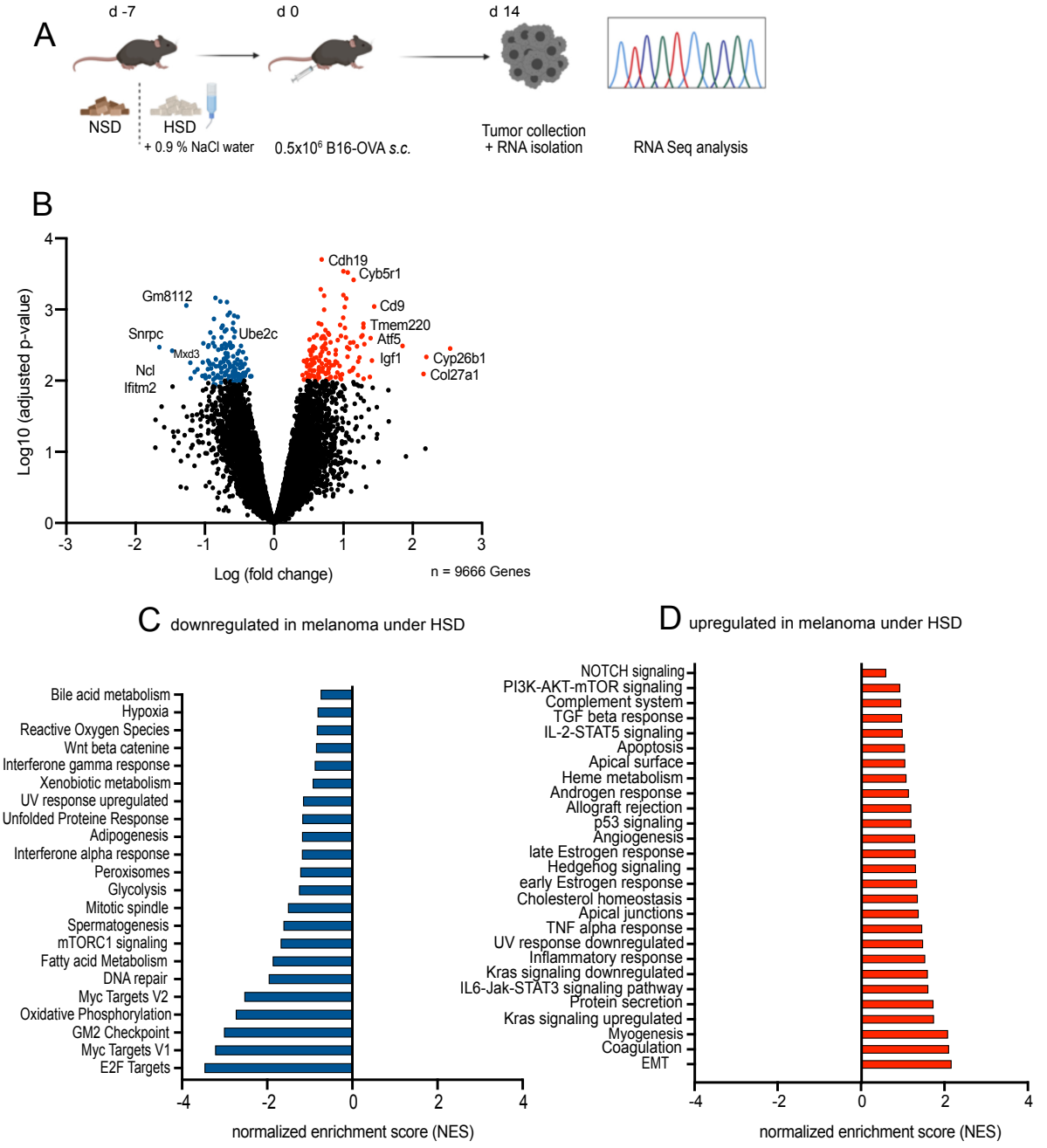

Figure 18: RNA sequencing data from melanoma cells under HSD and NSD. After isolation of tumor RNA from both groups, sequencing data were generated and analyzed. Differentially expressed genes were investigated and Gene Set Enrichment Analysis (GSEA) showed up-and downregulated pathways modulated by HSD. (A) Experimental Setup. (B) Volcano plot from differentially expressed genes. (C) GESA analysis of pathways either significantly downregulated (blue) or (D) upregulated (red) in melanoma cells under HSD. Data were generated from 1 experiment with 5 mice per group and diet. RNA sequencing was performed by A. Heimbach and analyzed with the help of M. Hölzel.

3.3.2. HSD has no impact on mTOR activity and Hif-1α production

Initial RNA sequencing data indicated that HSD significantly upregulates genes of pathways known to promote tumorigenesis. One of the most prominent pathways is the PI3K/AKT pathway which further activates the mammalian target of rapamycin (mTOR) kinase. Overactivation of mTOR leads to massive cell proliferation and survival (Pópulo, Lopes, and Soares 2012; Saxton and Sabatini 2017). To test whether HSD modulates mTOR activity, intracellular mTOR expression was measured in melanoma cells from both investigated groups. Contrary to what was shown in the RNA sequencing data, no difference in *Mtor* mRNA expression was detected in melanoma under HSD (Figure 19, A). The results were confirmed by FACS analysis (Figure 19, B) as well as Western blot, showing similar protein levels of mTOR expression in melanoma cells from HSD *versus* NSD mice (Figure 24, C+D). Although no differences in mTOR expression were found, HSD could activate the phosphorylation of mTOR. However, comparable levels of phosphorylated mTOR (p-mTOR) were measured by FACS (Figure 19, E) and Western blot (Figure 19, F+G). It has been shown that the transcription factor hypoxia-inducible factor 1-alpha (Hif-1α) and its target genes are activated by mTOR in the renal medulla in response to HSD (Z. Wang et al. 2010). Examination of *Hif-1α* gene expression in melanoma cells under HSD did not reveal any changes compared to the control group (Figure 19, H). Furthermore, similar protein levels of Hif-1α were measured in melanoma cells under HSD compared to the control diet (Figure 19, I+J).

Contrary to RNA sequencing data, HSD did not change the activation and phosphorylation of mTOR. Moreover, excessive salt intake did not affect Hif-1α expression.

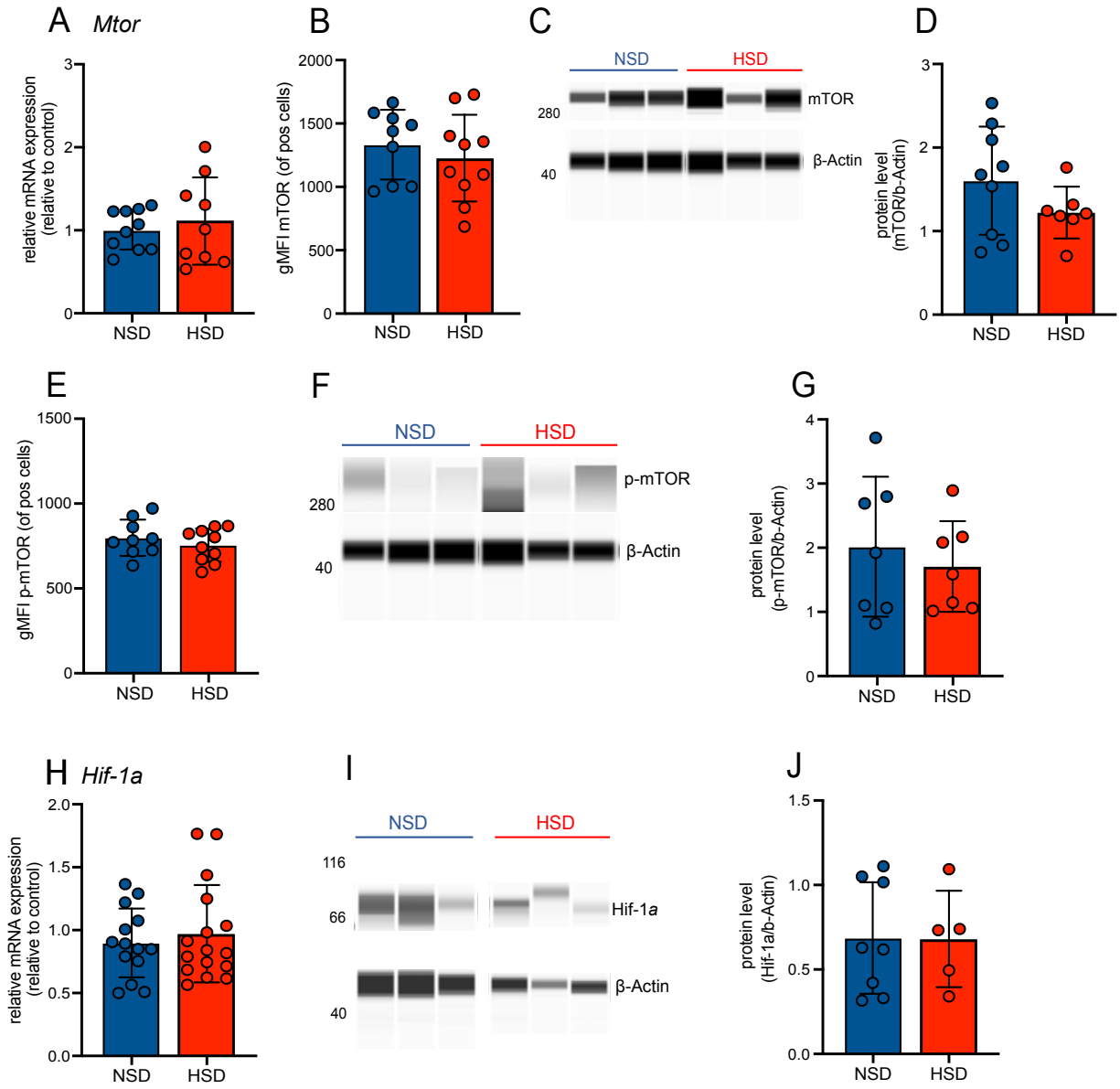

Figure 19: HSD has no effect on the expression of mTOR and Hif-1α. Melanoma cells were harvested from mice on either HSD or NSD after 14 days and further analyzed for their gene and protein levels. (A) Gene expression analysis of *Mtor* (n=10 mice/group). (B) FACS analysis of mTOR expression in tumor cells under HSD and NSD (n=10 mice/group). (C) Western blot of mTOR protein level and (D) statistical analysis of mTOR protein level (n=7-9 mice/group). (E) FACS analysis of phosphor-mTOR expression in tumor cells under HSD and NSD (n=10 mice/group). (F) Western blot of phosphor-mTOR and (G) statistical analysis of p-mTOR protein level (n=7 mice/group). (H) Gene expression analysis of *Hif1-*α in tumor cells under NSD and HSD (n=16 mice/group). (I) Western blot of Hif-1α levels and (J) statistical analysis of Hif-1α protein level (n=5-8 mice/group). Data show mean ± SD of 2-3 independent experiments and analyzed by unpaired t-Test. * - p<0.05; **- p<0.01; ***- p<0. 001.

3.3.3. HSD significantly impairs the metabolic activity of tumor cells

Further analysis of the RNA sequencing data indicated that HSD significantly downregulates genes involved in the metabolic activity of tumor cells. Deregulation of metabolic processes is one of the Hallmarks of Cancer, where cancer cells reprogram their glucose metabolism and thus their energy production (Hanahan and Weinberg 2011; WARBURG 1956). To examine whether HSD alters the metabolism of melanoma cells on a functional level, Seahorse® analysis was performed. Single-cell suspensions of tumors from HSD and NSD animals were seeded into a specific Seahorse® 96-well plate and the extracellular acidification rate (ECAR) and oxygen consumption rate (OCR) were measured (Figure 20, A+E). Melanoma cells from HSD-fed mice showed significantly lower glycolysis (Figure 20, B), lower glycolytic capacity (Figure 20, C) and lower glycolytic reserve activity (Figure 20, D) than cells of the control group. Based on the measured oxygen consumption rates (Figure 20, E), tumor cells under HSD also showed reduced basal mitochondrial respiration (Figure 20, F), a strong trend towards less ATP production (Figure 20, G), less maximal respiration (Figure 20, H), and significantly less spare respiratory capacity (Figure 20, I). In parallel with high glycolytic activity, elevated glucose also stimulates protein synthesis in most cells, including tumor cells (Jeyapalan et al. 2007; Avagliano et al. 2020). The protein synthesis rate of melanoma cells under HSD was measured by using the SCENITH assay. Cells were incubated with fluorescence-labeled puromycin, which will be taken up by cells and used during the protein synthesis. Melanoma cells under HSD showed significantly less puromycin incorporation than cells of the control group indicating less activity of protein synthesis (Figure 20, J+K).

In conclusion, confirming the previous results from RNA sequencing, melanoma cells under HSD performed significantly less glycolysis and oxidative phosphorylation than control cells, suggesting an impairment in the metabolic activity of the cells. In addition, HSD reduced the protein synthesis in these cells. Taken together, the reduced metabolic activity and reduced protein synthesis might be the cause of the reduced tumor growth under HSD.

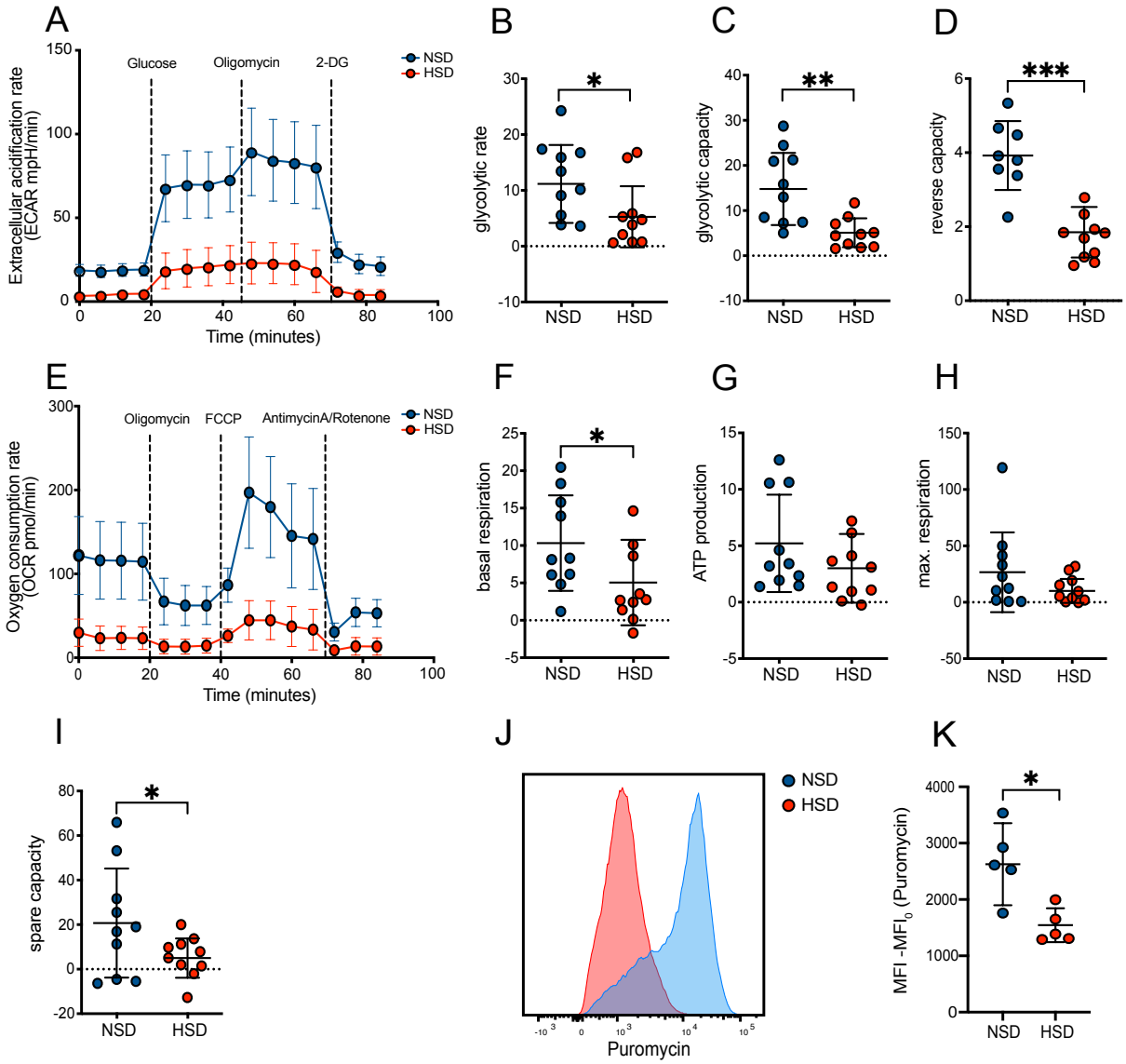

Figure 20: HSD significantly slows down tumor metabolism. Melanoma cells were analyzed for their energy production. Seahorse® analysis revealed changes in the glycolytic capacity as well as mitochondrial respiration in melanoma cells under HSD. In addition, protein synthesis was significantly reduced in tumor cells after excessive salt intake. (A) Seahorse® analysis of extracellular acidification rate (ECAR). (B) Analysis of glycolytic capacity, glycolytic capacity (C) and reverse capacity (D). (E) Seahorse® analysis of oxygen consumption rate (OCR). (F) Basal respiration and (G) ATP production of melanoma cells under HSD vs. NSD. (H) Maximal respiration as well as (I) spare capacity analysis. (J) Histogram of intracellular puromycin signal. (K) Statistical analysis of intracellular puromycin level (n=5 mice/group). Seahorse® experiments were done with the help of V. Schmitt. Data show mean ± SD of 3 independent experiments with 10 mice/group for Seahorse® assay (A-I) and analyzed by unpaired t-Test. Puromycin assay was performed once and data were analyzed by unpaired t-Test. * - $p<0.05$; **- $p<0.01$; ***- $p<0.001$.

3.3.4. Melanoma cells under HSD are able to take up more glucose while simultaneously reducing fatty acid uptake

As HSD impaired tumor metabolism, the question was addressed whether HSD might cause dysfunction in nutrient uptake. For this purpose, melanoma cells were collected from mice fed with HSD or NSD. The single-cell suspension was incubated with fluorescent-labeled glucose (2-NBDG) to examine the ability of the cells to take up glucose. FACS analysis revealed a significant increase in the uptake of glucose by melanoma cells under HSD compared to NSD cells (Figure 21, A+B). Interestingly, gene expression analysis of the glucose transporters 1 and 3 (*Slc2a1 and Slc2a3*) did not show a difference in mRNA levels between HSD and NSD (Figure 21, C+D). In addition, the influence of HSD on the uptake of fatty acids was investigated. Melanoma cells were incubated with a fluorescent-labeled fatty acid derivate (BODIPY-FL C_{16}) and the uptake was measured by FACS. In contrast to the increase in glucose uptake, HSD significantly diminished the uptake of long-chain fatty acids by tumor cells compared to NSD (Figure 21, E+F). However, similar mRNA expression levels of the fatty acid transporters were detected in both investigated groups (*Slc27a1*-*Slc27a6*, Figure 21, G-L). Analysis of the large neutral amino acid transporter (*Lat1*) consisting of heavy subunit (*Slc23a1*) and light subunit (*Slc7a5*), showed no differences in the mRNA level of the heavy subunit *Lat1* (Figure 21, M) but a significant increase in the mRNA level of the light subunit of *Lat1* upon HSD (Figure 21, N).

In conclusion, HSD increased the uptake of glucose and decreased the uptake of long-chain fatty acids in comparison to NSD, without affecting the mRNA levels of the respective nutrient transporters.

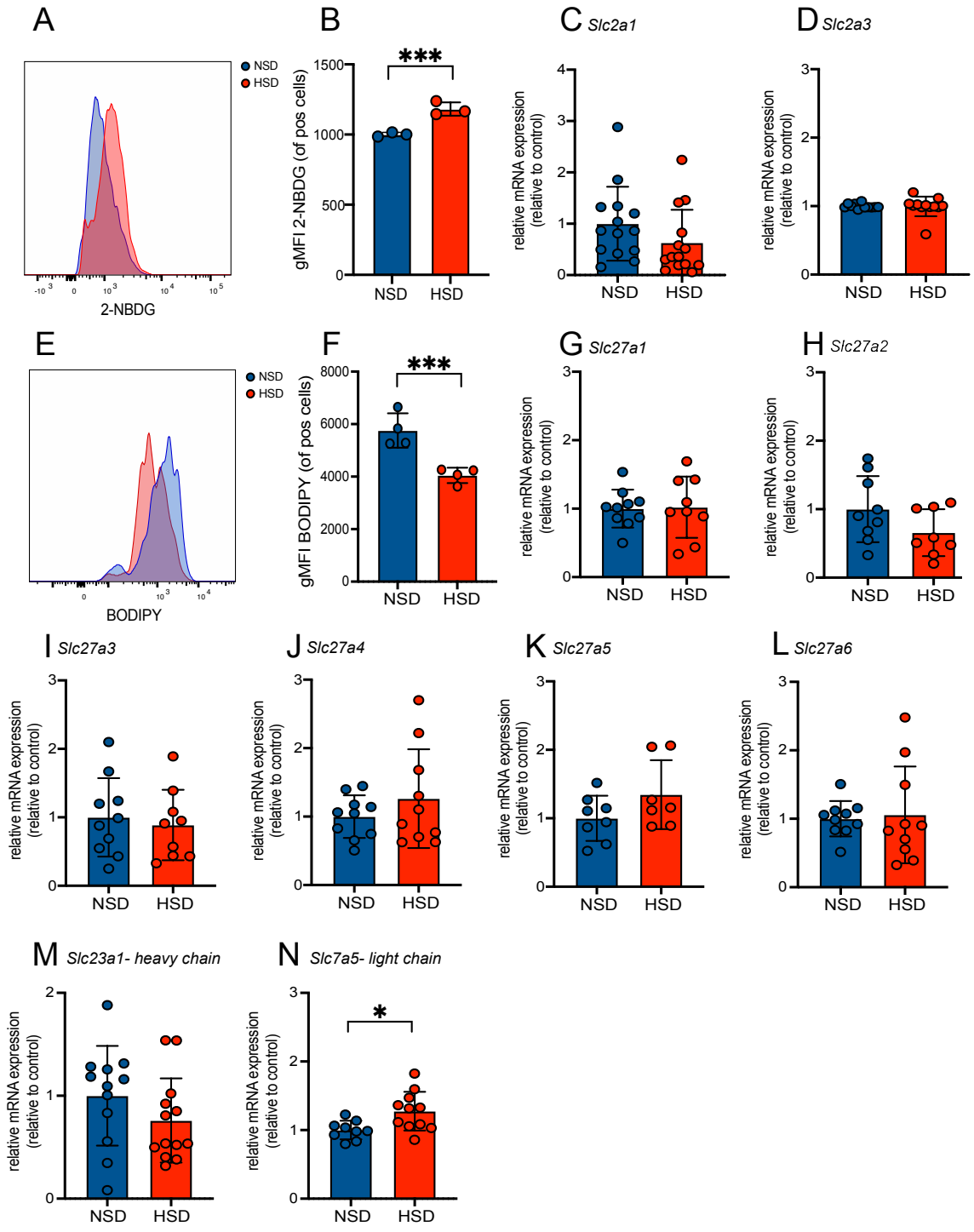

Figure 21: Nutrient uptake of melanoma cells under HSD. The capacity of nutrient uptake was examined by FACS. Glucose uptake was significantly increased while fatty acid insult was decreased. Gene expression analysis showed no further differences between HSD and NSD melanoma cells. (A) Representative histogram of intracellular 2-NDBG signal and (B) statistical analysis (n=3 mice/group). (C) Gene expression analysis of glucose transporter *Glut1* and (D) *Glut3* (n=10 mice/group). (E) Representative histogram of intracellular BODIPY signal in melanoma cells from HSD

versus NSD and (F) statistical analysis (n=4 mice/group). (G)–(L) Gene expression analysis of fatty acid transporter family (*Fatp*, n=7-10 mice/group). (M)+(N) Gene expression analysis of amino acid transporter (*Lat1*, n=7-10 mice/group). Data show mean ± SD of 1-2 independent experiments and analyzed by unpaired t-Test. * - p<0.05; **- p<0.01; ***- p<0. 001.

3.3.5. HSD does not impair mitochondrial function

Previous findings indicated that HSD diminishes glycolysis activity in melanoma cells and trends towards less mitochondrial respiration capacity. One possible explanation could be that HSD impairs the tricarboxylic acid cycle (TCA) and further diminishes the energy generation *via* the electron transport chain. To test this, melanoma cells were harvested from mice under HSD and NSD after 14 days and mitochondrial mass was quantified. Comparable levels of MitoTracker were detected in tumor cells from both investigated groups, indicating no changes in total mitochondrial mass upon HSD (Figure 22, A). Furthermore, tumor cells from both diet groups were stained with JC-1 to indicate changes in membrane potential. Melanoma cells under HSD showed a similar ratio of JC-1 compared to the control group, implying no defects in mitochondrial fitness (Figure 22, B). Next, the metabolites involved in the TCA cycle were examined by analyzing intracellular metabolome compounds. A similar metabolite composition was found in melanoma cells under HSD compared to NSD (Figure 22, C). To get a closer look of the electron transport chain, the individual complexes were analyzed on their gene levels. Overall, comparable levels of relative mRNA expression were measured for complex I (NADH-dehydrogenase) and complex II (succinate dehydrogenase) between HSD and NSD. Analysis of complex III (ubiquinol-cytochrome c reductase) showed significantly lower mRNA expression in tumor cells after HSD. Complex IV (cytochrome c oxidase), as well as complex V (ATP synthase), were unchanged on their gene level between HSD and NSD (Figure 22, D). Both pathways are connected *via* the succinate dehydrogenase, which is an enzyme in the TCA cycle and functions as complex II of the respiratory chain. Based on the reduced gene expression, complex II and complex III were further investigated. Melanoma cells were homogenized and mitochondria were obtained by buffer-based isolation. Similar levels of complex II and complex III activity were detected in mitochondria out of tumor cells after both diet forms (Figure 22, E+F).

In conclusion, HSD did not alter the totality of mitochondrial mass and its membrane potential. No changes in the metabolite composition were detected in melanoma cells under HSD. Slightly reduced gene expression was found in complex II and complex III of the electron transport chain in melanoma cells under HSD but its activity was not impaired.

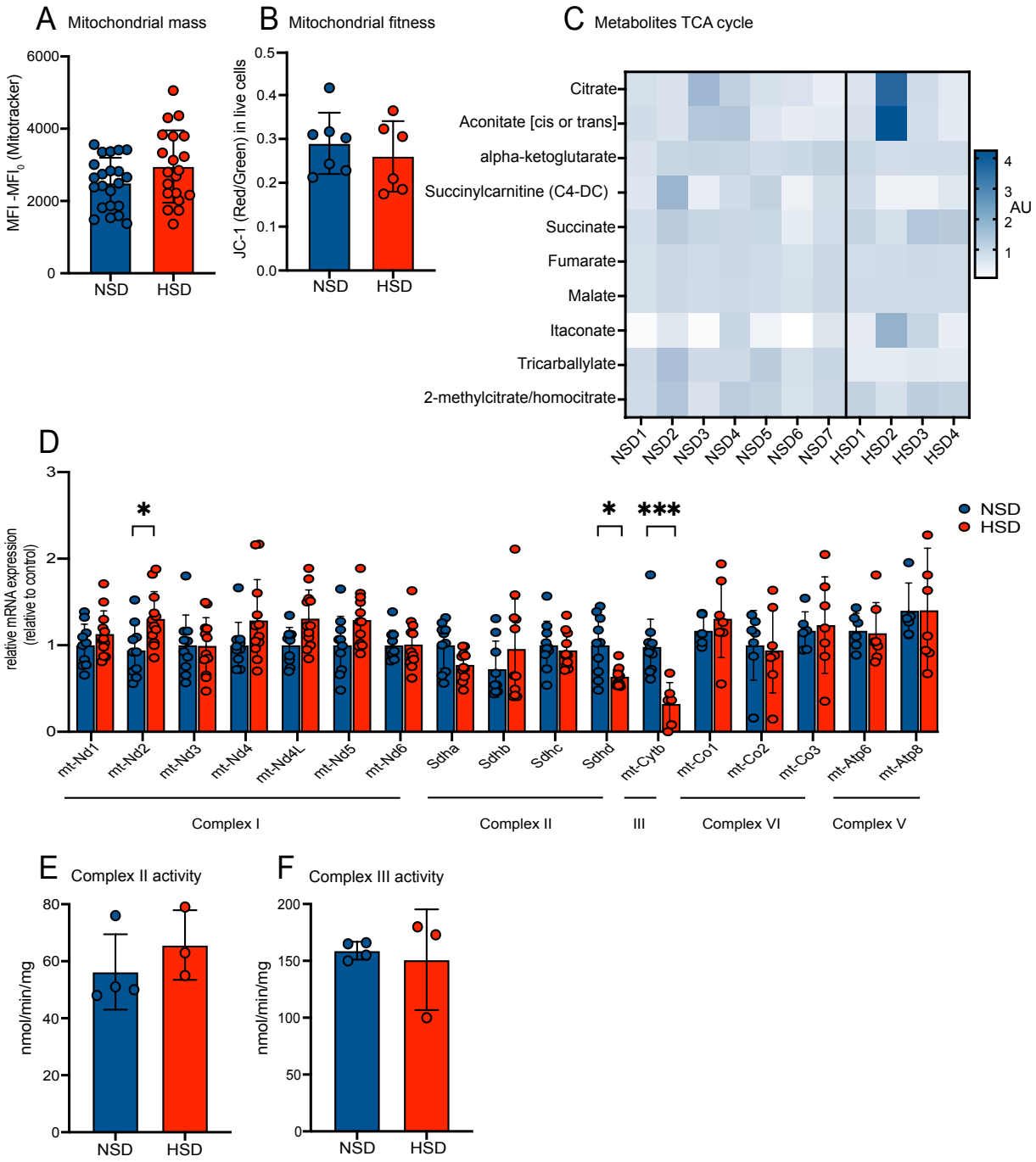

Figure 22: HSD does not affect mitochondrial mass and its functionality. (A) Quantification of mitochondrial mass using MitoTracker in melanoma cells under NSD

(blue) *versus* HSD (red) (n=20 mice/group). (B) JC-1 ratio in live melanoma cells under HSD vs. NSD (n=7 mice/group). (C) Metabolome analysis of metabolites involved in the TCA cycle. (D) Gene expression analysis of mitochondrial complexes (n=12 mice/group). (E) Analysis of complex II and (F) complex III activity of isolated mitochondria of both investigated groups. Each point represents 5 pooled mice. (E) +F). Complex activity was done with the help of T. Becker and M. Eckhard. Data show mean ± SD of 2 independent experiments and analyzed by unpaired t-Test * - $p<0.05$; **- $p<0.01$; ***- $p<0.001$.

3.3.6. Metabolome analysis reveals accumulation of metabolites involved in carbohydrate pathways in melanoma under HSD

Previous experiments have shown that HSD significantly reduces melanoma growth through less metabolic activity and lower protein synthesis. While a connection between reduced metabolic activity and reduced tumor growth is likely, it remained unclear how HSD caused the loss of metabolic activity. One possible explanation could be limited metabolite availability during HSD. To test this, melanoma cells were collected after 14 days under HSD and NSD and the metabolite composition was analyzed (Figure 23, A). METABOLON® analysis revealed changes in metabolites, necessary for carbohydrate synthesis, nucleotide as well as amino acid metabolism, whereas lipid compositions remained unchanged in melanoma cells under HSD (Figure 20, B) Detailed analysis of the carbohydrate synthesis pathway showed a significant increase in glucose and glucose 6-phosphate in melanoma cells under HSD compared to NSD (Figure 23, C). Moreover, elevated levels of metabolites involved in the pentose phosphate pathway were detected in melanoma during HSD (Figure 23, D). In addition to that, metabolites associated with the nucleotide sugar pathway were significantly increased in melanoma under HSD (Figure 23, E).

Taken together, melanoma cells under HSD showed an accumulation of metabolites essential for glycolysis. Furthermore, increased levels of intermediates involved in the pentose phosphate pathway and nucleotide sugar metabolism were found in melanoma cells after excessive salt intake.

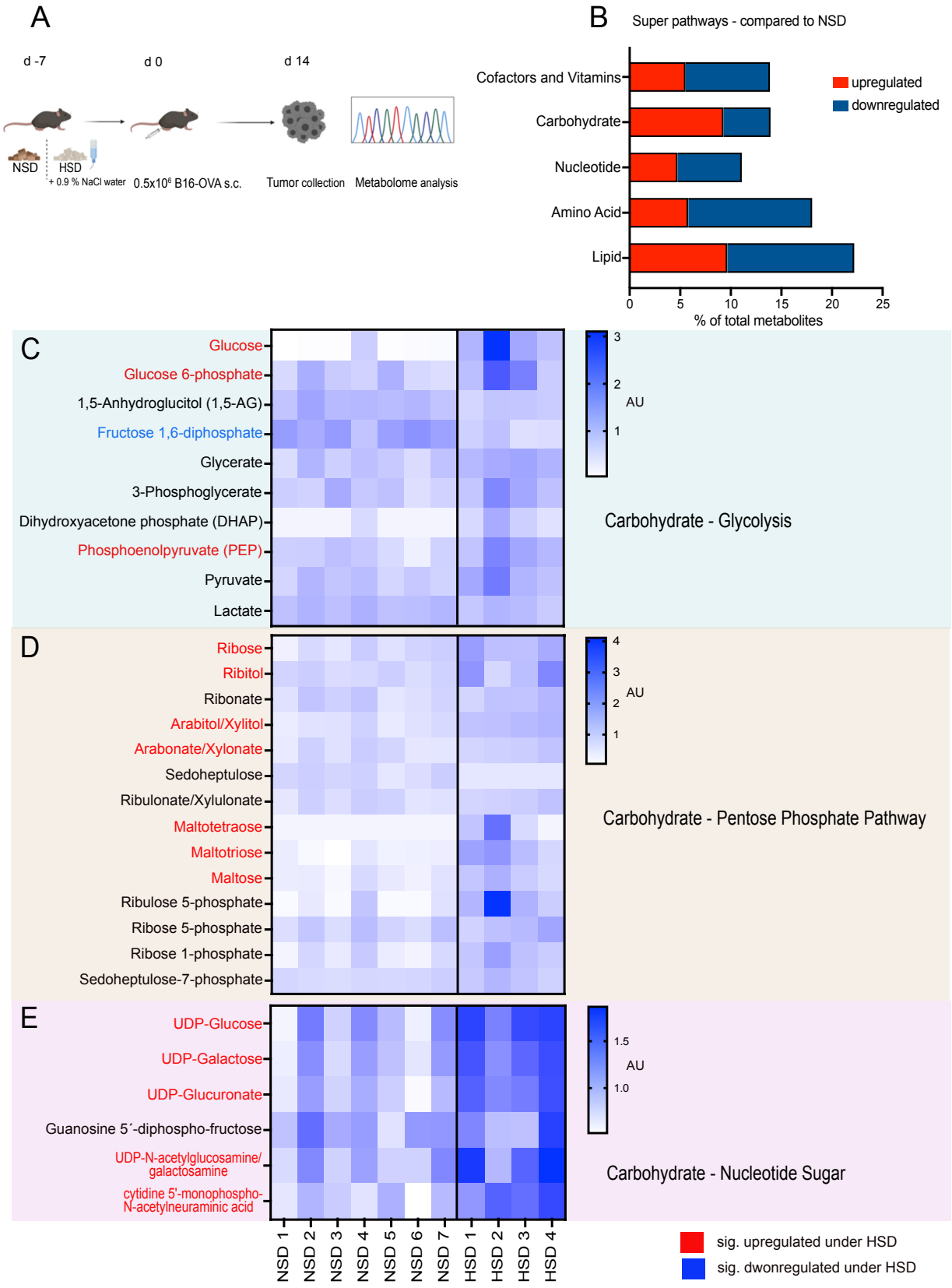

Figure 23: Melanoma cells under HSD accumulate metabolites involved in carbohydrate pathways. (A) Experimental setup. (B) Changes in super pathways in

melanoma cells under HSD in comparison to NSD. (C) METABOLON data show increased levels of several metabolites crucial for glycolysis, pentose phosphate pathways (D) and nucleotide sugar pathway. Data represented one experiment and was analyzed with 2way ANOVA.

3.3.7. HSD reduced the gene expression of enzymes involved in glycolysis

RNA sequencing data revealed downregulation of genes involved in glycolysis, Seahorse® assays confirmed this on a functional level and METABOLON® data showed an accumulation of metabolites crucial for carbohydrate metabolism. For deeper analysis, enzymes of the glycolysis pathways were examined for their gene expression level. HSD significantly decreased the gene expression of the first enzyme Hexokinase 1 and 2 (*Hk1* and *Hk2*) (Figure 24, A+B). Examination of Aldolase A (*Aldoa*) mRNA levels showed no changes in melanoma cells under HSD and NSD (Figure 24, C). Gene expression analysis of Phosphofructokinase (*Pfk*), Triosephosphate isomerase 1 (*Tpi1*) as well as Phosphoglycerate kinase 1 (*Pgk1*), were significantly downregulated in melanoma cells after excessive salt intake (Figure 24, D-F), whereas Phosphoglucomutase 2 (*Pgm2*) mRNA levels were not affected (Figure 24, G). Furthermore, Enolase (*Eno*) gene expression was significantly downregulated in melanoma cells under HSD (Figure 24, H). Finally, equal levels of Pyruvate dehydrogenase A (*Pdha*) and Lactate dehydrogenase A (*Ldha*) were measured in melanoma cells under HSD compared to NSD (Figure 24, I+J).

In conclusion, HSD significantly downregulated gene expression of several enzymes involved in glycolysis. In particular, the key glycolysis rate-limiting enzymes, *Hk1, Hk2* and *Pfk*, were significantly downregulated in melanoma cells under HSD.

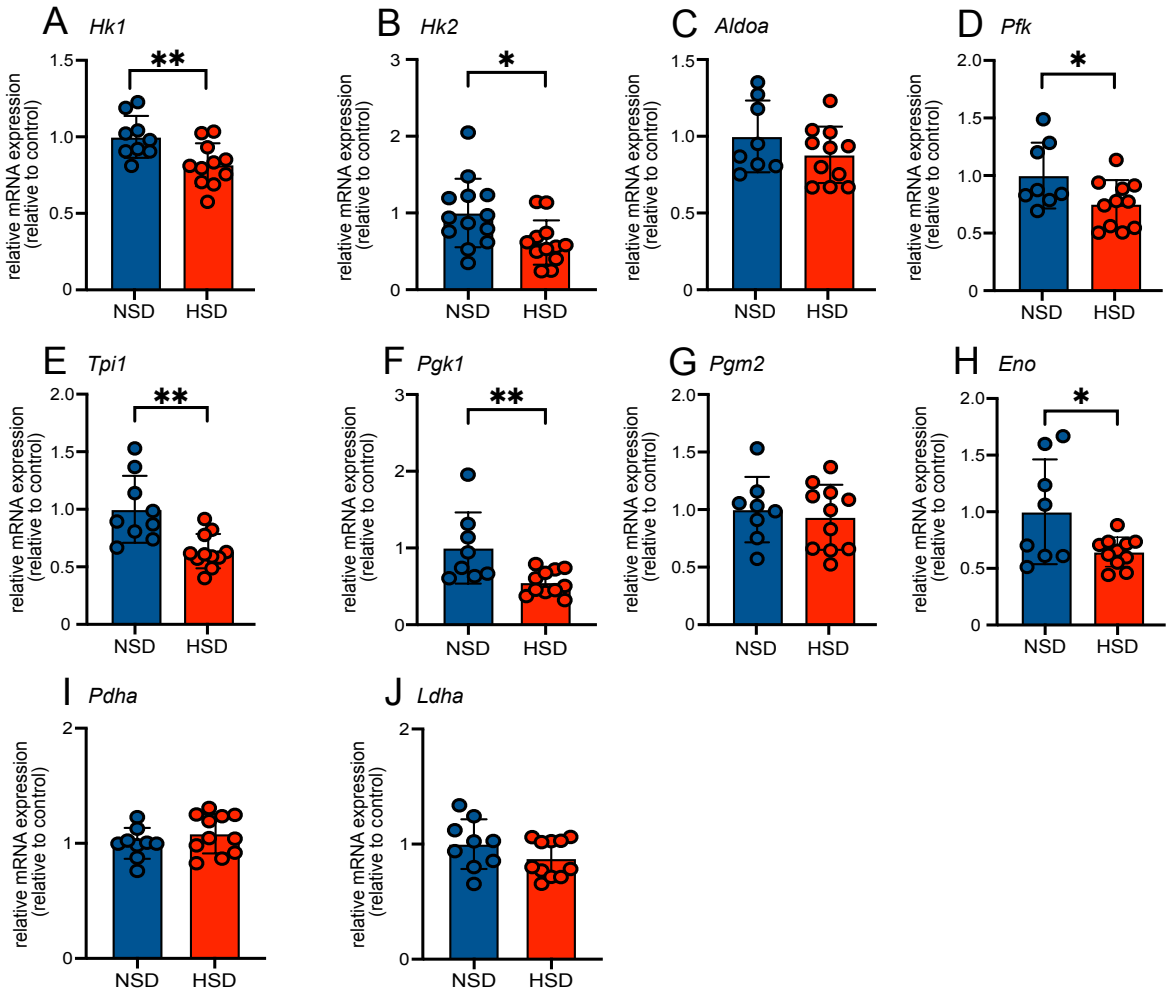

Figure 24: HSD significantly reduces mRNA expression of enzymes involved in glycolysis. (A) Gene expression analysis of Hexokinase 1 (*Hk1*, n=9 mice/group). (B) Gene expression analysis of Hexokinase 2 (*Hk2*, n=12 mice/group). (C) Gene expression analysis of Aldolase A (*Aldoa*, n=.9 mice/group). (D) Gene expression analysis of Phosphofructokinase (*Pfk*, n=9 mice/group). (E) Gene expression analysis of Triosephosphate isomerase 1 (*Tpi1*, n=9 mice/group). (F) Gene expression analysis of Phosphoglycerate kinase 1 (*Pgk1*, n=9 mice/group). (G) Gene expression analysis of Phosphoglucomutase 2 (*Pgm2*, n=9 mice/group). (H) Gene expression analysis of Enolase (*Eno*, n=9 mice/group). (I) Gene expression analysis of Pyruvate dehydrogenase A (*Pdha*, n=11 mice/group). (J) Gene expression analysis of Lactate dehydrogenase A (*Ldha*, n=11 mice/group). Data show mean ± SD of 2 independent experiments and analyzed by unpaired t-Test. * - p<0.05; **- p<0.01; ***- p<0. 001.

3.4. HSD-mediated tumor reduction specifically affects melanoma growth by promoting melanogenesis

3.4.1. HSD promotes melanin biosynthesis in B16 melanoma cells

Melanoma cells under HSD showed impaired energy metabolism, especially a downregulation of glycolysis. To determine the underlying mechanisms between HSD, the decrease in metabolic activity and the resulting tumor reduction, the proteome of the melanoma cells was analyzed. Tumor tissue was collected from mice under HSD or NSD after 14 days. Using MACS isolation, tumor tissue was depleted of immune cells and the proteome was analyzed *via* mass spectrometry (Figure 25, A). Proteome analysis revealed 6197 proteins differentially expressed between melanoma cells under HSD and NSD (Figure 25, B). Protein Set Enrichment Analysis (PSEA) revealed a significant increase in proteins involved in melanin biosynthesis, melanosome formation, and tyrosine metabolism under HSD (Figure 25, C).
In conclusion, HSD significantly enhanced proteins necessary for melanogenesis-related processes in melanoma.

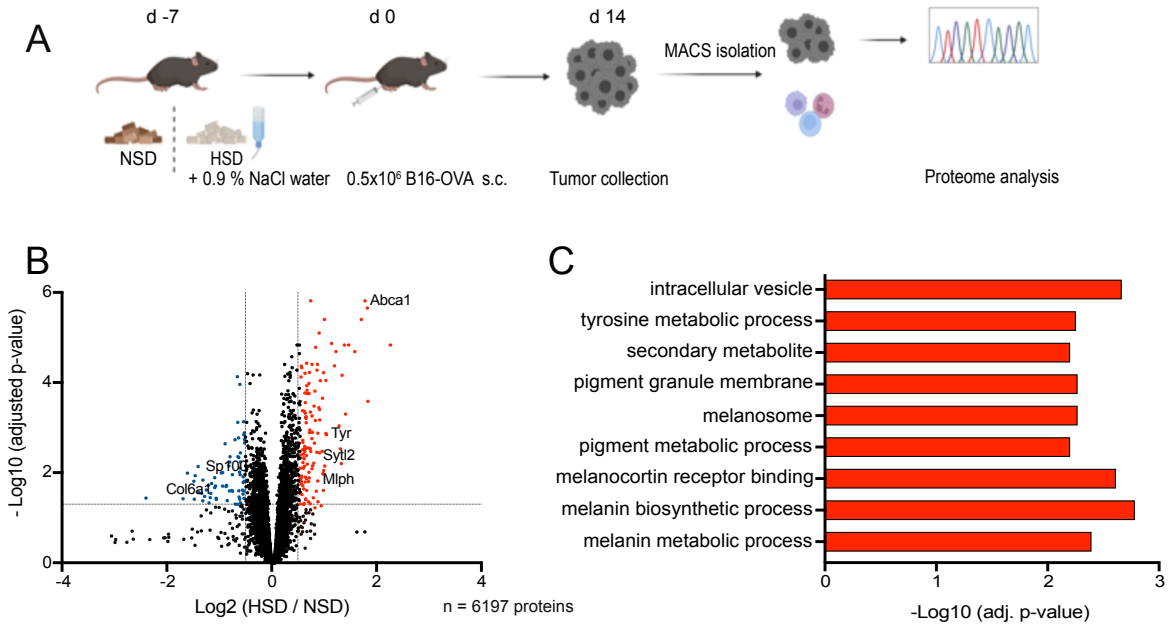

Figure 25: HSD upregulates proteins involved in melanogenesis. Melanoma cells were harvested from mice on HSD or NSD after 14 days and tumor cells were purified by

MACS isolation. Proteomics was performed by mass spectrometry by our collaborators. (A) Experimental setup. (B) Volcano plot of up- and downregulated proteins under HSD. (C) Analysis of upregulated processes of isolated melanoma under HSD. Proteomics was done with the help of C. Münch and S. Bozkurt. Data represents 1 experiment with 10 mice per group.

3.4.2. HSD significantly increases modulators required for melanogenesis

Analysis of the protein composition of melanoma cells under HSD revealed an increase in melanogenesis activity in these cells. Researchers found a connection between increased melanogenesis and anti-proliferative effects in B16 murine melanoma cells (Smalley and Eisen 2000). As described in detail in section 1.5. during melanogenesis, the alpha-melanocyte stimulating hormone (α-MSH) binds to its receptor (Mc1r) on melanocytes as well as melanoma and activates downstream the transcription of the master regulator *Mitf*. The transcription factor leads to the conversion of tyrosine to melanin *via* the enzyme *tyrosinase*. To further analyze melanogenesis activity during HSD, blood and tumor tissue were collected from mice on HSD and NSD after 14 days and were further investigated. Analysis of α-MSH levels in the serum of mice under HSD revealed significantly lower α-MSH levels in comparison to the control diet (Figure 26, A). Metabolome data indicated a significant increase of tyrosine and its isomer o-tyrosine in melanoma under HSD compared to NSD (Figure 26, B). Moreover, melanoma cells under HSD showed significantly higher *Mc1r* mRNA expression compared to the control group (Figure 26, C). In line with this, Western blot analysis of isolated tumor cells revealed significantly elevated protein levels of Mc1r in melanoma under HSD (Figure 26, D+E). Moreover, significantly increased *Mitf* mRNA expression and protein levels were measured in tumor cells under HSD compared to NSD (Figure 26, F-H). *Tyrosinase* (*Tyr*) mRNA expression, the key enzyme for melanogenesis, was significantly increased in melanoma cells when exposed to HSD (Figure 26, I). RNA sequencing data of genes regulated by *Mitf* showed a trend toward downregulation of genes involved in cell cycle progression, cell proliferation and cell survival. On the other hand, genes encoded for cell differentiation were slightly increased in melanoma cells under HSD compared to NSD (Figure 26, J).

In summary, HSD reduced serum levels of α-MSH, but significantly upregulated key regulators involved in the melanogenesis pathway.

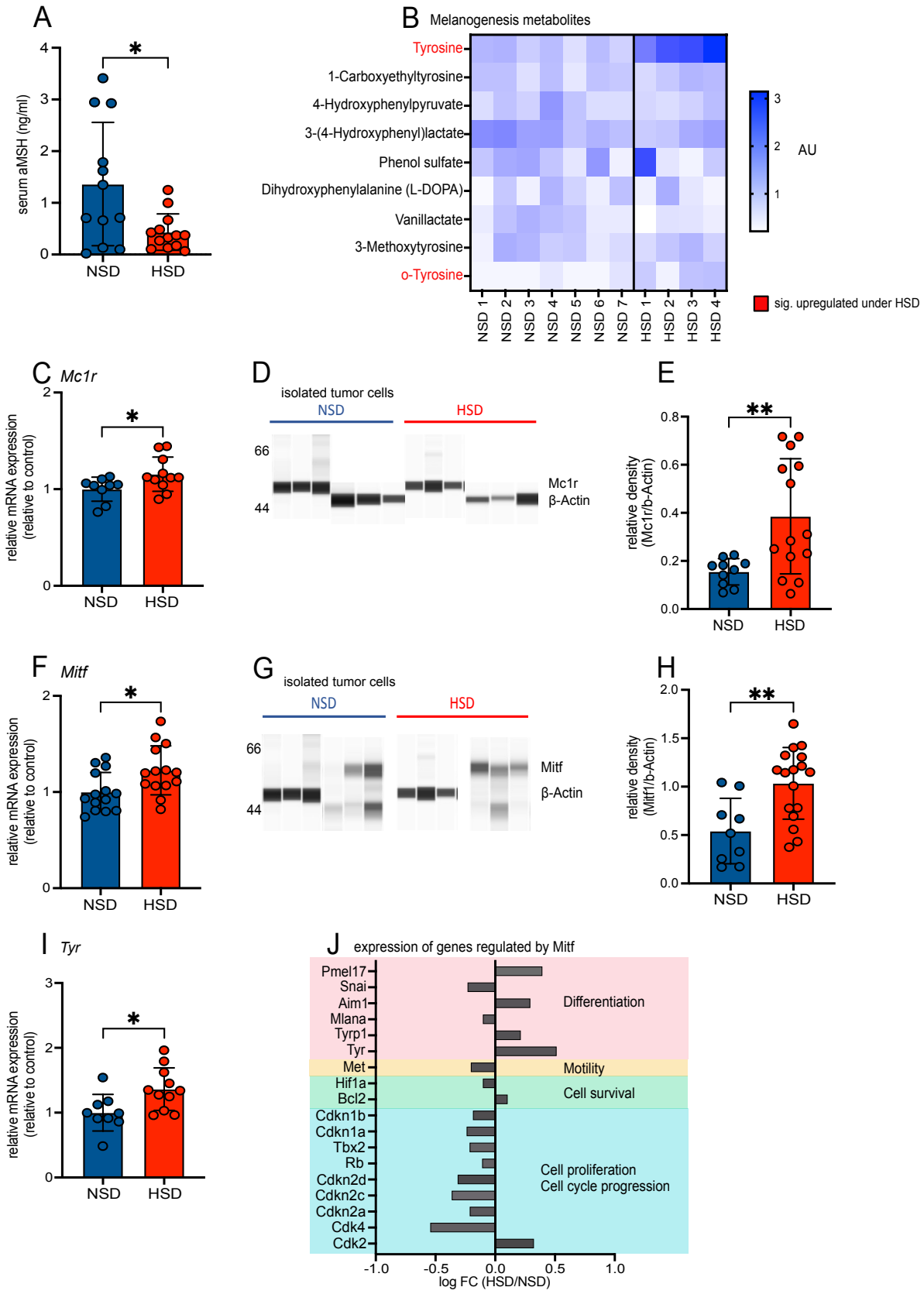

Figure 26: HSD significantly increases melanogenesis-associated molecules. Tumor cells were harvested after 14 days from mice fed either with HSD or NSD. Modulators

involved in melanogenesis were investigated by Western Blot and RT-PCR. (A) Gene expression analysis of Melanocortin 1 receptor (*Mc1r*, n=11 mice/group). (B) Representative example of Western blot analysis of Mc1r in isolated tumor cells and (C) statistical analysis of Western blot of Mc1r (n=10-14 mice/group). (D) Gene expression analysis of melanogenesis associated transcription factor (*Mitf*, n=14 mice/group). (E) Representative image of Western blot analysis of Mitf in isolated tumor cells and (F) statistical analysis of Mitf expression based on Western blot (n=10-14 mice/group). (G) Gene expression analysis of dopachrome tautomerase (*Dct*, n=10 mice/group). (H) Gene expression analysis of tyrosinase-related protein (*Tyrp1*, n=10 mice/group). (I) Gene expression analysis of tyrosinase (*Tyr*, n=10 mice/group). (J) Metabolome data of tyrosine pathway. Red-marked metabolites were significantly upregulated in melanoma cells under HSD. (K) ELISA of serum a-MSH levels in mice under HSD vs. NSD (n=14 mice/group). Data show mean ± SD of 2-3 independent experiments and analyzed by unpaired t-Test. * - p<0.05; **- p<0.01; ***- p<0. 001.

3.4.3. Melanoma cells lacking tyrosinase growth similar under high salt conditions compared to control cells *in vitro*

Melanoma cells under HSD showed increased melanogenesis activity by higher mRNA levels of the master transcription factor *Mitf*. Moreover, proteome analysis as well as RNA sequencing data revealed an upregulation of tyrosinase, the key enzyme in melanin synthesis. To prove that salt-mediated tumor reduction is dependent on melanogenesis, melanoma cells lacking tyrosinase (B16-TyrKO) were generated and treated *in vitro* as described in section 2.2.28. Briefly, 0.1 x10^5 B16-TyrKO cells were seeded into each well of a 12-well plate and cultured either in regular medium, under high sodium (HS), or under high Mannitol (Man) conditions. The confluence of these cells was measured daily and the media was refreshed every other day (Figure 27, A). Until day 7, a similar increase in cell confluence could be observed in all three groups (Figure 27, B). Then B16-TyrKO cells under Man cells started to grow less compared to the control group, which was significant from day 8 until the end of the experiment. Interestingly, B16-TyrKO cells under high sodium showed a similar cell growth compared to the control cells. In addition, a significant difference between B16-TyrKO cells under HS and Man was measured on days 10 and 11 of the experiment. However, B16-TyrKO cells did not reach 100 % of confluence as they started to be confluent and detached due to media change.

In conclusion, B16-TyrKO cells under high sodium showed similar cell proliferation compared to the control cells. This may strengthen the theory, that HSD promotes melanogenesis in B16 melanoma and thereby stopping cell proliferation.

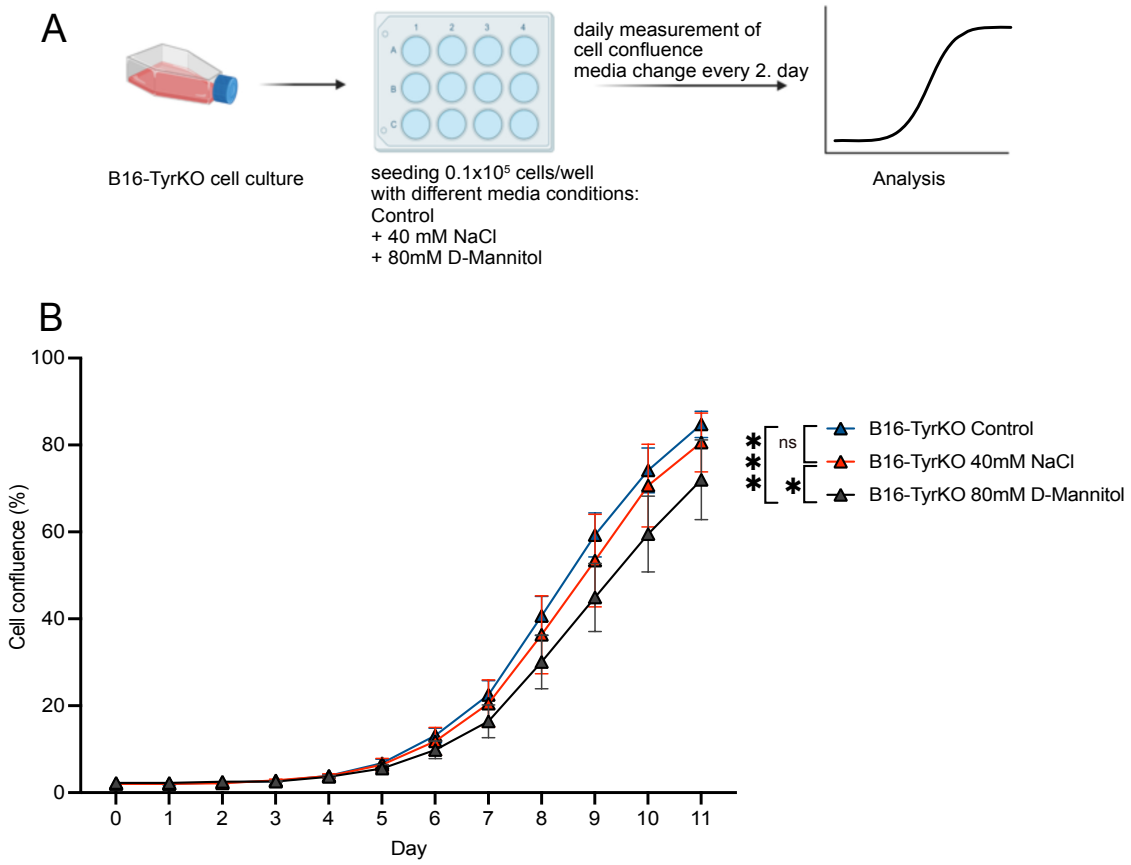

Figure 27: Melanoma cells lacking tyrosinase activity growth similar under high sodium compared to control cells. 0.1 x 10^5 B16-TyrKO cells were seeded into a 12-well plate under different media conditions: control media, high sodium (+ 40 mM NaCl) or D-Mannitol (+ 80 mM). Cell confluence was daily measured *via* Tecan and media was changed every second day. (A) Experimental setup. (B) Quantification of cell confluence (%). Data show mean ± SD of 3 independent experiments and analyzed with 2-way ANOVA. * - p<0.05; **- p<0.01; ***- p<0. 001.

3.4.4. HSD does not affect tumor growth in other epithelial-derived cancers

To prove the hypothesis, that HSD reduced melanoma proliferation by promoting melanogenesis, the experiment was repeated by using another murine cancer model which is not capable of melanogenesis. CCL79 tumor cells are murine epithelial-derived

cancer cells isolated from the adrenal gland (ATCC). Mice were placed on either HSD or control diet one week prior to tumor injection. Then 0.5 x 10^6 CCL79 cells were injected *subcutaneously* into the mice and tumor volume was monitored for 14 days (Figure 28, A). Mice under NSD showed a continuous increase in tumor volume over the experimental period. Surprisingly, mice on HSD showed similar tumor formation compared to the control diet (Figure 28, B).

In conclusion, HSD specifically inhibited melanoma growth but apparently no other epithelial-derived tumors. These results supported the hypothesis that HSD limits the growth of B16 tumors by promoting melanin biosynthesis.

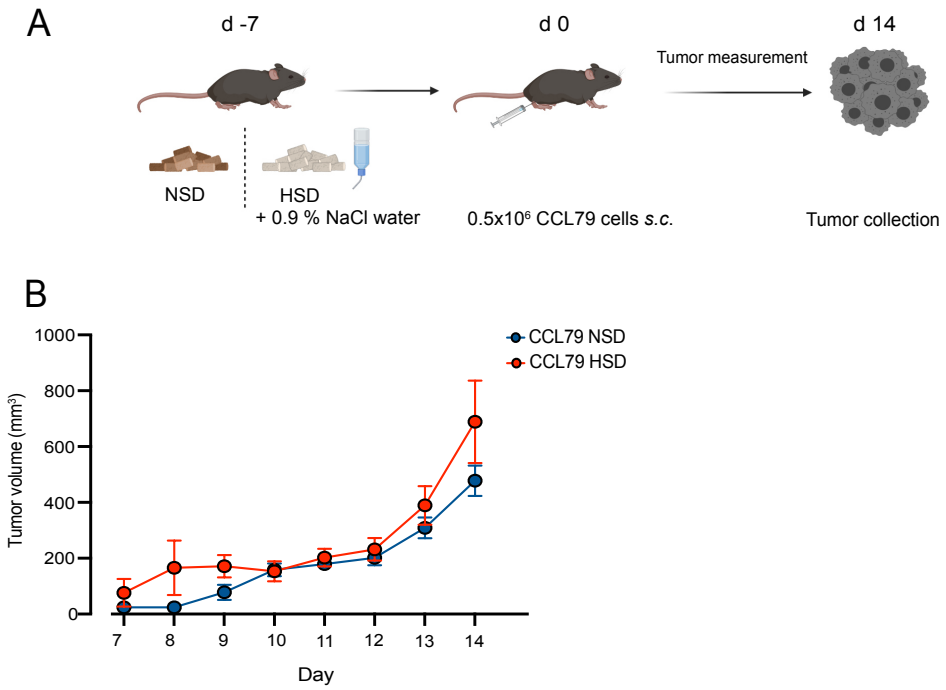

Figure 28: HSD has no growth-inhibiting effect on other epithelial-derived tumor cells. (A) Experimental setup. After one week on either HSD or control diet, mice were injected with 0.5 x 10^6 CCL79 cells and the tumor formation was measured for 14 days. The tumors were then harvested for further analysis. (B) Tumor formation over the experimental period between mice on HSD (red) *versus* NSD (blue) (n=10 mice/group). Data show mean ± SEM of 2 independent experiments and analyzed with 2way ANOVA. * - p<0.05; **- p<0.01; ***- p<0. 001. Cells were kindly provided by J. Yin.

4. Discussion

Malignant melanoma is an aggressive form of cancer that develops in the pigment-containing cells of the skin, called melanocytes. The primary cause of melanoma is unprotected exposure to ultraviolet light (UV) or artificial UV sources, which causes DNA damage (Pfeifer and Besaratinia 2012). As a consequence, genetic mutations within melanocytes promote malignancy and trigger uncontrolled proliferation. Untreated or late diagnostic cancer leads to poor survival in patients with melanoma (Clark 1991). Another risk factor in developed countries is the so-called Western diet. This diet is characterized by high levels of fat, glucose, and proteins. Many researchers have found a link between high glucose intake and tumorigenesis in various tissues, such as breast or colon cancer (Stoll 1998; Mehta et al. 2017). Additionally, the Western diet consists of twice the amount of salt (up to 12 grams/day) as the recommended daily intake (5-6 grams/day) (Manzel et al. 2014). The increased consumption of salt leads to changes in body homeostasis and affects physiological and immunological processes. For example, sodium accumulation in the skin compromises wound healing and impairs dermal tissue remodeling, resulting in dermatitis progression (Pajtók et al. 2021). On the other hand, excess salt was shown to be stored in the skin creating an hypertonic microenvironment, in which the immune system is markedly activated (Jantsch et al. 2015).
The aim of the thesis was to elucidate the effect of high-salt diet (HSD) on cutaneous cancer growth and to gain insight into various factors involved in disease progression.

4.1. High-salt diet reduces tumor growth independent of the immune system

4.1.1. Myeloid-derived suppressor cells are not key players in the HSD-mediated tumor reduction

Reduced melanoma growth under excessive salt intake was first described in 2019. HSD inhibited myeloid-derived suppressor cells (MDSCs), which promotes the activation of tumor-specific lymphocytes (Willebrand et al. 2019). Further studies then identified the underlying mechanism. HSD leads to sodium accumulation in the skin and activates Nfat5 expression in MDSCs, which in turn alters their differentiation (He et al. 2020). Specifically, monocytic MDSCs (M-MDSCs) were significantly decreased in abundance in the tumor

and the spleen, as well as in the circulation, whereas granulocytic MDSCs (PMN-MDSCs) were unchanged. To assess, whether HSD abolished myeloid-derived suppressor cells in our mouse model, the total number of MDSCs was quantified by FACS in mice on HSD and NSD. Based on the literature, M-MDSCs were identified as $CD45^+$ $CD11b^+$ $Ly6C^{hi}$ cells, whereas PMN-MDSCs were positive for $CD45^+$ $CD11b^+$ $Ly6G^+$ (Bronte et al. 2016). No differences in the frequency of M-MDSC and PMN-MDSC in the blood and the tumor microenvironment (TME) were observed between HSD-fed mice and the control diet. However, no specific claim can be made based on the gating strategy, as neutrophils and monocytes express similar surface markers as MDSCs (Z. Liu et al. 2020). Moreover, the authors depleted the MDSC population with anti-GR1 (anti-Ly6G/anti-Ly6C) treatment to reverse the salt-induced tumor reduction. However, anti-GR1 is commonly used in experimental studies to successfully deplete neutrophils (*via* anti-Ly6G) and additionally monocytes (*via* anti-Ly6C) (Fleming, Fleming, and Malek 1993). In the current study, the absence of MDSCs was investigated by treating the mice with Gemcitabine *i.p.* every third day (Le et al. 2009; Dawod et al. 2020). In addition to MDSCs depletion, Gemcitabine is a cytostatic drug that is effectively used in cancer therapy, especially in patients with pancreatic cancer and non-small cell lung carcinoma (Conroy et al. 2011; van der Lee et al. 2001). Gemcitabine treatment resulted in similar tumor growth in mice on HSD and NSD. The depletion of MDSCs in combination with HSD should further decrease tumor reduction, as the absence of suppressor cells should promote T cell infiltration. Contrary to the literature, HSD did not abolish myeloid-derived suppressor cells in our model. In addition to the influence of MDSCs on salt-induced tumor reduction, other immune cells were investigated.

4.1.2. Immune cell composition in the TME and tumor-draining lymph nodes were unchanged during HSD

As introduced in chapter 1.7. melanoma formation has an enormous impact on the body's immune system to defend against the disease. Immune cell infiltration of specific $CD8^+$ and $CD4^+$ T cells into the tumor microenvironment is a positive prognostic factor for tumor regression (Clark 1991; Mahmoud et al. 2011). Furthermore, sodium accumulation itself is known to alter several immune responses in different organs, including the skin. Skin-

resident macrophages polarize in response to the osmotic stress and change their function into a pro-inflammatory one (Jantsch et al. 2015). Moreover, the excessive Na^+ accumulation leads to an increase in Th17 T cells (Kleinewietfeld et al. 2013), which improved anti-tumor immunity (Muranski et al. 2008). Therefore, UMAP analysis of immune cells found in the TME as well as tumor-draining lymph nodes were performed. In the current model, HSD did not have a strong effect on the innate immune cell compartment in the TME as well as in the tumor-draining lymph nodes. Furthermore, a similar distribution of cells belonging to the adaptive immune system was observed. These data are surprising, as they ruled out the involvement of the immune system in HSD-mediated tumor reduction. However, overall low immune cell numbers were found in the TME of both investigated groups. One possible explanation could be that murine B16 melanoma cells are not sufficient to induce inflammation that promotes T cell infiltration. Leick et al. described that B16-OVA growth in mice leads to spare infiltration of immune cells around the intratumoral vessels. Additionally, low expression of critical homing receptor ligands on endothelial cells fails to recruit immune cells from the circulation in the TME during melanoma formation (Leick et al. 2019). RNA-sequencing data from Id et al. identified low expression of markers on B-16 melanoma required for NK function, macrophage activity, T cell co-stimulatory receptors, and antigen processing. Moreover, the authors described that only 4 % of all cells in the TME are immune cells (Id et al. 2018), which is in line with the low numbers of immune cells found in the current melanoma model. In addition to the FACS data, melanoma was used in different knockout mice to rule out the influence of specific immune cells in HSD-mediated tumor regression.

$RAG2^{-/-}$ mice (T and B cells), $CCR2^{-/-}$ mice (monocytes) as well as depletion of NK cells (anti-NK1.1), neutrophils (anti-Ly6G) and macrophages (Clodronate-Liposomes), still showed reduced tumor growth upon HSD, supporting previous findings that diminished melanoma growth is independent of the immune system (data not shown). However, further analysis of the immune cells at the functional level should be done to exclude the role of the immune system in HSD-reduced tumor growth.

After finding, that HSD did not change the immune cell compartment in the TME, the tumor-draining lymph nodes were analyzed. Tumor-draining lymph nodes are formed during melanoma, where tumor antigens are presented by DC to naïve T cells to elicit antitumor immunity (Fisher and Fisher 1971; Shu et al. 2006; Toki et al. 2020). No

differences were found in the number of immune cells in the tumor-draining lymph nodes between HSD and NSD. So far, no data are available investigating the role of HSD on tumor-draining lymph nodes during melanoma growth.
In conclusion, our melanoma mouse model did not recruit many immune cells in the TME. Furthermore, HSD had no further impact on immune cell distribution, thus, the reduced tumor growth is mainly immune cell-independent, contrary to the current beliefs. This theory was supported by further *in vitro* experiments. Melanoma cells under high sodium conditions (+ 40mM NaCl) showed significantly less cell growth compared to control cells, indicating a direct effect of salt on melanoma proliferation, independent of the immune cells or other circulating factors, such as hormones. Similar results were described by Arimochi et al. showing that glioma cells under high salt culture stopped cell growth and arrested cell cycle (Arimochi and Morita 2005). On the other hand, reduced melanoma growth could also be mediated by osmotic stress, induced by the use of D-Mannitol (Peña-Oyarzun et al. 2017). With the *in vitro* experiment, we cannot distinguish between salt-specific cell inhibition and osmotic stress responses. Nevertheless, reduced melanoma growth could be explained by the osmotic stress of cancer cells, independent of the immune system.

4.1.3. Reduced tumor formation under HSD is not limited to the skin

To rule out the possibility that local sodium accumulation in the skin alone led to reduced tumor growth, another mouse metastasis model was chosen, in which tumor cells grew in the lungs. Luciferase-expressing tumor cells were injected *intravenously* and the malignant cells attached to the lung tissue. Using the In Vivo Imaging System (IVIS), a reduced melanoma formation in the lung upon HSD was observed. In line with this, Willebrand et al. showed a reduction of Lewis lung carcinoma cells (LLC) growth in the lungs of mice on HSD (Willebrand et al. 2019). Interestingly, He et al. detected similar levels of sodium and chloride in the lungs of mice fed with HSD compared to NSD (He et al. 2020).
In conclusion, the results indicate that excessive salt intake promotes tumor suppression in an immune cell and sodium accumulation-independent manner.

4.2. Salt-sensitive factors are not key players in HSD-mediated tumor reduction

High consumption of salt leads to the accumulation of sodium in the skin, thereby generating an hypertonic environment (Wiig et al. 2013). In response to osmotic stress, cells upregulate the osmoprotective transcription factor *Nfat5* and the enzyme Sgk1. Both lead to the activation of ion channels to rebalance cell osmolarity (Miyakawa et al. 1999; Yang et al. 2020). Besides this, both modulators were found in melanoma to promote tumor growth. Kim et al. identified *Nfat5* as an oncogenic gene in melanoma where it is involved in metastasis formation (D.-H. Kim, Kim, and Ramakrishna 2018). In line with this, Zhu et al. found an accumulation of Sgk1 in several tumors, leading to increased mTOR signaling which is believed to trigger tumor progression (Zhu et al. 2020). We asked whether HSD triggers salt-sensitive regulators to protect melanoma against hypertonic stress. Contrary to expectations, both investigated mediators were unchanged in terms of gene expression and protein levels in melanoma cells grown under HSD. In addition to that, the absence of either *Nfat5* or Sgk1 could not restore sodium-mediated tumor reduction.

HSD is associated with increased glucocorticoid production and its anti-inflammatory function (Baudrand et al. 2014; Hayashi et al. 2004). In addition, researchers described an unfavorable function of glucocorticoids on epithelial-derived tumors by increasing local Sgk1 and activation of mitogen-activated protein kinase (MAPK) (Lin and Wang 2016). Therefore, the involvement of Glucocorticoid receptor (GR) expression in melanoma cells under HSD was investigated. Glucocorticoid receptor analysis showed significantly lower mRNA expression and a trend toward less protein level in melanoma cells exposed to HSD. Moreover, melanoma cells lacking glucocorticoid receptor still exhibited less tumor formation under HSD compared to NSD. This may explain why HSD did not induce Sgk1 expression, as glucocorticoid receptor levels trend to be downregulated. Furthermore, analysis of downstream mTOR activity revealed no changes in melanoma cells exposed to HSD compared to the control diet.

In conclusion, the observed tumor reduction by HSD was independent of Nfat5, Sgk1, and glucocorticoid receptor signaling.

4.3. High-salt diet significantly modulates energy production in melanoma cells

Metabolic rewiring is one of the Hallmarks of Cancer across all cancer types and is markedly different from the surrounding tissue (Ward and Thompson 2012). The TME is often low in oxygen and nutrients, driving metabolic rewiring to ensure survival and growth. Increased cell proliferation requires additional energy as well as precursors of amino acids, lipids, and nucleotides. As a result, the central carbon metabolism is highly activated in malignant cells (Denko 2008). In general, melanoma prefers glycolysis and lactic acid fermentation as it produces energy faster than mitochondrial respiration (Avagliano et al. 2020). Thus, melanoma cells under HSD were deeply analyzed on their metabolic signature. RNA-sequencing data revealed a downregulation of genes involved in tumor metabolism and cell cycle progression. The data were confirmed by Seahorse® experiments showing a significant reduction of glycolysis and a trend towards less mitochondrial respiration in melanoma cells exposed to HSD. In line with this, Aykin-Burns et al. showed that the blockade of glycolysis was sufficient to induce cell cycle arrest and further force cell death in cancer cells (Aykin-Burns et al. 2009; Saito et al. 2009). Ruocco et al. investigated higher glucose uptake and its transporters in tumor cells, which is associated with a high tumor progression (Ruocco et al. 2019). In line with this, the excessive salt intake significantly increased glucose uptake compared to the control group. However, gene expression analysis of glucose transporter 1 and 3 (*Slc2a1* and *Slc2a3*) were unchanged in melanoma under HSD compared to NSD. Contrary to the literature, the increase in glucose did not lead to tumor progression in melanoma cells under HSD. Metabolomic data revealed an accumulation of glucose in these cells, possibly indicating that HSD somehow impairs glycolysis. Additionally, *in vitro* data supported the theory that HSD may directly inhibit glycolysis in tumor cells. Seahorse® experiments with melanoma cells under high sodium conditions showed a trend towards lower ECAR as well as OCR, suggesting a direct effect of high salt on melanoma metabolism (data not shown). Therefore, glycolytic enzymes were further investigated. Shimada et al. showed that HSD leads to increased mRNA expression of genes encoding for key glycolytic enzymes and the release of pyruvate in the kidneys of Sprague Dawley rats (Shimada et al. 2023). In line with this, Amara and colleagues showed increased glycolytic activity and elevated expression of key rate-limiting enzymes of aerobic

glycolysis in breast cancer cells under HSD (Amara, Zheng, and Tiriveedhi 2016). Contrary to the literature, several glycolytic enzymes were significantly downregulated on mRNA levels in melanoma cells under HSD. In addition, the key rate-limiting enzymes Hexokinase (*Hk1* and *Hk2*) and Phosphofructokinase (*Pfk*) were significantly downregulated in melanoma under HSD, strengthening the theory that excessive salt intake affects glycolysis.

In conclusion, these findings suggest that HSD directly inhibits melanoma glycolysis and by this inhibits cell proliferation. These data were supported by the results that mitochondrial mass and fitness were not altered upon HSD. Analysis of mRNA expression of the electron chain transporter revealed overall no differences between melanoma cells under HSD compared to NSD. Moreover, complex activity was not affected by high sodium levels and metabolomic data revealed similar metabolite occurrence in melanoma cells under HSD. This data may surprise as Geisberger et al. showed that high salt (HS) reduces mitochondrial membrane potential in macrophages. Especially the activity of complex II (succinate dehydrogenase) of the electron transport chain was inhibited by HS (Geisberger et al. 2021). These results support the theory that HSD primarily affects glycolysis rather than mitochondrial respiration.

Taken together, the reduced glycolysis in melanoma cells due to HSD may be a unique phenomenon that can be used for future treatment strategies specifically for melanoma. Downstream of glycolysis, other metabolic pathways get activated. The generated Acetyl-CoA produced from glucose is used for fatty acid synthesis to build up new lipids (Folch and Bisschops 2021). Several alterations in fatty acid metabolism have been described to contribute to melanoma progression. A recent study reported that melanoma cells upregulate fatty acid transporter 2 (Fatp2/*Slc27a2*) to increase fatty acid uptake (Alicea et al. 2020). Moreover, fatty acid uptake and lipid storage were induced by Hif1-α expression and further promoted melanoma growth and survival (Bensaad et al. 2014). Contrary to the literature, HSD significantly diminished fatty acid uptake in the current melanoma study, and RNA-sequencing data indicated downregulation of pathways involved in the fatty acid synthesis. In line with this, Li et al. revealed downregulation of pathways involved in lipid metabolism in liver tissue from HSD-fed mice (Li et al. 2021). This data may indicate a negative effect of HSD on fatty acid synthesis. The unchanged expression of Hif1-α as

well as reduced gene expression of hypoxia-related genes supported a negative effect of melanoma metabolism under HSD.
Although, these data suggest an inhibitory effect of HSD on tumor metabolism. Excessive salt consumption somehow impairs glycolysis and further inhibits cell proliferation. Furthermore, the lower energy production could explain the impaired cell cycle activity and thus arrest melanoma cell division. These new findings could represent a new therapeutic approach in the treatment of melanoma formation. By additionally blocking specific glucose transporters (Koch et al. 2015) in combination with increased salt, glycolysis could markedly inhibit and force tumor reduction.

4.4. Melanogenesis is a unique characteristic of melanoma cells that may explain HSD-mediated inhibition

The effect of excessive salt consumption on cancer growth has been described by several researchers. Chen et al. investigated that excessive salt promotes the progression of breast tumors by remodeling the immune response towards an increased Th17 T cells population (J. Chen et al. 2020). Studies about salt consumption in humans showed a high correlation between excessive sodium intake and increased risk of colorectal cancer (Yakoob and Baig-ansari 2019). Furthermore, long-term dietary sodium intake favors the risk of developing renal cell cancer (Deckers et al. 2014). In summary, the current state of knowledge suggests that HSD promotes tumor growth. However, skin cancer growth was significantly reduced by dietary salt consumption. A possible explanation may be that melanoma cells are unique in their ability to perform melanogenesis, which can be altered by excessive salt intake. Recent publications reported that HSD leads to an accumulation of sodium in the brain of mice and further the activation of pro-opiomelanocortin (POMC) neurons (Zhang et al. 2022). Enzymatic cleavage of POMC gives rise to multiple peptide hormones, including adrenocorticotropic hormone (ACTH) which is further cleaved into alpha-melanocyte stimulating hormone (α-MSH). Both hormones can bind to the melanocortin 1 receptor (Mc1r) on melanocytes as well as melanoma cells (Orth et al. 1970; Wolf Horrell, Boulanger, and D'Orazio 2016). In our model, serum α-MSH levels were dramatically lower in mice exposed to HSD. One explanation could be that α-MSH

has already bound to the receptor in the tissue and on melanoma cells. Further experiments should be done to measure α-MSH in melanoma cells and the surrounding tissue to reinforce the hypothesis. Jobin et al. measured high corticosterone levels in mice fed with HSD (Jobin et al. 2020). In line with this, Costello et al. investigated that ACTH, the precursor of corticosterone, was more produced in mice under HSD (Costello et al. 2022). Suzuki et al. showed that ACTH could also bind to Mc1r on melanoma cells and promote downstream signaling pathways that activate melanogenesis (Suzuki et al. 1996). We asked whether HSD increases ACTH, which in turn binds on Mc1r instead of α-MSH. Dr. med. Sebastian Schwab found elevated levels of ACTH in the serum of mice exposed to HSD for one week (data not shown). This may indicate that ACTH binds to Mc1r and activates downstream pathways to promote melanogenesis. Analysis of Mc1r revealed significantly higher mRNA expression and protein levels in melanoma under HSD compared to NSD. The master transcription factor that regulates melanogenesis is the microphthalmia-associated transcription factor (*Mitf*). *Mitf* is known to be upregulated in malignant cells and has been described as a key player in melanoma progression, proliferation, and migration (Hoek et al. 2008; Giuliano et al. 2010). On the other hand, *Mitf* can stimulate melanogenesis which in turn promotes cell differentiation. The differentiation step is associated with the loss of the replicative immortality characteristic of melanoma cells and thus limits uncontrolled cell growth (Valyi-Nagy et al. 1993). Melanoma cells under HSD showed significantly elevated levels of *Mitf* at mRNA expression and protein levels, supporting the theory of altered melanogenesis activity caused by high sodium intake. Distinct gene expression signatures regulated by *Mitf* were identified and further cell characteristics were determined (D'Mello et al. 2016). RNA sequencing data showed less expression of genes associated with cell proliferation and cell cycle progression regulated by *Mitf.* On the other hand, RNA sequencing data and proteomic data confirmed an increased expression of genes involved in melanogenesis and the resulting differentiation when melanoma are exposed to HSD. The results presented here suggest a role for altered melanogenesis activity under HSD. One possible explanation could be that the increased activity of POMC neurons in mice under HSD promotes the production of ACTH. Through the bloodstream, ACTH enters skin tissue and binds to Mc1r on melanoma cells which leads to the downstream activation of melanogenesis. As a result, melanoma cells differentiate and fail to proliferate in the

aggressive manner of cancer cells. To strengthen this theory, adenocarcinoma cells (CCL79) were injected in mice under HSD or NSD and tumor formation was observed. Like melanoma cells, CCL79 cells are epithelial-derived cells but are not able to perform melanogenesis. Indeed, CCL79 cells grew similarly under HSD compared to the control group. These results reinforce the idea that HSD specifically promotes melanogenesis activity in melanoma, which in turn stops cell proliferation.

Taken together, HSD significantly diminishes tumor metabolism and irreversibly stops cell proliferation. Furthermore, the current state of the project investigates the influence of HSD on melanogenesis activity, which can lead to stop tumor cell proliferation.

Furthermore, melanoma cells lacking tyrosinase (B16-TyrKO) were used *in vitro* to investigate cell proliferation by measuring cell confluence. The loss of tyrosinase prevents melanogenesis and thus may reverse cell proliferation. Culturing of B16-TyrKO cells under high sodium showed similar cell proliferation compared to the control cells. Furthermore, treatment of B16-TyrKO cells with D-Mannitol showed significantly less cell proliferation in comparison to the control cells and to cells under HS. This may strengthen the theory, that HSD promotes melanogenesis thereby stopping cell proliferation. However, these data have to be confirmed *in vivo.*

Taken together, HSD significantly diminishes tumor metabolism and irreversibly stops cell proliferation. Furthermore, the current state of the project investigates that HSD specifically influences melanogenesis activity, which can lead to stopping tumor cell proliferation.

5. Summary

Malignant melanoma is one of the most aggressive cancers in the world and is on the rise. Therapeutic treatments for patients with metastatic melanoma have a low success rate and many side effects. As a result, melanoma mortality has increased dramatically over the past 40 years. Furthermore, new diseases of the Western world are being identified due to changes in their diary patterns. In particular, salt consumption, which has increased due to the high consumption of processed foods, has many effects on the body´s health.

In this thesis, the effect of high-salt diet (HSD) on melanoma growth was investigated. The results showed a significant decrease in tumor formation in mice fed with HSD compared to a normal diet. In addition, tumor formation in the lungs was also reduced when mice were fed with HSD. The initial hypothesis was an activation of the immune system due to the increased sodium content. Analysis of the tumor microenvironment revealed a similar abundance of immune cells in both investigated groups. Furthermore, the distribution of immune cells in the tumor-draining lymph nodes was not altered by the increased salt intake. Blood analysis indicated no differences in the immune cell compartment of mice fed with HSD compared to the control diet. *In vitro* experiments indicated a direct effect of high sodium on reduced melanoma growth.

The next question was whether salt-sensitive mediators are activated in melanoma cells in response to excessive salt consumption. No changes in the expression of *Nfat5* and Sgk1 were found. Glucocorticoid receptor levels were slightly downregulated in melanoma cells under HSD, ruling out a direct effect of these modulators involved in tumor suppression.

Therefore, the direct effect of HSD on melanoma cells was analyzed. Surprisingly, HSD significantly diminished tumor metabolism, especially glycolysis activity. Analyzing glycolytic enzymes showed downregulation of mRNA levels in melanoma cells under HSD, strengthening the theory that excessive salt intake impaired glycolysis. By analyzing the activity of mitochondrial complexes, no defects were detected in melanoma cells under HSD, and therefore the impaired tumor metabolism could be attributed to the inhibition of glycolysis.

Finally, melanogenesis activity was highly increased in melanoma cells, suggesting a direct effect of HSD on reduced tumor growth. Here, the Mc1r, as well as downstream pathways were significantly increased in melanoma cells exposed to HSD. This activity may rather promote melanoma toward cell differentiation and result in the inhibition of cell proliferation.

In conclusion, the thesis revealed new insights into how HSD influences melanoma growth. The direct effect of HSD affects tumor metabolism and could be considered in future therapeutic approaches. Furthermore, the presented data indicate changes in melanogenesis activity in melanoma cells exposed to HSD and may explain the salt-mediated tumor reduction.

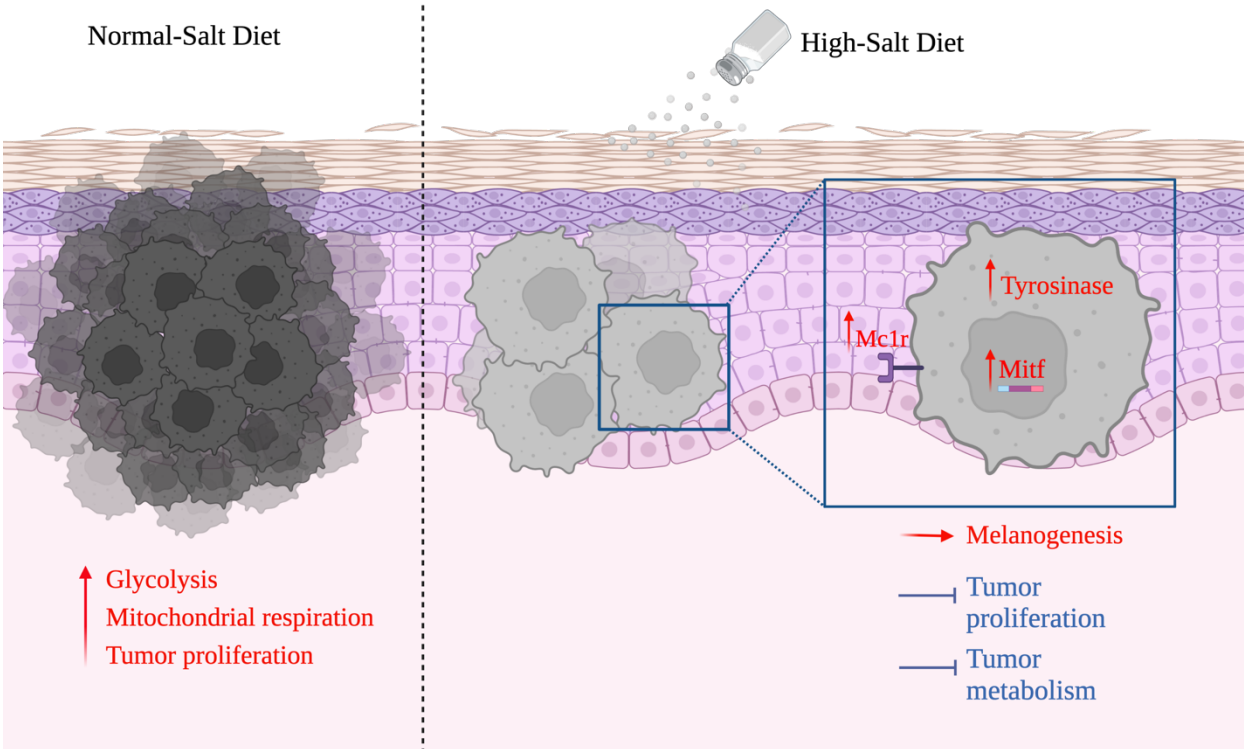

Figure 29: Summary of HSD-mediated modifications of melanoma cells. In the present thesis, melanoma cells under high-salt diet showed less tumor formation compared to the control group. The reduced tumor growth was associated with a lower tumor proliferation rate and less metabolic activity. On the other hand, HSD promotes melanogenesis and results in the inhibition of massive cell proliferation.

6. List of Figures

7. List of Tables

8. References

Abbasi, Naheed R, Helen M Shaw, Darrell S Rigel, Robert J Friedman, William H McCarthy, Iman Osman, Alfred W Kopf, and David Polsky. 2004. “Early Diagnosis of Cutaneous Melanoma: Revisiting the ABCD Criteria.” *JAMA* 292 (22): 2771–76. https://doi.org/10.1001/jama.292.22.2771.

Aguiar, Sarah Leão Fiorini, Mariana Camila Gonçalves Miranda, Mauro Andrade Freitas Guimarães, Helton Costa Santiago, Camila Pereira Queiroz, Pricila da Silva Cunha, Denise Carmona Cara, et al. 2018. “High-Salt Diet Induces IL-17-Dependent Gut Inflammation and Exacerbates Colitis in Mice.” *Frontiers in Immunology* 8 (January): 1969. https://doi.org/10.3389/fimmu.2017.01969.

Ali, Niwa, and Michael D Rosenblum. 2017. “Regulatory T Cells in Skin.” *Immunology* 152 (3): 372–81. https://doi.org/10.1111/imm.12791.

Alicea, Gretchen M, Vito W Rebecca, Aaron R Goldman, Mitchell E Fane, Stephen M Douglass, Reeti Behera, Marie R Webster, et al. 2020. “Changes in Aged Fibroblast Lipid Metabolism Induce Age-Dependent Melanoma Cell Resistance to Targeted Therapy via the Fatty Acid Transporter FATP2.” *Cancer Discovery* 10 (9): 1282–95. https://doi.org/10.1158/2159-8290.CD-20-0329.

Amara, Suneetha, Mu Zheng, and Venkataswarup Tiriveedhi. 2016. “Oleanolic Acid Inhibits High Salt-Induced Exaggeration of Warburg-like Metabolism in Breast Cancer Cells.” *Cell Biochemistry and Biophysics* 74 (September). https://doi.org/10.1007/s12013-016-0736-7.

Appel, Lawrence J. 2008. “Editorial: Dietary Patterns and Longevity Expanding the Blue Zones.” *Circulation* 118 (3): 214–15. https://doi.org/10.1161/CIRCULATIONAHA.108.788497.

Arimochi, Hideki, and Kyoji Morita. 2005. “High Salt Culture Conditions Suppress Proliferation of Rat C6 Glioma Cell by Arresting Cell-Cycle Progression at S-Phase.” *Journal of Molecular Neuroscience : MN* 27 (3): 293–301. https://doi.org/10.1385/JMN:27:3:293.

Ariotti, Silvia, Marc A Hogenbirk, Feline E Dijkgraaf, Lindy L Visser, Mirjam E Hoekstra, Ji-Ying Song, Heinz Jacobs, John B Haanen, and Ton N Schumacher. 2014. “T Cell Memory. Skin-Resident Memory $CD8^+$ T Cells Trigger a State of Tissue-Wide Pathogen Alert.” *Science (New York, N.Y.)* 346 (6205): 101–5. https://doi.org/10.1126/science.1254803.

Arnold, Melina, Esther de Vries, David C Whiteman, Ahmedin Jemal, Freddie Bray, Donald Maxwell Parkin, and Isabelle Soerjomataram. 2018. “Global Burden of Cutaneous Melanoma Attributable to Ultraviolet Radiation in 2012.” *International Journal of Cancer* 143 (6): 1305–14. https://doi.org/10.1002/ijc.31527.

Ascierto, Paolo A, John M Kirkwood, Jean-Jacques Grob, Ester Simeone, Antonio M Grimaldi, Michele Maio, Giuseppe Palmieri, Alessandro Testori, Francesco M Marincola, and Nicola Mozzillo. 2012. “The Role of BRAF V600 Mutation in Melanoma.” *Journal of Translational Medicine*. England. https://doi.org/10.1186/1479-5876-10-85.

Avagliano, Angelica, Giuseppe Fiume, Alessandra Pelagalli, Gennaro Sanità, Maria Rosaria Ruocco, Stefania Montagnani, and Alessandro Arcucci. 2020. “Metabolic Plasticity of Melanoma Cells and Their Crosstalk With Tumor Microenvironment.” *Frontiers in Oncology* 10 (May): 722. https://doi.org/10.3389/fonc.2020.00722.

Aykin-Burns, Nùkhet, Iman M Ahmad, Yueming Zhu, Larry W Oberley, and Douglas R Spitz. 2009. “Increased Levels of Superoxide and H2O2 Mediate the Differential

Susceptibility of Cancer Cells versus Normal Cells to Glucose Deprivation." *The Biochemical Journal* 418 (1): 29–37. https://doi.org/10.1042/BJ20081258.

Bae, Jeong-Hyeon, Min-Young Shin, Eun Ha Kang, Yun Jong Lee, and You-Jung Ha. 2021. "Association of Rheumatoid Arthritis and High Sodium Intake with Major Adverse Cardiovascular Events: A Cross-Sectional Study from the Seventh Korean National Health and Nutrition Examination Survey." *BMJ Open* 11 (12): e056255. https://doi.org/10.1136/bmjopen-2021-056255.

Baek, Se Hwan, Ho Won Lee, Prakash Gangadaran, Ji Min Oh, Liya Zhu, Ramya Lakshmi Rajendran, Jaetae Lee, and Byeong-Cheol Ahn. 2020. "Role of M2-like Macrophages in the Progression of Ovarian Cancer." *Experimental Cell Research* 395 (2): 112211. https://doi.org/https://doi.org/10.1016/j.yexcr.2020.112211.

Batista, Facundo D, and Naomi E Harwood. 2009. "The Who, How and Where of Antigen Presentation to B Cells." *Nature Reviews. Immunology* 9 (1): 15–27. https://doi.org/10.1038/nri2454.

Baudrand, R, C Campino, C A Carvajal, O Olivieri, G Guidi, G Faccini, P A Vöhringer, et al. 2014. "High Sodium Intake Is Associated with Increased Glucocorticoid Production, Insulin Resistance and Metabolic Syndrome." *Clinical Endocrinology* 80 (5): 677–84. https://doi.org/10.1111/cen.12225.

Bazzoni, Gianfranco, and Elisabetta Dejana. 2002. "Keratinocyte Junctions and the Epidermal Barrier: How to Make a Skin-Tight Dress." *The Journal of Cell Biology* 156 (6): 947–49. https://doi.org/10.1083/jcb.200202116.

Bensaad, Karim, Elena Favaro, Caroline A Lewis, Barrie Peck, Simon Lord, Jennifer M Collins, Katherine E Pinnick, et al. 2014. "Fatty Acid Uptake and Lipid Storage Induced by HIF-1α Contribute to Cell Growth and Survival after Hypoxia-Reoxygenation." *Cell Reports* 9 (1): 349–65. https://doi.org/10.1016/j.celrep.2014.08.056.

Berardinis, Ralph J. De, and Navdeep S. Chandel. 2016. "Fundamentals of Cancer Metabolism." *Science Advances* 2 (5). https://doi.org/10.1126/sciadv.1600200.

Binger, Katrina J, Matthias Gebhardt, Matthias Heinig, Carola Rintisch, Agnes Schroeder, Wolfgang Neuhofer, Karl Hilgers, et al. 2015. "High Salt Reduces the Activation of IL-4- and IL-13-Stimulated Macrophages." *The Journal of Clinical Investigation* 125 (11): 4223–38. https://doi.org/10.1172/JCI80919.

Blanpain, Cédric, and Elaine Fuchs. 2006. "Epidermal Stem Cells of the Skin." *Annual Review of Cell and Developmental Biology* 22: 339–73. https://doi.org/10.1146/annurev.cellbio.22.010305.104357.

Bonaventure, Jacky, Melanie J Domingues, and Lionel Larue. 2013. "Cellular and Molecular Mechanisms Controlling the Migration of Melanocytes and Melanoma Cells." *Pigment Cell & Melanoma Research* 26 (3): 316–25. https://doi.org/10.1111/pcmr.12080.

Boroughs, Lindsey K, and Ralph J DeBerardinis. 2015. "Metabolic Pathways Promoting Cancer Cell Survival and Growth." *Nature Cell Biology* 17 (4): 351–59. https://doi.org/10.1038/ncb3124.

Breitkreutz, Dirk, Nicolae Mirancea, and Roswitha Nischt. 2009. "Basement Membranes in Skin: Unique Matrix Structures with Diverse Functions?" *Histochemistry and Cell Biology* 132 (1): 1–10. https://doi.org/10.1007/s00418-009-0586-0.

Bronte, Vincenzo, Sven Brandau, Shu-hsia Chen, and Mario P Colombo. 2016. "Recommendations for Myeloid-Derived Suppressor Cell Nomenclature and Characterization Standards." *Nature Communications* 7 (July): 1–10.

https://doi.org/10.1038/ncomms12150.
Brożyna, Anna A, Wojciech Jóźwicki, J Andrew Carlson, and Andrzej T Slominski. 2013. “Melanogenesis Affects Overall and Disease-Free Survival in Patients with Stage III and IV Melanoma.” *Human Pathology* 44 (10): 2071–74. https://doi.org/10.1016/j.humpath.2013.02.022.
Bulgarelli, Jenny, Marcella Tazzari, Anna Maria Granato, Laura Ridolfi, Serena Maiocchi, Francesco de Rosa, Massimiliano Petrini, et al. 2019. “Dendritic Cell Vaccination in Metastatic Melanoma Turns ‘Non-T Cell Inflamed’ Into ‘T-Cell Inflamed’ Tumors.” *Frontiers in Immunology* 10 (October). https://doi.org/10.3389/fimmu.2019.02353.
Chapman, Paul B, Axel Hauschild, Caroline Robert, John B Haanen, Paolo Ascierto, James Larkin, Reinhard Dummer, et al. 2011. “Improved Survival with Vemurafenib in Melanoma with BRAF V600E Mutation.” *The New England Journal of Medicine* 364 (26): 2507–16. https://doi.org/10.1056/NEJMoa1103782.
Chen, Angela X, Andrea V Haas, Gordon H Williams, and Anand Vaidya. 2020. “Dietary Sodium Intake and Cortisol Measurements.” *Clinical Endocrinology* 93 (5): 539–45. https://doi.org/10.1111/cen.14262.
Chen, Jiewen, Xiyuan Liu, Hongyan Huang, Fangfang Zhang, Yongjun Lu, and Hai Hu. 2020. “High Salt Diet May Promote Progression of Breast Tumor through Eliciting Immune Response.” *International Immunopharmacology* 87: 106816. https://doi.org/https://doi.org/10.1016/j.intimp.2020.106816.
Chen, Songcang, Christopher L Grigsby, Christopher S Law, Xiping Ni, Nada Nekrep, Keith Olsen, Michael H Humphreys, and David G Gardner. 2009. “Tonicity-Dependent Induction of Sgk1 Expression Has a Potential Role in Dehydration-Induced Natriuresis in Rodents.” *The Journal of Clinical Investigation* 119 (6): 1647–58. https://doi.org/10.1172/JCI35314.
Cheung, Chris Yk, and Ben Cb Ko. 2013. “NFAT5 in Cellular Adaptation to Hypertonic Stress - Regulations and Functional Significance.” *Journal of Molecular Signaling* 8 (1): 5. https://doi.org/10.1186/1750-2187-8-5.
Choi, H W, H J Ahn, M K Shin, Y S Son, and K S Kim. 2018. “Pretreatment with Substance P Alleviates Irritation Due to Sodium Lauryl Sulphate Exposure by Maintaining E-Cadherin Expression on Human Keratinocytes.” *Clinical and Experimental Dermatology* 43 (3): 291–95. https://doi.org/10.1111/ced.13363.
Clark, Wallace H. 1991. “Human Cutaneous Malignant Melanoma as a Model for Cancer.” *Cancer and Metastasis Reviews* 10 (2): 83–88. https://doi.org/10.1007/BF00049406.
Coderch, Luisa, Olga López, Alfonso de la Maza, and José L Parra. 2003. “Ceramides and Skin Function.” *American Journal of Clinical Dermatology* 4 (2): 107–29. https://doi.org/10.2165/00128071-200304020-00004.
Commerford, Catharina D., Lothar C. Dieterich, Yuliang He, Tanja Hell, Javier A. Montoya-Zegarra, Simon F. Noerrelykke, Erica Russo, Martin Röcken, and Michael Detmar. 2018. “Mechanisms of Tumor-Induced Lymphovascular Niche Formation in Draining Lymph Nodes.” *Cell Reports* 25 (13): 3554-3563.e4. https://doi.org/10.1016/j.celrep.2018.12.002.
Conroy, Thierry, Françoise Desseigne, Marc Ychou, Olivier Bouché, Rosine Guimbaud, Yves Bécouarn, Antoine Adenis, et al. 2011. “FOLFIRINOX versus Gemcitabine for Metastatic Pancreatic Cancer.” *New England Journal of Medicine* 364 (19): 1817–25. https://doi.org/10.1056/nejmoa1011923.

Cordain, Loren, S Boyd Eaton, Anthony Sebastian, Neil Mann, Staffan Lindeberg, Bruce A Watkins, James H O'Keefe, and Janette Brand-Miller. 2005. "Origins and Evolution of the Western Diet: Health Implications for the 21st Century." *The American Journal of Clinical Nutrition* 81 (2): 341–54. https://doi.org/10.1093/ajcn.81.2.341.

Costello, Hannah M, Georgios Krilis, Celine Grenier, David Severs, Jessica R Ivy, Mark Nixon, Megan C Holmes, et al. 2022. "High Salt Intake Activates the Hypothalamic-Pituitary-Adrenal Axis, Amplifies the Stress Response, and Alters Tissue Glucocorticoid Exposure in Mice." *BioRxiv*, January, 2022.03.04.481654. https://doi.org/10.1101/2022.03.04.481654.

Coussens, Lisa M, and Zena Werb. 2002. "Inflammation and Cancer." *Nature* 420 (6917): 860–67. https://doi.org/10.1038/nature01322.

D'Mello, Stacey A.N., Graeme J. Finlay, Bruce C. Baguley, and Marjan E. Askarian-Amiri. 2016. "Signaling Pathways in Melanogenesis." *International Journal of Molecular Sciences* 17 (7): 1–18. https://doi.org/10.3390/ijms17071144.

Davar, Diwakar, Amiran K Dzutsev, John A McCulloch, Richard R Rodrigues, Joe-Marc Chauvin, Robert M Morrison, Richelle N Deblasio, et al. 2021. "Fecal Microbiota Transplant Overcomes Resistance to Anti-PD-1 Therapy in Melanoma Patients." *Science (New York, N.Y.)* 371 (6529): 595–602. https://doi.org/10.1126/science.abf3363.

Dawod, Bassel, Jinghua Liu, Simon Gebremeskel, Chi Yan, Antonia Sappong, Brent Johnston, David W Hoskin, Jean S Marshall, and Jun Wang. 2020. "Myeloid-Derived Suppressor Cell Depletion Therapy Targets IL-17A-Expressing Mammary Carcinomas." *Scientific Reports* 10 (1): 13343. https://doi.org/10.1038/s41598-020-70231-7.

Deckers, I A G, P A van den Brandt, M van Engeland, P M M B Soetekouw, M M L L Baldewijns, R A Goldbohm, and L J Schouten. 2014. "Long-Term Dietary Sodium, Potassium and Fluid Intake; Exploring Potential Novel Risk Factors for Renal Cell Cancer in the Netherlands Cohort Study on Diet and Cancer." *British Journal of Cancer* 110 (3): 797–801. https://doi.org/10.1038/bjc.2013.771.

Denko, Nicholas C. 2008. "Hypoxia, HIF1 and Glucose Metabolism in the Solid Tumour." *Nature Reviews. Cancer*. England. https://doi.org/10.1038/nrc2468.

Dick, J C. 1947. "Observations on the Elastic Tissue of the Skin with a Note on the Reticular Layer at the Junction of the Dermis and Epidermis." *Journal of Anatomy* 81 (Pt 3): 201–11.

Drenjančević-Perić, I, B Jelaković, J H Lombard, M P Kunert, A Kibel, and M Gros. 2011. "High-Salt Diet and Hypertension: Focus on the Renin-Angiotensin System." *Kidney & Blood Pressure Research* 34 (1): 1–11. https://doi.org/10.1159/000320387.

Dunn, Gavin P, Lloyd J Old, and Robert D Schreiber. 2004. "The Three Es of Cancer Immunoediting." *Annual Review of Immunology* 22: 329–60. https://doi.org/10.1146/annurev.immunol.22.012703.104803.

Egbuniwe, Isioma U, Sophia N Karagiannis, Frank O Nestle, and Katie E Lacy. 2015. "Revisiting the Role of B Cells in Skin Immune Surveillance." *Trends in Immunology* 36 (2): 102–11. https://doi.org/10.1016/j.it.2014.12.006.

Elbe, A, C A Foster, and G Stingl. 1996. "T-Cell Receptor Alpha Beta and Gamma Delta T Cells in Rat and Human Skin--Are They Equivalent?" *Seminars in Immunology* 8 (6): 341–49. https://doi.org/10.1006/smim.1996.0045.

Elwood, J Mark, and Janet Jopson. 1997. “Melanoma and Sun Exposure: An Overview of Published Studies.” *International Journal of Cancer* 73 (2): 198–203. https://doi.org/https://doi.org/10.1002/(SICI)1097-0215(19971009)73:2<198::AID-IJC6>3.0.CO;2-R.

Ewart, William. 1842. “Remarks on the Physiology and Pathological Bearings of the Skin and Mucous Membrane.” *Edinburgh Medical and Surgical Journal* 58 (153): 413–26.

Farjah, Mariam, Bryan P. Roxas, David L. Geenen, and Robert S. Danziger. 2003. “Dietary Salt Regulates Renal SGK1 Abundance: Relevance to Salt Sensitivity in the Dahl Rat.” *Hypertension* 41 (4): 874–78. https://doi.org/10.1161/01.HYP.0000063885.48344.EA.

Fecher, Leslie A, Ravi K Amaravadi, and Keith T Flaherty. 2008. “The MAPK Pathway in Melanoma.” *Current Opinion in Oncology* 20 (2). https://journals.lww.com/co-oncology/Fulltext/2008/03000/The_MAPK_pathway_in_melanoma.7.aspx.

Fisher, B, and E R Fisher. 1971. “Studies Concerning the Regional Lymph Node in Cancer. I. Initiation of Immunity.” *Cancer* 27 (5): 1001–4. https://doi.org/10.1002/1097-0142(197105)27:5<1001::aid-cncr2820270502>3.0.co;2-u.

Fleming, T J, M L Fleming, and T R Malek. 1993. “Selective Expression of Ly-6G on Myeloid Lineage Cells in Mouse Bone Marrow. RB6-8C5 MAb to Granulocyte-Differentiation Antigen (Gr-1) Detects Members of the Ly-6 Family.” *Journal of Immunology (Baltimore, Md. : 1950)* 151 (5): 2399–2408.

Folch, Pauline L, and Markus M M Bisschops. 2021. “Minireview Metabolic Energy Conservation for Fermentative Product Formation.” https://doi.org/10.1111/1751-7915.13746.

Fridman, Wolf Herman, Franck Pagès, Catherine Sautès-Fridman, and Jérôme Galon. 2012. “The Immune Contexture in Human Tumours: Impact on Clinical Outcome.” *Nature Reviews. Cancer*. England. https://doi.org/10.1038/nrc3245.

Gabrilovich, Dmitry I. 2017. “Myeloid-Derived Suppressor Cells.” *Cancer Immunology Research* 5 (1): 3–8. https://doi.org/10.1158/2326-6066.CIR-16-0297.

Galon, Jérôme, Wolf-Herman Fridman, and Franck Pagès. 2007. “The Adaptive Immunologic Microenvironment in Colorectal Cancer: A Novel Perspective.” *Cancer Research* 67 (5): 1883–86. https://doi.org/10.1158/0008-5472.CAN-06-4806.

Geisberger, Sabrina, Hendrik Bartolomaeus, Patrick Neubert, Ralf Willebrand, Christin Zasada, Thomas Bartolomaeus, Victoria McParland, et al. 2021. “Salt Transiently Inhibits Mitochondrial Energetics in Mononuclear Phagocytes.” *Circulation* 144 (2): 144–58. https://doi.org/10.1161/CIRCULATIONAHA.120.052788.

Ghigo, Clément, Isabelle Mondor, Audrey Jorquera, Jonathan Nowak, Stephan Wienert, Sonja P Zahner, Björn E Clausen, et al. 2013. “Multicolor Fate Mapping of Langerhans Cell Homeostasis.” *The Journal of Experimental Medicine* 210 (9): 1657–64. https://doi.org/10.1084/jem.20130403.

Gilboa, Eli. 2007. “DC-Based Cancer Vaccines.” *The Journal of Clinical Investigation* 117 (5): 1195–1203. https://doi.org/10.1172/JCI31205.

Gilchrest, B A, H Y Park, M S Eller, and M Yaar. 1996. “Mechanisms of Ultraviolet Light-Induced Pigmentation.” *Photochemistry and Photobiology* 63 (1): 1–10. https://doi.org/10.1111/j.1751-1097.1996.tb02988.x.

Ginhoux, Florent, and Steffen Jung. 2014. “Monocytes and Macrophages: Developmental Pathways and Tissue Homeostasis.” *Nature Reviews Immunology*

14 (6): 392–404. https://doi.org/10.1038/nri3671.
Giuliano, Sandy, Yann Cheli, Mickaël Ohanna, Caroline Bonet, Laurent Beuret, Karine Bille, Agnès Loubat, et al. 2010. “Microphthalmia-Associated Transcription Factor Controls the DNA Damage Response and a Lineage-Specific Senescence Program in Melanomas.” *Cancer Research* 70 (9): 3813–22. https://doi.org/10.1158/0008-5472.CAN-09-2913.
Granot, Zvi, and Jadwiga Jablonska. 2015. “Distinct Functions of Neutrophil in Cancer and Its Regulation.” *Mediators of Inflammation* 2015: 701067. https://doi.org/10.1155/2015/701067.
Gregory, Alyssa D, and A McGarry Houghton. 2011. “Tumor-Associated Neutrophils: New Targets for Cancer Therapy.” *Cancer Research* 71 (7): 2411–16. https://doi.org/10.1158/0008-5472.CAN-10-2583.
Gutschner, Tony, and Sven Diederichs. 2012. “The Hallmarks of Cancer: A Long Non-Coding RNA Point of View.” *RNA Biology* 9 (6): 703–19. https://doi.org/10.4161/rna.20481.
Hanahan, Douglas, and Robert A Weinberg. 2000. “The Hallmarks of Cancer.” *Cell* 100 (1): 57–70. https://doi.org/https://doi.org/10.1016/S0092-8674(00)81683-9.
———. 2011. “Hallmarks of Cancer: The next Generation.” *Cell* 144 (5): 646–74. https://doi.org/10.1016/j.cell.2011.02.013.
Hassanshahi, Alireza, Mohammad Moradzad, Saman Ghalamkari, Moosa Fadaei, Allison J. Cowin, and Mohammadhossein Hassanshahi. 2022. “Macrophage-Mediated Inflammation in Skin Wound Healing.” *Cells* 11 (19). https://doi.org/10.3390/cells11192953.
Hayashi, Ryuji, Hiroo Wada, Kazuhiro Ito, and Ian M. Adcock. 2004. “Effects of Glucocorticoids on Gene Transcription.” *European Journal of Pharmacology* 500 (1-3 SPEC. ISS.): 51–62. https://doi.org/10.1016/j.ejphar.2004.07.011.
He, Wei, Jinzhi Xu, Ruoyu Mu, Qiu Li, Da-lun Lv, Zhen Huang, Junfeng Zhang, Chunming Wang, and Lei Dong. 2020. “High-Salt Diet Inhibits Tumour Growth in Mice via Regulating Myeloid-Derived Suppressor Cell Differentiation.” *Nature Communications* 11 (1): 1732. https://doi.org/10.1038/s41467-020-15524-1.
Hearing, Vincent J. 1999. “Biochemical Control of Melanogenesis and Melanosomal Organization.” *Journal of Investigative Dermatology Symposium Proceedings* 4 (1): 24–28. https://doi.org/10.1038/sj.jidsp.5640176.
Hida, Tokimasa, Takafumi Kamiya, Akinori Kawakami, Jiro Ogino, Hitoshi Sohma, Hisashi Uhara, and Kowichi Jimbow. 2020. “Elucidation of Melanogenesis Cascade for Identifying Pathophysiology and Therapeutic Approach of Pigmentary Disorders and Melanoma.” *International Journal of Molecular Sciences* . https://doi.org/10.3390/ijms21176129.
Hoath, Steven B, and D G Leahy. 2003. “The Organization of Human Epidermis: Functional Epidermal Units and Phi Proportionality.” *The Journal of Investigative Dermatology* 121 (6): 1440–46. https://doi.org/10.1046/j.1523-1747.2003.12606.x.
Hodi, F Stephen, Steven J O’Day, David F McDermott, Robert W Weber, Jeffrey A Sosman, John B Haanen, Rene Gonzalez, et al. 2010. “Improved Survival with Ipilimumab in Patients with Metastatic Melanoma.” *The New England Journal of Medicine* 363 (8): 711–23. https://doi.org/10.1056/NEJMoa1003466.
Hoek, Keith S, Natalie C Schlegel, Ossia M Eichhoff, Daniel S Widmer, Christian Praetorius, Steingrimur O Einarsson, Sigridur Valgeirsdottir, et al. 2008. “Novel MITF Targets Identified Using a Two-Step DNA Microarray Strategy.” *Pigment Cell*

& Melanoma Research 21 (6): 665–76. https://doi.org/10.1111/j.1755-148X.2008.00505.x.

Holbrook, J T, K Y Patterson, J E Bodner, L W Douglas, C Veillon, J L Kelsay, W Mertz, and J C Jr Smith. 1984. "Sodium and Potassium Intake and Balance in Adults Consuming Self-Selected Diets." *The American Journal of Clinical Nutrition* 40 (4): 786–93. https://doi.org/10.1093/ajcn/40.4.786.

Hussein, Mahmoud R. 2006. "Tumour-Associated Macrophages and Melanoma Tumourigenesis: Integrating the Complexity." *International Journal of Experimental Pathology* 87 (3): 163–76. https://doi.org/10.1111/j.1365-2613.2006.00478.x.

Id, Jong W Yu, Sabyasachi Bhattacharya, Niranjan Yanamandra, David Kilian, Hong Shi, Sapna Yadavilli, Yuliya Katlinskaya, et al. 2018. "Tumor-Immune Profiling of Murine Syngeneic Tumor Models as a Framework to Guide Mechanistic Studies and Predict Therapy Response in Distinct Tumor Microenvironments," 1–27.

Ip, W K Eddie, and Ruslan Medzhitov. 2015. "Macrophages Monitor Tissue Osmolarity and Induce Inflammatory Response through NLRP3 and NLRC4 Inflammasome Activation." *Nature Communications* 6 (May): 6931. https://doi.org/10.1038/ncomms7931.

Jameson, Julie M., Leslie L. Sharp, Deborah A. Witherden, and Wendy L. Havran. 2004. "Regulation of Skin Cell Homeostasis by Gamma Delta T Cells." *Frontiers in Bioscience : A Journal and Virtual Library*. https://doi.org/10.2741/1423.

Jantsch, Jonathan, Valentin Schatz, Diana Friedrich, Agnes Schröder, Christoph Kopp, Isabel Siegert, Andreas Maronna, et al. 2015. "Cutaneous Na+ Storage Strengthens the Antimicrobial Barrier Function of the Skin and Boosts Macrophage-Driven Host Defense." *Cell Metabolism* 21 (3): 493–501. https://doi.org/10.1016/j.cmet.2015.02.003.

Jeannin, Pascale, Sébastien Jaillon, and Yves Delneste. 2008. "Pattern Recognition Receptors in the Immune Response against Dying Cells." *Current Opinion in Immunology* 20 (5): 530–37. https://doi.org/10.1016/j.coi.2008.04.013.

Jeyapalan, Asumthia S, Renan A Orellana, Agus Suryawan, Pamela M J O'Connor, Hanh V Nguyen, Jeffery Escobar, Jason W Frank, and Teresa A Davis. 2007. "Glucose Stimulates Protein Synthesis in Skeletal Muscle of Neonatal Pigs through an AMPK- and MTOR-Independent Process." *American Journal of Physiology-Endocrinology and Metabolism* 293 (2): E595–603. https://doi.org/10.1152/ajpendo.00121.2007.

Jobin, Katarzyna, Natascha E Stumpf, Sebastian Schwab, Melanie Eichler, Patrick Neubert, Manfred Rauh, Marek Adamowski, et al. 2020. "A High-Salt Diet Compromises Antibacterial Neutrophil Responses through Hormonal Perturbation." *Science Translational Medicine* 12 (536): eaay3850. https://doi.org/10.1126/scitranslmed.aay3850.

Kim, Dong-Ho, Kye-Seong Kim, and Suresh Ramakrishna. 2018. "NFAT5 Promotes in Vivo Development of Murine Melanoma Metastasis." *Biochemical and Biophysical Research Communications* 505 (3): 748–54. https://doi.org/10.1016/j.bbrc.2018.09.171.

Kim, Ryungsa, Manabu Emi, and Kazuaki Tanabe. 2007. "Cancer Immunoediting from Immune Surveillance to Immune Escape." *Immunology* 121 (1): 1–14. https://doi.org/10.1111/j.1365-2567.2007.02587.x.

Kino, Tomoshige, Hiroaki Takatori, Irini Manoli, Yonghong Wang, Anatoly Tiulpakov, Marc R Blackman, Yan A Su, George P Chrousos, Alan H DeCherney, and James

H Segars. 2009. “Brx Mediates the Response of Lymphocytes to Osmotic Stress through the Activation of NFAT5.” *Science Signaling* 2 (57): ra5. https://doi.org/10.1126/scisignal.2000081.

Kirchner, K A. 1992. “Increased Loop Chloride Uptake Precedes Hypertension in Dahl Salt-Sensitive Rats.” *American Journal of Physiology-Regulatory, Integrative and Comparative Physiology* 262 (2): R263–68. https://doi.org/10.1152/ajpregu.1992.262.2.R263.

Kitada, Kento, Steffen Daub, Yahua Zhang, Janet D Klein, Daisuke Nakano, Tetyana Pedchenko, Louise Lantier, et al. 2017. “High Salt Intake Reprioritizes Osmolyte and Energy Metabolism for Body Fluid Conservation.” *The Journal of Clinical Investigation* 127 (5): 1944–59. https://doi.org/10.1172/JCI88532.

Kleinewietfeld, Markus, Arndt Manzel, Jens Titze, Heda Kvakan, Nir Yosef, Ralf A Linker, Dominik N Muller, and David A Hafler. 2013. “Sodium Chloride Drives Autoimmune Disease by the Induction of Pathogenic TH17 Cells.” *Nature* 496 (7446): 518–22. https://doi.org/10.1038/nature11868.

Koch, Andreas, Sven Arke Lang, Peter Johannes Wild, Susanne Gantner, Abdo Mahli, Gerrit Spanier, Mark Berneburg, Martina Müller, Anja Katrin Bosserhoff, and Claus Hellerbrand. 2015. “Glucose Transporter Isoform 1 Expression Enhances Metastasis of Malignant Melanoma Cells.” *Oncotarget* 6 (32): 32748–60. https://doi.org/10.18632/oncotarget.4977.

Kong, Benjamin Y, Matteo S Carlino, and Alexander M Menzies. 2016. “Biology and Treatment of BRAF Mutant Metastatic Melanoma.” *Melanoma Management* 3 (1): 33–45. https://doi.org/10.2217/mmt.15.38.

Kuang, Rebecca, Stephen J D O’Keefe, Claudia Ramos del Aguila de Rivers, Filippos Koutroumpakis, and David G Binion. 2023. “Is Salt at Fault? Dietary Salt Consumption and Inflammatory Bowel Disease.” *Inflammatory Bowel Diseases* 29 (1): 140–50. https://doi.org/10.1093/ibd/izac058.

Kumar, Vinit, Sima Patel, Evgenii Tcyganov, and Dmitry I. Gabrilovich. 2016. “The Nature of Myeloid-Derived Suppressor Cells in the Tumor Microenvironment.” *Trends in Immunology* 37 (3): 208–20. https://doi.org/10.1016/j.it.2016.01.004.

la Sierra, A de, M M Lluch, A Coca, M T Aguilera, V Giner, E Bragulat, and A Urbano-Márquez. 1996. “Fluid, Ionic and Hormonal Changes Induced by High Salt Intake in Salt-Sensitive and Salt-Resistant Hypertensive Patients.” *Clinical Science (London, England : 1979)* 91 (2): 155–61. https://doi.org/10.1042/cs0910155.

Laberge, Greggory S., Eric Duvall, Zachary Grasmick, Kay Haedicke, Anjela Galan, Jesse Leverett, Sudhir Baswan, Sunghan Yim, and John Pawelek. 2020. “Recent Advances in Studies of Skin Color and Skin Cancer.” *Yale Journal of Biology and Medicine* 93 (1): 69–80.

Larkin, James, Paolo A Ascierto, Brigitte Dréno, Victoria Atkinson, Gabriella Liszkay, Michele Maio, Mario Mandalà, et al. 2014. “Combined Vemurafenib and Cobimetinib in BRAF-Mutated Melanoma.” *The New England Journal of Medicine* 371 (20): 1867–76. https://doi.org/10.1056/NEJMoa1408868.

Le, Hanh K, Laura Graham, Esther Cha, Johanna K Morales, Masoud H Manjili, and Harry D Bear. 2009. “Gemcitabine Directly Inhibits Myeloid Derived Suppressor Cells in BALB/c Mice Bearing 4T1 Mammary Carcinoma and Augments Expansion of T Cells from Tumor-Bearing Mice.” *International Immunopharmacology* 9 (7–8): 900–909. https://doi.org/10.1016/j.intimp.2009.03.015.

Lee, I van der, E F Smit, J W van Putten, H J Groen, N J Schlösser, P E Postmus, and F

M Schramel. 2001. “Single-Agent Gemcitabine in Patients with Resistant Small-Cell Lung Cancer.” *Annals of Oncology : Official Journal of the European Society for Medical Oncology* 12 (4): 557–61. https://doi.org/10.1023/a:1011104509759.

Lei, Tie Chi, Victoria Virador, Ken-Ichi Yasumoto, Wilfred D Vieira, Kazutomo Toyofuku, and Vincent J Hearing. 2002. “Stimulation of Melanoblast Pigmentation by 8-Methoxypsoralen:The Involvement of Microphthalmia-Associated Transcription Factor, the Protein Kinase a Signal Pathway, and Proteasome-Mediated Degradation.” *The Journal of Investigative Dermatology* 119 (6): 1341–49. https://doi.org/10.1046/j.1523-1747.2002.19607.x.

Leick, Katie M, Joel Pinczewski, Ileana S Mauldin, Samuel J Young, Donna H Deacon, Amber N Woods, Marcus W Bosenberg, Victor H Engelhard, and Craig L Slingluff Jr. 2019. “Patterns of Immune-Cell Infiltration in Murine Models of Melanoma: Roles of Antigen and Tissue Site in Creating Inflamed Tumors.” *Cancer Immunology, Immunotherapy : CII* 68 (7): 1121–32. https://doi.org/10.1007/s00262-019-02345-5.

Li, Yanping, Yufei Lyu, Jing Huang, Kun Huang, and Jiufei Yu. 2021. “Transcriptome Sequencing Reveals High-Salt Diet-Induced Abnormal Liver Metabolic Pathways in Mice.” *BMC Gastroenterology* 21 (1): 335. https://doi.org/10.1186/s12876-021-01912-4.

Lin, Kai-Ti, and Lu-Hai Wang. 2016. “New Dimension of Glucocorticoids in Cancer Treatment.” *Steroids* 111 (July): 84–88. https://doi.org/10.1016/j.steroids.2016.02.019.

Liu, Chao-Ying, Juan-Ying Xu, Xiao-Yan Shi, Wei Huang, Ting-Yan Ruan, Ping Xie, and Jun-Li Ding. 2013. “M2-Polarized Tumor-Associated Macrophages Promoted Epithelial–Mesenchymal Transition in Pancreatic Cancer Cells, Partially through TLR4/IL-10 Signaling Pathway.” *Laboratory Investigation* 93 (7): 844–54. https://doi.org/https://doi.org/10.1038/labinvest.2013.69.

Liu, Yanan, and Gang Zeng. 2012. “Cancer and Innate Immune System Interactions: Translational Potentials for Cancer Immunotherapy.” *Journal of Immunotherapy (Hagerstown, Md. : 1997)* 35 (4): 299–308. https://doi.org/10.1097/CJI.0b013e3182518e83.

Liu, Zhaoyuan, Zhaoyuan Liu, Yaqi Gu, Amanda Shin, Shuangyan Zhang, and Florent Ginhoux. 2020. “Protocol Analysis of Myeloid Cells in Mouse Tissues with Flow Cytometry Protocol Analysis of Myeloid Cells in Mouse Tissues with Flow Cytometry.” *STAR Protocols* 1 (1): 100029. https://doi.org/10.1016/j.xpro.2020.100029.

Lo, Jennifer A, and David E Fisher. 2014. “The Melanoma Revolution: From UV Carcinogenesis to a New Era in Therapeutics.” *Science (New York, N.Y.)* 346 (6212): 945–49. https://doi.org/10.1126/science.1253735.

Loffing, J, D Loffing-Cueni, V Valderrabano, L Kläusli, S C Hebert, B C Rossier, J G Hoenderop, R J Bindels, and B Kaissling. 2001. “Distribution of Transcellular Calcium and Sodium Transport Pathways along Mouse Distal Nephron.” *American Journal of Physiology. Renal Physiology* 281 (6): F1021-7. https://doi.org/10.1152/ajprenal.0085.2001.

Lu, Pengfei, Valerie M Weaver, and Zena Werb. 2012. “The Extracellular Matrix: A Dynamic Niche in Cancer Progression.” *The Journal of Cell Biology* 196 (4): 395–406. https://doi.org/10.1083/jcb.201102147.

MacGregor, G A, F P Cappuccio, and N D Markandu. 1987. “Sodium Intake, High Blood Pressure, and Calcium Channel Blockers.” *The American Journal of Medicine* 82

(3B): 16–22. https://doi.org/10.1016/0002-9343(87)90206-3.
Machnik, Agnes, Wolfgang Neuhofer, Jonathan Jantsch, Anke Dahlmann, Tuomas Tammela, Katharina Machura, Joon-Keun Park, et al. 2009. “Macrophages Regulate Salt-Dependent Volume and Blood Pressure by a Vascular Endothelial Growth Factor-C–Dependent Buffering Mechanism.” *Nature Medicine* 15 (5): 545–52. https://doi.org/10.1038/nm.1960.
Mackay, Laura K, Azad Rahimpour, Joel Z Ma, Nicholas Collins, Angus T Stock, Ming-Li Hafon, Javier Vega-Ramos, et al. 2013. “The Developmental Pathway for CD103(+)CD8+ Tissue-Resident Memory T Cells of Skin.” *Nature Immunology* 14 (12): 1294–1301. https://doi.org/10.1038/ni.2744.
Mackiewicz, Jacek, and Andrzej Mackiewicz. 2018. “BRAF and MEK Inhibitors in the Era of Immunotherapy in Melanoma Patients.” *Contemporary Oncology (Poznan, Poland)* 22 (1A): 68–72. https://doi.org/10.5114/wo.2018.73890.
MacLeod, Amanda S, Saskia Hemmers, Olivia Garijo, Marianne Chabod, Kerri Mowen, Deborah A Witherden, and Wendy L Havran. 2013. “Dendritic Epidermal T Cells Regulate Skin Antimicrobial Barrier Function.” *The Journal of Clinical Investigation* 123 (10): 4364–74. https://doi.org/10.1172/JCI70064.
Madison, Kathi C. 2003. “Barrier Function of the Skin: ‘La Raison d’être’ of the Epidermis.” *The Journal of Investigative Dermatology* 121 (2): 231–41. https://doi.org/10.1046/j.1523-1747.2003.12359.x.
Mahmoud, Sahar M A, Emma Claire Paish, Desmond G Powe, R Douglas Macmillan, Matthew J Grainge, Andrew H S Lee, Ian O Ellis, and Andrew R Green. 2011. “Tumor-Infiltrating CD8+ Lymphocytes Predict Clinical Outcome in Breast Cancer.” *Journal of Clinical Oncology : Official Journal of the American Society of Clinical Oncology* 29 (15): 1949–55. https://doi.org/10.1200/JCO.2010.30.5037.
Malissen, Bernard, Samira Tamoutounour, and Sandrine Henri. 2014. “The Origins and Functions of Dendritic Cells and Macrophages in the Skin.” *Nature Reviews. Immunology* 14 (6): 417–28. https://doi.org/10.1038/nri3683.
Manicassamy, Santhakumar, and Bali Pulendran. 2011. “Dendritic Cell Control of Tolerogenic Responses.” *Immunological Reviews* 241 (1): 206–27. https://doi.org/10.1111/j.1600-065X.2011.01015.x.
Manzel, Arndt, Dominik N Muller, David A Hafler, Susan E Erdman, Ralf A Linker, and Markus Kleinewietfeld. 2014. “Role of ‘Western Diet’ in Inflammatory Autoimmune Diseases.” *Current Allergy and Asthma Reports* 14 (1): 404. https://doi.org/10.1007/s11882-013-0404-6.
Mao, Yumeng, Isabel Poschke, Erik Wennerberg, Yago Pico de Coaña, Suzanne Egyhazi Brage, Inkeri Schultz, Johan Hansson, Giuseppe Masucci, Andreas Lundqvist, and Rolf Kiessling. 2013. “Melanoma-Educated CD14+ Cells Acquire a Myeloid-Derived Suppressor Cell Phenotype through COX-2-Dependent Mechanisms.” *Cancer Research* 73 (13): 3877–87. https://doi.org/10.1158/0008-5472.CAN-12-4115.
McArthur, Grant A, Paul B Chapman, Caroline Robert, James Larkin, John B Haanen, Reinhard Dummer, Antoni Ribas, et al. 2014. “Safety and Efficacy of Vemurafenib in BRAF(V600E) and BRAF(V600K) Mutation-Positive Melanoma (BRIM-3): Extended Follow-up of a Phase 3, Randomised, Open-Label Study.” *The Lancet. Oncology* 15 (3): 323–32. https://doi.org/10.1016/S1470-2045(14)70012-9.
Mehta, Raaj S, Mingyang Song, Reiko Nishihara, David A Drew, Kana Wu, Zhi Rong Qian, Teresa T Fung, et al. 2017. “Dietary Patterns and Risk of Colorectal Cancer:

Analysis by Tumor Location and Molecular Subtypes." *Gastroenterology* 152 (8): 1944-1953.e1. https://doi.org/10.1053/j.gastro.2017.02.015.

Mente, Andrew, Martin J O'Donnell, Sumathy Rangarajan, Matthew J McQueen, Paul Poirier, Andreas Wielgosz, Howard Morrison, et al. 2014. "Association of Urinary Sodium and Potassium Excretion with Blood Pressure." *The New England Journal of Medicine* 371 (7): 601–11. https://doi.org/10.1056/NEJMoa1311989.

Merlo, A, J G Herman, L Mao, D J Lee, E Gabrielson, P C Burger, S B Baylin, and D Sidransky. 1995. "5' CpG Island Methylation Is Associated with Transcriptional Silencing of the Tumour Suppressor P16/CDKN2/MTS1 in Human Cancers." *Nature Medicine* 1 (7): 686–92. https://doi.org/10.1038/nm0795-686.

Miranda, Pedro M, Giada De Palma, Viktoria Serkis, Jun Lu, Marc P Louis-Auguste, Justin L McCarville, Elena F Verdu, Stephen M Collins, and Premysl Bercik. 2018. "High Salt Diet Exacerbates Colitis in Mice by Decreasing Lactobacillus Levels and Butyrate Production." *Microbiome* 6 (1): 57. https://doi.org/10.1186/s40168-018-0433-4.

Miskolczi, Zsofia, Michael P Smith, Emily J Rowling, Jennifer Ferguson, Jorge Barriuso, and Claudia Wellbrock. 2018. "Collagen Abundance Controls Melanoma Phenotypes through Lineage-Specific Microenvironment Sensing." *Oncogene* 37 (23): 3166–82. https://doi.org/10.1038/s41388-018-0209-0.

Miyakawa, H, S K Woo, S C Dahl, J S Handler, and H M Kwon. 1999. "Tonicity-Responsive Enhancer Binding Protein, a Rel-like Protein That Stimulates Transcription in Response to Hypertonicity." *Proceedings of the National Academy of Sciences of the United States of America* 96 (5): 2538–42. https://doi.org/10.1073/pnas.96.5.2538.

Moore, Douglas E. 2002. "Drug-Induced Cutaneous Photosensitivity: Incidence, Mechanism, Prevention and Management." *Drug Safety* 25 (5): 345–72. https://doi.org/10.2165/00002018-200225050-00004.

Muller, Olivier G, Rimma G Parnova, Gabriel Centeno, Bernard C Rossier, Dmitri Firsov, and Jean-Daniel Horisberger. 2003. "Mineralocorticoid Effects in the Kidney: Correlation between AENaC, GILZ, and Sgk-1 MRNA Expression and Urinary Excretion of Na⁺ and K⁺" *Journal of the American Society of Nephrology* 14 (5): 1107 LP – 1115. https://doi.org/10.1097/01.ASN.0000061777.67332.77.

Muranski, Pawel, Andrea Boni, Paul A Antony, Lydie Cassard, Kari R Irvine, Andrew Kaiser, Chrystal M Paulos, et al. 2008. "Tumor-Specific Th17-Polarized Cells Eradicate Large Established Melanoma." *Blood* 112 (2): 362–73. https://doi.org/10.1182/blood-2007-11-120998.

Neuhofer, Wolfgang. 2010. "Role of NFAT5 in Inflammatory Disorders Associated with Osmotic Stress." *Current Genomics* 11 (8): 584–90. https://doi.org/10.2174/138920210793360961.

Nguyen, Alan V, and Athena M Soulika. 2019. "The Dynamics of the Skin's Immune System." *International Journal of Molecular Sciences* 20 (8): 1811. https://doi.org/10.3390/ijms20081811.

Omholt, Katarina, Anton Platz, Lena Kanter, Ulrik Ringborg, and Johan Hansson. 2003. "NRAS and BRAF Mutations Arise Early during Melanoma Pathogenesis and Are Preserved throughout Tumor Progression." *Clinical Cancer Research* 9 (17): 6483–88.

Orth, D N, W E Nicholson, M Shapiro, and R Byyny. 1970. "Adrenocorticotropic

Hormone (ACTH) and Melanocyte-Stimulating Hormone (MSH) Production by a Single Cell." In *Program of the 52nd Meeting of the Endocrine Society, St. Louis, Mo. 140.(Abstr.)*.

Ostrand-Rosenberg, Suzanne, Pratima Sinha, Daniel W Beury, and Virginia K Clements. 2012. "Cross-Talk between Myeloid-Derived Suppressor Cells (MDSC), Macrophages, and Dendritic Cells Enhances Tumor-Induced Immune Suppression." *Seminars in Cancer Biology* 22 (4): 275–81. https://doi.org/10.1016/j.semcancer.2012.01.011.

Pagliuca, Chiara, Luca Di Leo, and Daniela De Zio. 2022. "New Insights into the Phenotype Switching of Melanoma." *Cancers*. https://doi.org/10.3390/cancers14246118.

Pajtók, Csenge, Apor Veres-Székely, Róbert Agócs, Beáta Szebeni, Péter Dobosy, István Németh, Zoltán Veréb, et al. 2021. "High Salt Diet Impairs Dermal Tissue Remodeling in a Mouse Model of IMQ Induced Dermatitis." *PLoS ONE* 16 (11 November): 1–16. https://doi.org/10.1371/journal.pone.0258502.

Pandey, R, S Mehrotra, R S Ray, P C Joshi, and R K Hans. 2002. "EVALUATION OF UV-RADIATION INDUCED SINGLET OXYGEN GENERATION POTENTIAL OF SELECTED DRUGS." *Drug and Chemical Toxicology* 25 (2): 215–25. https://doi.org/10.1081/DCT-120003261.

Patra, Krushna C, Qi Wang, Prashanth T Bhaskar, Luke Miller, Zebin Wang, Will Wheaton, Navdeep Chandel, et al. 2013. "Hexokinase 2 Is Required for Tumor Initiation and Maintenance and Its Systemic Deletion Is Therapeutic in Mouse Models of Cancer." *Cancer Cell* 24 (2): 213–28. https://doi.org/10.1016/j.ccr.2013.06.014.

Pavlova, Natalya N, and Craig B Thompson. 2016. "The Emerging Hallmarks of Cancer Metabolism." *Cell Metabolism* 23 (1): 27–47. https://doi.org/10.1016/j.cmet.2015.12.006.

Pazirandeh, Ahmad, Yintong Xue, Tore Prestegaard, Mikael Jondal, and Sam Okret. 2002. "Effects of Altered Glucocorticoid Sensitivity in the T-Cell Lineage on Thymocyte and T-Cell Homeostasis." *The FASEB Journal* 16 (7): 727–29. https://doi.org/https://doi.org/10.1096/fj.01-0891fje.

Peña-Oyarzun, Daniel, Rodrigo Troncoso, Catalina Kretschmar, Cecilia Hernando, Mauricio Budini, Eugenia Morselli, Sergio Lavandero, and Alfredo Criollo. 2017. "Hyperosmotic Stress Stimulates Autophagy via Polycystin-2." *Oncotarget* 8 (34): 55984–97. https://doi.org/10.18632/oncotarget.18995.

Peyssonnaux, C, and A Eychène. 2001. "The Raf/MEK/ERK Pathway: New Concepts of Activation." *Biology of the Cell* 93 (1–2): 53–62. https://doi.org/10.1016/s0248-4900(01)01125-x.

Pfeifer, Gerd P, and Ahmad Besaratinia. 2012. "UV Wavelength-Dependent DNA Damage and Human Non-Melanoma and Melanoma Skin Cancer." *Photochemical & Photobiological Sciences : Official Journal of the European Photochemistry Association and the European Society for Photobiology* 11 (1): 90–97. https://doi.org/10.1039/c1pp05144j.

Pham, Duc Daniel M, Samantha Guhan, and Hensin Tsao. 2020. "KIT and Melanoma: Biological Insights and Clinical Implications." *Yonsei Medical Journal* 61 (7): 562–71. https://doi.org/10.3349/ymj.2020.61.7.562.

Piepkorn, M. 2000. "Melanoma Genetics: An Update with Focus on the CDKN2A(P16)/ARF Tumor Suppressors." *Journal of the American Academy of*

Dermatology 42 (5 Pt 1): 705–6. https://doi.org/10.1067/mjd.2000.104687.
Pópulo, Helena, José Manuel Lopes, and Paula Soares. 2012. “The MTOR Signalling Pathway in Human Cancer.” *International Journal of Molecular Sciences* 13 (2): 1886–1918. https://doi.org/10.3390/ijms13021886.
Priesnitz, Chantal, Nikolaus Pfanner, and Thomas Becker. 2020. “Studying Protein Import into Mitochondria.” *Methods in Cell Biology* 155: 45–79. https://doi.org/10.1016/bs.mcb.2019.11.006.
Proksch, Ehrhardt, Johanna M Brandner, and Jens-Michael Jensen. 2008. “The Skin: An Indispensable Barrier.” *Experimental Dermatology* 17 (12): 1063–72. https://doi.org/10.1111/j.1600-0625.2008.00786.x.
PROTTEY, C. 1977. “Investigation of Functions of Essential Fatty Acids in the Skin.” *British Journal of Dermatology* 97 (1): 29–38. https://doi.org/https://doi.org/10.1111/j.1365-2133.1977.tb15424.x.
Rakova, Natalia, Kento Kitada, Kathrin Lerchl, Anke Dahlmann, Anna Birukov, Steffen Daub, Christoph Kopp, et al. 2017. “Increased Salt Consumption Induces Body Water Conservation and Decreases Fluid Intake.” *The Journal of Clinical Investigation* 127 (5): 1932–43. https://doi.org/10.1172/JCI88530.
Ribas, Antoni. 2012. “Tumor Immunotherapy Directed at PD-1.” *The New England Journal of Medicine*. United States. https://doi.org/10.1056/NEJMe1205943.
Robert, Caroline, Antoni Ribas, Jedd D Wolchok, F Stephen Hodi, Omid Hamid, Richard Kefford, Jeffrey S Weber, et al. 2014. “Anti-Programmed-Death-Receptor-1 Treatment with Pembrolizumab in Ipilimumab-Refractory Advanced Melanoma: A Randomised Dose-Comparison Cohort of a Phase 1 Trial.” *The Lancet* 384 (9948): 1109–17. https://doi.org/10.1016/S0140-6736(14)60958-2.
Romani, N, S Koide, M Crowley, M Witmer-Pack, A M Livingstone, C G Fathman, K Inaba, and R M Steinman. 1989. “Presentation of Exogenous Protein Antigens by Dendritic Cells to T Cell Clones. Intact Protein Is Presented Best by Immature, Epidermal Langerhans Cells.” *The Journal of Experimental Medicine* 169 (3): 1169–78. https://doi.org/10.1084/jem.169.3.1169.
Ruocco, Maria Rosaria, Angelica Avagliano, Giuseppina Granato, Elena Vigliar, Stefania Masone, Stefania Montagnani, and Alessandro Arcucci. 2019. “Metabolic Flexibility in Melanoma: A Potential Therapeutic Target.” *Seminars in Cancer Biology* 59 (December): 187–207. https://doi.org/10.1016/j.semcancer.2019.07.016.
Sadowski, Tomasz, Christian Klose, Mathias J Gerl, Anna Wójcik-Maciejewicz, Ronny Herzog, Kai Simons, Adam Reich, and Michal A Surma. 2017. “Large-Scale Human Skin Lipidomics by Quantitative, High-Throughput Shotgun Mass Spectrometry.” *Scientific Reports* 7 (March): 43761. https://doi.org/10.1038/srep43761.
Saito, Sakae, Aki Furuno, Junko Sakurai, Asami Sakamoto, Hae-Ryong Park, Kazuo Shin-ya, Takashi Tsuruo, and Akihiro Tomida. 2009. “Chemical Genomics Identifies the Unfolded Protein Response as a Target for Selective Cancer Cell Killing during Glucose Deprivation.” *Cancer Research* 69 (10): 4225–34. https://doi.org/10.1158/0008-5472.CAN-08-2689.
Salmi, Satu, Anton Lin, Benjamin Hirschovits-Gerz, Mari Valkonen, Niina Aaltonen, Reijo Sironen, Hanna Siiskonen, and Sanna Pasonen-Seppänen. 2021. “The Role of FoxP3+ Regulatory T Cells and IDO+ Immune and Tumor Cells in Malignant Melanoma – an Immunohistochemical Study.” *BMC Cancer* 21 (1): 641. https://doi.org/10.1186/s12885-021-08385-4.
Sandru, A, S Voinea, E Panaitescu, and A Blidaru. 2014. “Survival Rates of Patients

with Metastatic Malignant Melanoma." *Journal of Medicine and Life* 7 (4): 572.
Sansal, Isabelle, and William R Sellers. 2004. "The Biology and Clinical Relevance of the PTEN Tumor Suppressor Pathway." *Journal of Clinical Oncology : Official Journal of the American Society of Clinical Oncology* 22 (14): 2954–63. https://doi.org/10.1200/JCO.2004.02.141.
Sapolsky, R M, L M Romero, and A U Munck. 2000. "How Do Glucocorticoids Influence Stress Responses? Integrating Permissive, Suppressive, Stimulatory, and Preparative Actions." *Endocrine Reviews* 21 (1): 55–89. https://doi.org/10.1210/edrv.21.1.0389.
Sari, Murat, and Pinar Saip. 2018. "Prolonged Disease Control with Nivolumab in Metastatic Lung Adenocarcinoma During Immunotherapy Era." *Journal of the College of Physicians and Surgeons--Pakistan: JCPSP* 28 (October): 891–92. https://doi.org/10.29271/jcpsp.2018.11.891.
Saxton, Robert A, and David M Sabatini. 2017. "MTOR Signaling in Growth, Metabolism, and Disease." *Cell* 169 (2): 361–71. https://doi.org/10.1016/j.cell.2017.03.035.
Schirmacher, Peter, Amrit Mann, Kai Breuhahn, and Manfred Blessing. 2001. "Keratinocyte-Derived Granulocyte-Macrophage Colony Stimulating Factor Accelerates Wound Healing: Stimulation of Keratinocyte Proliferation, Granulation Tissue Formation, and Vascularization." *Journal of Investigative Dermatology* 117 (6): 1382–90. https://doi.org/https://doi.org/10.1046/j.0022-202x.2001.01600.x.
Seggewiss, Ruth, and Hermann Einsele. 2007. "Hematopoietic Growth Factors Including Keratinocyte Growth Factor in Allogeneic and Autologous Stem Cell Transplantation." *Seminars in Hematology* 44 (3): 203–11. https://doi.org/https://doi.org/10.1053/j.seminhematol.2007.04.009.
Seidel, J A, M Vukmanovic-Stejic, B Muller-Durovic, N Patel, J Fuentes-Duculan, S M Henson, J G Krueger, et al. 2018. "Skin Resident Memory CD8(+) T Cells Are Phenotypically and Functionally Distinct from Circulating Populations and Lack Immediate Cytotoxic Function." *Clinical and Experimental Immunology* 194 (1): 79–92. https://doi.org/10.1111/cei.13189.
Shimada, Satoshi, Brian R Hoffmann, Chun Yang, Theresa Kurth, Andrew S Greene, Mingyu Liang, Ranjan K Dash, and Allen W Cowley. 2023. "Metabolic Responses of Normal Rat Kidneys to a High Salt Intake." *BioRxiv : The Preprint Server for Biology*. United States. https://doi.org/10.1101/2023.01.18.524636.
Shirshin, Evgeny A, Yury I Gurfinkel, Alexander V Priezzhev, Victor V Fadeev, Juergen Lademann, and Maxim E Darvin. 2017. "Two-Photon Autofluorescence Lifetime Imaging of Human Skin Papillary Dermis in Vivo: Assessment of Blood Capillaries and Structural Proteins Localization." *Scientific Reports* 7 (1): 1171. https://doi.org/10.1038/s41598-017-01238-w.
Shu, Suyu, Alistair J. Cochran, Rong Rong Huang, Donald L. Morton, and Holden T. Maecker. 2006. "Immune Responses in the Draining Lymph Nodes against Cancer: Implications for Immunotherapy." *Cancer and Metastasis Reviews* 25 (2): 233–42. https://doi.org/10.1007/s10555-006-8503-7.
Siegel, Rebecca L, Kimberly D Miller, Hannah E Fuchs, and Ahmedin Jemal. 2022. "Cancer Statistics, 2022." *CA: A Cancer Journal for Clinicians* 72 (1): 7–33. https://doi.org/10.3322/caac.21708.
Silva, Ines Pires da, Anne Gallois, Sonia Jimenez-Baranda, Shaukat Khan, Ana C Anderson, Vijay K Kuchroo, Iman Osman, and Nina Bhardwaj. 2014. "Reversal of NK-Cell Exhaustion in Advanced Melanoma by Tim-3 Blockade." *Cancer*

Immunology Research 2 (5): 410–22. https://doi.org/10.1158/2326-6066.CIR-13-0171.

Slominski, Andrzej, Desmond J Tobin, Shigeki Shibahara, and Jacobo Wortsman. 2004. "Melanin Pigmentation in Mammalian Skin and Its Hormonal Regulation." *Physiological Reviews* 84 (4): 1155–1228. https://doi.org/10.1152/physrev.00044.2003.

Smalley, K, and T Eisen. 2000. "The Involvement of P38 Mitogen-Activated Protein Kinase in the Alpha-Melanocyte Stimulating Hormone (Alpha-MSH)-Induced Melanogenic and Anti-Proliferative Effects in B16 Murine Melanoma Cells." *FEBS Letters* 476 (3): 198–202. https://doi.org/10.1016/s0014-5793(00)01726-9.

Spurrell, Emma L, and Michelle Lockley. 2014. "Adaptive Immunity in Cancer Immunology and Therapeutics." *Ecancermedicalscience* 8: 441. https://doi.org/10.3332/ecancer.2014.441.

Stoll, B A. 1998. "Breast Cancer and the Western Diet: Role of Fatty Acids and Antioxidant Vitamins." *European Journal of Cancer (Oxford, England : 1990)* 34 (12): 1852–56. https://doi.org/10.1016/s0959-8049(98)00204-4.

Sung, Hyuna, Jacques Ferlay, Rebecca L Siegel, Mathieu Laversanne, Isabelle Soerjomataram, Ahmedin Jemal, and Freddie Bray. 2021. "Global Cancer Statistics 2020: GLOBOCAN Estimates of Incidence and Mortality Worldwide for 36 Cancers in 185 Countries." *CA: A Cancer Journal for Clinicians* 71 (3): 209–49. https://doi.org/https://doi.org/10.3322/caac.21660.

Suzuki, I, R D Cone, S Im, J Nordlund, and Z A Abdel-Malek. 1996. "Binding of Melanotropic Hormones to the Melanocortin Receptor MC1R on Human Melanocytes Stimulates Proliferation and Melanogenesis." *Endocrinology* 137 (5): 1627–33. https://doi.org/10.1210/endo.137.5.8612494.

Tazzyman, Simon, Claire E Lewis, and Craig Murdoch. 2009. "Neutrophils: Key Mediators of Tumour Angiogenesis." *International Journal of Experimental Pathology* 90 (3): 222–31. https://doi.org/10.1111/j.1365-2613.2009.00641.x.

Thompson, John F, and Helen M Shaw. 2000. "Sentinel Node Metastasis From Thin Melanomas With Vertical Growth Phase." *Annals of Surgical Oncology* 7 (4): 251–52. https://doi.org/10.1007/s10434-000-0251-2.

Toki, Maria I, Deepika Kumar, Fahad S Ahmed, David L Rimm, and Mina L Xu. 2020. "Benign Lymph Node Microenvironment Is Associated with Response to Immunotherapy." *Precision Clinical Medicine* 3 (1): 44–53. https://doi.org/10.1093/pcmedi/pbaa003.

Valyi-Nagy, Istvan, Ie-Ming Shih, Tibor Györfi, David Greenstein, Istvan Juhasz, Meenhard Herlyn, and David E Elder. 1993. "Spontaneous and Induced Differentiation of Human Melanoma Cells." *International Journal of Cancer* 54 (1): 159–65. https://doi.org/https://doi.org/10.1002/ijc.2910540125.

Videira, Inês Ferreira dos Santos, Daniel Filipe Lima Moura, and Sofia Magina. 2013. "Mechanisms Regulating Melanogenesis." *Anais Brasileiros de Dermatologia* 88 (1): 76–83. https://doi.org/10.1590/s0365-05962013000100009.

Villanueva, Jessie, and Meenhard Herlyn. 2008. "Melanoma and the Tumor Microenvironment." *Current Oncology Reports* 10 (5): 439–46. https://doi.org/10.1007/s11912-008-0067-y.

Vliet, Amanda A van, Anna-Maria Georgoudaki, Monica Raimo, Tanja D de Gruijl, and Jan Spanholtz. 2021. "Adoptive NK Cell Therapy: A Promising Treatment Prospect for Metastatic Melanoma." *Cancers* 13 (18).

https://doi.org/10.3390/cancers13184722.
Wang, Guang, Cheung-kwan Yeung, Wing-Yan Wong, Nuan Zhang, Yi-fan Wei, Jing-li Zhang, Yu Yan, et al. 2016. “Liver Fibrosis Can Be Induced by High Salt Intake through Excess Reactive Oxygen Species (ROS) Production.” *Journal of Agricultural and Food Chemistry* 64 (7): 1610–17. https://doi.org/10.1021/acs.jafc.5b05897.
Wang, Zhengchao, Qing Zhu, Min Xia, Pin-Lan Li, Shante J Hinton, and Ningjun Li. 2010. “Hypoxia-Inducible Factor Prolyl-Hydroxylase 2 Senses High-Salt Intake to Increase Hypoxia Inducible Factor 1alpha Levels in the Renal Medulla.” *Hypertension (Dallas, Tex. : 1979)* 55 (5): 1129–36. https://doi.org/10.1161/HYPERTENSIONAHA.109.145896.
WARBURG, O. 1956. “On the Origin of Cancer Cells.” *Science (New York, N.Y.)* 123 (3191): 309–14. https://doi.org/10.1126/science.123.3191.309.
Ward, Patrick S, and Craig B Thompson. 2012. “Metabolic Reprogramming: A Cancer Hallmark Even Warburg Did Not Anticipate.” *Cancer Cell* 21 (3): 297–308. https://doi.org/10.1016/j.ccr.2012.02.014.
Weber, Jeffrey. 2008. “Overcoming Immunologic Tolerance to Melanoma: Targeting CTLA-4 with Ipilimumab (MDX-010).” *The Oncologist* 13 Suppl 4: 16–25. https://doi.org/10.1634/theoncologist.13-S4-16.
Weinberger, M H. 1996. “Salt Sensitivity of Blood Pressure in Humans.” *Hypertension (Dallas, Tex. : 1979)* 27 (3 Pt 2): 481–90. https://doi.org/10.1161/01.hyp.27.3.481.
Welling, Paul A, and Kevin Ho. 2009. “A Comprehensive Guide to the ROMK Potassium Channel: Form and Function in Health and Disease.” *American Journal of Physiology. Renal Physiology* 297 (4): F849–63. https://doi.org/10.1152/ajprenal.00181.2009.
Wiig, Helge, Agnes Schröder, Wolfgang Neuhofer, Jonathan Jantsch, Christoph Kopp, Tine V Karlsen, Michael Boschmann, et al. 2013. “Immune Cells Control Skin Lymphatic Electrolyte Homeostasis and Blood Pressure.” *The Journal of Clinical Investigation* 123 (7): 2803–15. https://doi.org/10.1172/JCI60113.
Wilck, Nicola, András Balogh, Lajos Markó, Hendrik Bartolomaeus, and Dominik N Müller. 2019. “The Role of Sodium in Modulating Immune Cell Function.” *Nature Reviews Nephrology* 15 (9): 546–58. https://doi.org/10.1038/s41581-019-0167-y.
Willebrand, Ralf, Ibrahim Hamad, Lauren Van Zeebroeck, Máté Kiss, Kirsten Bruderek, Anneleen Geuzens, Dries Swinnen, et al. 2019. “High Salt Inhibits Tumor Growth by Enhancing Anti-Tumor Immunity .” *Frontiers in Immunology* . https://www.frontiersin.org/article/10.3389/fimmu.2019.01141.
Wolchok, Jedd D, Harriet Kluger, Margaret K Callahan, Michael A Postow, Naiyer A Rizvi, Alexander M Lesokhin, Neil H Segal, et al. 2013. “Nivolumab plus Ipilimumab in Advanced Melanoma.” *The New England Journal of Medicine* 369 (2): 122–33. https://doi.org/10.1056/NEJMoa1302369.
Wolf Horrell, Erin M, Mary C Boulanger, and John A D’Orazio. 2016. “Melanocortin 1 Receptor: Structure, Function, and Regulation.” *Frontiers in Genetics* 7 (May): 95. https://doi.org/10.3389/fgene.2016.00095.
Xiong, Na, and David H Raulet. 2007. “Development and Selection of Gammadelta T Cells.” *Immunological Reviews* 215 (February): 15–31. https://doi.org/10.1111/j.1600-065X.2006.00478.x.
Xu, Bing-e, Steve Stippec, Po-Yin Chu, Ahmed Lazrak, Xin-Ji Li, Byung-Hoon Lee, Jessie M English, Bernardo Ortega, Chou-Long Huang, and Melanie H Cobb. 2005.

"WNK1 Activates SGK1 to Regulate the Epithelial Sodium Channel." *Proceedings of the National Academy of Sciences of the United States of America* 102 (29): 10315–20. https://doi.org/10.1073/pnas.0504422102.

Yakoob, Mohammad Yawar, and Naila Baig-ansari. 2019. "Dietary Sodium (Salt) Intake and Risk of Colorectal Cancer: A Systematic Review (P05-039-19)." *Current Developments in Nutrition*. https://doi.org/10.1093/cdn/nzz030.P05-039-19.

Yancey, Paul H. 2005. "Organic Osmolytes as Compatible, Metabolic and Counteracting Cytoprotectants in High Osmolarity and Other Stresses." *The Journal of Experimental Biology* 208 (Pt 15): 2819–30. https://doi.org/10.1242/jeb.01730.

Yang, Yujian H, Roman Istomine, Fernando Alvarez, Tho-Alfakar Al-Aubodah, Xiang Qun Shi, Tomoko Takano, Angela M Thornton, Ethan M Shevach, Ji Zhang, and Ciriaco A Piccirillo. 2020. "Salt Sensing by Serum/Glucocorticoid-Regulated Kinase 1 Promotes Th17-like Inflammatory Adaptation of Foxp3(+) Regulatory T Cells." *Cell Reports* 30 (5): 1515-1529.e4. https://doi.org/10.1016/j.celrep.2020.01.002.

Yokoyama, Wayne M, and Beatrice F M Plougastel. 2003. "Immune Functions Encoded by the Natural Killer Gene Complex." *Nature Reviews. Immunology* 3 (4): 304–16. https://doi.org/10.1038/nri1055.

Yu, H C, L M Burrell, M J Black, L L Wu, R J Dilley, M E Cooper, and C I Johnston. 1998. "Salt Induces Myocardial and Renal Fibrosis in Normotensive and Hypertensive Rats." *Circulation* 98 (23): 2621–28. https://doi.org/10.1161/01.cir.98.23.2621.

Yuzawa, Satoru, Yarden Opatowsky, Zhongtao Zhang, Valsan Mandiyan, Irit Lax, and Joseph Schlessinger. 2007. "Structural Basis for Activation of the Receptor Tyrosine Kinase KIT by Stem Cell Factor." *Cell* 130 (2): 323–34. https://doi.org/10.1016/j.cell.2007.05.055.

Zeng, Xiaokang, Yan Li, Weibiao Lv, Xinhuai Dong, Chong Zeng, Liming Zeng, Zibo Wei, Xu Lin, Yanning Ma, and Qiang Xiao. 2020. "A High-Salt Diet Disturbs the Development and Function of Natural Killer Cells in Mice." *Journal of Immunology Research* 2020: 6687143. https://doi.org/10.1155/2020/6687143.

Zhang, Boyang, Kazuomi Kario, Toshihiko Yada, and Masanori Nakata. 2022. "TRPV1-Mediated Sensing of Sodium and Osmotic Pressure in POMC Neurons in the Arcuate Nucleus of the Hypothalamus."

Zheng, Jie. 2012. "Energy Metabolism of Cancer: Glycolysis versus Oxidative Phosphorylation (Review)." *Oncology Letters* 4 (6): 1151–57. https://doi.org/10.3892/ol.2012.928.

Zhu, Ruizhe, Gang Yang, Zhe Cao, Kexin Shen, Lianfang Zheng, Jianchun Xiao, Lei You, and Taiping Zhang. 2020. "The Prospect of Serum and Glucocorticoid-Inducible Kinase 1 (SGK1) in Cancer Therapy: A Rising Star." *Therapeutic Advances in Medical Oncology* 12 (July): 1758835920940946–1758835920940946. https://doi.org/10.1177/1758835920940946.

Zou, Weiping, and Lieping Chen. 2008. "Inhibitory B7-Family Molecules in the Tumour Microenvironment." *Nature Reviews. Immunology* 8 (6): 467–77. https://doi.org/10.1038/nri2326.

9. Acknowledgments

First and foremost, I want to thank my supervisor Prof. Christian Kurts who provided me the opportunity to perform my PhD studies in his group. His experience in immunology always led to exciting experimental theories and provided the basis for this thesis. Thank you for your continuous support, encouragement and trust.

Thanks to Prof. Jonathan Jantsch, for the great collaboration between Bonn and Regensburg and for kindly acting as my second examiner for my thesis.

I would also like to thank the other members of my PhD committee, Prof. Annkristin Heine and Prof. Natalio Garbi. In addition to reviewing my dissertation, I was able to rely on their support for subject-specific questions.

Furthermore, I would like to thank Dr. Katarzyna Jobin, who initiated the project. Many times, we had to think in new directions and try out new experimental approaches. Thank you for the great support and for supervising me during the initial period of my PhD. Thanks to Dr. Mirjam Meißner, for supporting the project with good ideas and her engagement. Special thanks to Dr. Clivia Lisowski for the great cooperation in the later state of the project. Thank you for supporting me and for often keeping track of things.

I would like to thank Melanie, who helped me a lot during my studies and being my right-hand during experiments. Thanks also to Daniela, for the technical support during lab work.

Many thanks go also to all other collaboration partners that contributed to this work.

Within the last years, many of my colleagues became friends and shared many precious moments with me. They constantly supported and encouraged me also during the difficult phases of my PhD thesis. Thanks to Susanne who reviewed my thesis and for the long friendship. Special thanks to Nina my office partner, for your support and our coffee breaks. Marigona and Annika, thank you for being my friends. You make the lab work even funnier.

Most importantly, I want to thank my family for backing me up and providing confidence. You were there at any phase of the PhD journey and were always there for me so I would not lose my sanity. This thesis would not have been possible without your support.

Thank you very much!

10. List of Publications

Böhner,…, Stumpf, ..., Kurts. 2021 *JASN* 32(10):2445–53)
Renal Denervation Exacerbates LPS- and Antibody-Induced Acute Kidney Injury, but Protects from Pyelonephritis in Mice. DOI: 10.1126/scitranslmed.aay3850

Krebs, …, Stumpf, …, Mittrücker. 2020 *Science Immunology* 5(5).
“Pathogen-Induced Tissue-Resident Memory T(H)17 (T(RM)17) Cells Amplify Autoimmune Kidney Disease. DOI: 10.1126/sciimmunol.aba4163

Jobin, Stumpf, …, Kurts. 2020 *Science Translational Medicine* 12(536).
“A High-Salt Diet Compromises Antibacterial Neutrophil Responses through Hormonal Perturbation.” DOI: 10.1126/scitranslmed.aay3850